PHYSICAL REVIEW D **78,** 073006 (2008)

Electroweak corrections using effective field theory: Applications to the CERN LHC

Jui-yu Chiu, Randall Kelley, and Aneesh V. Manohar
Department of Physics, University of California at San Diego, La Jolla, California 92093, USA
(Received 9 June 2008; published 9 October 2008)

Electroweak Sudakov logarithms at high energy, of the form $(\alpha/\sin^2\theta_W)^n \log^m s/M_{Z,W}^2$, are summed using effective theory (EFT) methods. The exponentiation of Sudakov logarithms and factorization is discussed in the EFT formalism. Radiative corrections are computed to scattering processes in the standard model involving an arbitrary number of external particles. The computations include nonzero particle masses such as the t-quark mass, electroweak mixing effects which lead to unequal W and Z masses and a massless photon, and Higgs corrections proportional to the top-quark Yukawa coupling. The structure of the radiative corrections, and which terms are summed by the EFT renormalization group is discussed in detail. The omitted terms are smaller than 1%. We give numerical results for the corrections to dijet production, dilepton production, $t\bar{t}$ production, and squark pair production. The purely electroweak corrections are significant—about 15% at 1 TeV, increasing to 30% at 5 TeV, and they change both the scattering rate and angular distribution. The QCD corrections (which are well-known) are also computed with the EFT. They are much larger—about a factor of 4 at 1 TeV, increasing to a factor of 30 at 5 TeV. Mass effects are also significant; the $q\bar{q} \to t\bar{t}$ rate is enhanced relative to the light-quark production rate by 40%.

DOI: 10.1103/PhysRevD.78.073006 PACS numbers: 12.15.Lk, 12.38.Cy, 13.40.Ks, 13.85.−t

I. INTRODUCTION

Radiative corrections to high-energy scattering processes have two powers of a large logarithm for each order in perturbation theory. These logarithms, referred to as Sudakov logarithms, lead to a breakdown of fixed-order perturbation theory, and have to be summed to all orders. The Large Hadron Collider (LHC) has a center-of-mass energy of $\sqrt{s} = 14$ TeV, and will be able to measure collisions with a partonic center-of-mass energy of several TeV, more than an order of magnitude larger than the masses of the electroweak gauge bosons. Electroweak Sudakov corrections are not small at LHC energies, since $\alpha \log^2 s/M_{W,Z}^2/(4\pi \sin^2\theta_W) \sim 0.15$ at $\sqrt{s} = 4$ TeV. In this paper, we will apply effective theory methods developed in two previous publications [1,2] to processes relevant for the LHC; in particular, we consider in detail dijet production, dilepton pair production, $t\bar{t}$ production, and squark pair production. In Refs. [1,2], electroweak Sudakov corrections to the matrix element of an external current were found to be of order 10%. Electroweak corrections to LHC cross-sections are about 4 times larger. Naively, one factor of 2 arises because scattering processes lead to four-particle operators, which have (approximately) twice the radiative correction of the two-particle current operator. The other factor of 2 arises in squaring the amplitude to obtain the cross-section. Thus purely electroweak corrections at the LHC are significant, and resummed contributions must be properly included to obtain a reliable prediction for the cross-section. There are, of course, QCD corrections which are even larger, and are also included.

There is an extensive literature on electroweak Sudakov effects [3–18]. The computations use infrared evolution equations [5], based on an analysis of the infrared structure of the perturbation theory amplitude and a factorization theorem for the Sudakov form factor [19]. These summations have been checked against one-loop [10–12] and two-loop [13–17] computations.

The Sudakov logarithm $\log(s/M_{W,Z}^2)$ can be thought of as an infrared logarithm in the electroweak theory, since it diverges as $M_{W,Z} \to 0$. By using an effective field theory (EFT), these infrared logarithms in the original theory can be converted to ultraviolet logarithms in the effective theory, and summed using standard renormalization group techniques. The effective theory needed is soft-collinear effective theory (SCET) [20–23], which has been used to study high energy processes in QCD [24], and to perform Sudakov resummations arising from radiative gluon corrections.

This paper studies high energy electroweak corrections to processes relevant for the LHC, such as dijet production, dilepton pair production, $t\bar{t}$ production, and squark pair production, and expands on our previous works [1,2], which will be referred to as CGKM1 and CGKM2, respectively. In CGKM1 we showed how to compute $\log s/M_{W,Z}^2$ corrections to the Sudakov form factor for massless fermions using EFT methods. In CGKM2 the results were generalized to massive fermions such as the top quark, including radiative corrections due to Higgs exchange. The corrections were computed without assuming that the Higgs and electroweak gauge bosons were degenerate in mass. The Higgs corrections when expanded to fixed order agree with previous results of Melles [18]. The

electroweak corrections to processes involving four external particles are computed in this paper. We will show that the results can be obtained by summing the Sudakov form-factor results of CGKM2 over all pairs of external particles with appropriate group theoretic factors. We also show how the results can be generalized to processes involving an arbitrary number of external particles.

There are different methods of counting the order of radiative corrections for the case of Sudakov corrections depending on whether one uses the amplitude or the logarithm of the amplitude. We discuss this issue in detail in Sec. III, where we also explain precisely which terms are summed in our computation. Roughly speaking, we use NLL running in QCD and LL running in the electroweak sector. The neglected terms are numerically less than 1%.

The paper is organized as follows: the outline of the calculation and notation is given in Sec. II. The general structure of Sudakov double-logarithms, exponentiation, and the log-counting rules we use are given in Sec. III. We also discuss the numerical convergence of the perturbation series. The SCET formalism we use for our calculation is described in Sec. IV, including the formalism for Wilson lines needed in multiparticle processes computed using an analytic regulator [25,26]. The calculation of quark scattering and production is first calculated in a toy theory in Sec. V. Results are also given for massive quark production and squark production. The toy theory illustrates the theoretical tools needed for the standard model computation without the added complications of a chiral gauge theory with three gauge groups and particles in many different gauge representations. It also illustrates how one can compute the radiative corrections for theories with scalar particles, such as supersymmetric extensions of the standard model. Some observations on the factorization of amplitudes are made in Sec. VI. Radiative corrections in the standard model are given in Sec. VII. There are a total of 80 different amplitudes that are needed, which are computed in this section. Detailed numerical results and plots are given in Sec. VIII. Appendix A discusses the box graphs needed for the high scale matching computation, as well as the crossing matrix needed for the case of identical particles. The parameter integrals we require in Sec. VII are tabulated in Appendix B. The top quark computation in CGKM2 was incorrect, and the corrected result is given in Appendix C. The numerical values change by about 1%.

II. OUTLINE OF CALCULATION AND NOTATION

The Sudakov logarithms are summed by integrating the renormalization group equations in SCET. The formalism we use has been explained in detail in CGKM2. In this section, we outline the computation of four-particle processes; most of the results are well-known but will serve to define the notation we use in the rest of the paper. As in CGKM2, we first consider a toy gauge theory, a $SU(2)$ spontaneously broken gauge theory with coupling constant α, where all gauge bosons have a common mass M. This is the theory used in many previous computations [2,6–9,17], and allows us to compare with previous results. The results will then be generalized to the realistic case of the standard model. When extending the results of the toy theory to the standard model in Sec. VII, Higgs exchange effects will be included as in CGKM2.

We consider two-to-two scattering at center-of-mass energies much larger than M_Z. We will generically use $Q \gg M_Z$ to denote the energetic scale, and work in the regime where s, t, u are all of order Q^2, so that one has hard scattering kinematics. Our results apply to high energy scattering processes at fixed angles, such as jet production, but not to processes such as diffractive scattering.

The scattering amplitude in the full theory arises from processes such as gauge boson exchange, as shown in Fig. 1(a). The exchanged particle has virtuality of order Q^2. At the scale $\mu \sim Q$, we make a transition to SCET, which is an effective theory describing energetic particles with virtualities parameterically smaller than Q^2. The full theory process is treated in SCET as scattering by a set of local operators, as shown in the right-hand graph in Fig. 1,

$$iA_{\text{full}} = \sum_i C_i(\mu)\langle p_4 p_2|\mathcal{O}_i(\mu)|p_1 p_3\rangle, \tag{1}$$

where $\mathcal{O}_i$ are local SCET operators, and $C_i(\mu)$ are matching coefficients chosen so that the right-hand side reproduces the full theory amplitude up to power corrections of order M^2/Q^2. Power corrections can be systematically included by keeping higher dimension operators suppressed by powers of Q^2. In our computation, we work to leading order in M^2/Q^2. The full and EFT have the same infrared physics but different ultraviolet behavior, and so we must introduce a set of matching coefficients, $C_i(\mu)$ which correct for the different short distance properties of the two theories. The matching coefficients $C_i(\mu)$ are computed by comparing on-shell matrix elements in the full and effective theories at a scale $\mu \sim Q$. At this scale, infrared effects such as gauge boson and particle masses can be neglected, and so $C_i(\mu)$ can be computed using the unbroken gauge theory with massless particles.

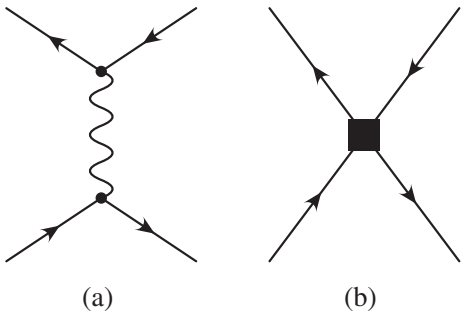

FIG. 1. The full-theory amplitude in (a) turns into scattering by a local operator in the effective theory, as shown in (b).

The coefficients $C_i(\mu)$ are evolved from $\mu \sim Q$ down to the scale $\mu \sim M$ using the SCET anomalous dimensions. The evolution equation for the matching coefficients involves the (matrix) anomalous dimension, γ_{ij}, and is

$$\mu \frac{d}{d\mu} C_i(\mu) = \gamma_{ij}(\mu) C_j(\mu). \tag{2}$$

The anomalous dimension depends on the ultraviolet behavior of SCET, and is independent of particle masses. Like the matching at Q, it can be computed using the unbroken theory with massless particles. In SCET, the anomalous dimension matrix can depend on $\log Q^2/\mu^2$, so integrating Eq. (2) sums the Sudakov double logarithms.

Once the coefficients $C_i(\mu)$ have been evolved down to a low scale of order M, we transition to a new effective theory, which is also SCET, but with the massive gauge bosons integrated out. In our toy example, this new theory has no gauge interactions, since all the gauge bosons are massive. In the standard model, the transition is from a theory with $SU(3) \times SU(2) \times U(1)$ gauge bosons which we call $\mathrm{SCET}_{\mathrm{EW}}$ to a new theory where the only gauge interactions are due to gluons and photons which we call SCET_γ. Operators $\mathcal{O}_i$ in $\mathrm{SCET}_{\mathrm{EW}}$ are matched onto a set of operators $\hat{\mathcal{O}}_i$ in SCET_γ. A single $SU(3) \times SU(2) \times U(1)$ invariant operator $\mathcal{O}_i$ can break up into several operators $\hat{\mathcal{O}}_i$ which are $SU(3) \times U(1)_{\mathrm{em}}$ invariant, but need not have full electroweak gauge invariance. The $\mathrm{SCET}_{\mathrm{EW}} \rightarrow \mathrm{SCET}_\gamma$ matching requires treating massive gauge bosons in SCET, using the formalism developed in CGKM1, CGKM2..

The operators in SCET_γ are evolved down to a scale set by the experimental observables of interest, and then used to compute the desired observables. For example, if one is interested in jet production, then the operators would be scaled down to μ of order the typical jet invariant mass. The operators can then be used to compute jet observables. This paper focuses on electroweak corrections, and we will not discuss this final step of the computation, since it is performed as discussed in earlier work [27]. In our numerical results, we will choose this low energy scale to be 30 GeV. The electroweak corrections are not very sensitive to this scale, since the only effects below M_Z are electromagnetic. The QCD corrections are scale dependent; the μ dependence in the SCET running cancels the μ dependence of the jet matrix elements to the order of the computation. We have not analyzed this in detail since we concentrate on electroweak effects in this paper. In Sec. VIII, only Figs. 12 and 13 have significant μ dependence.

The bulk of the paper discusses the computation of the anomalous dimensions in $\mathrm{SCET}_{\mathrm{EW}}$ and SCET_γ, and the matching between $\mathrm{SCET}_{\mathrm{EW}}$ and SCET_γ, which require SCET operators involving four-particles. We introduce the notation necessary to deal with an arbitrary number of particles. Most of the notation is standard to SCET, and we only discuss those features which are necessary for the extension to r-particles.

The r energetic particles are described by SCET fields ξ_{n_i,p_i} labeled by momentum p_i and light-cone direction n_i, $i = 1, \ldots, r$. There are r light-cone directions n_i, $n_i^2 = 0$, where $n_i^\mu = (1, \mathbf{n}_i)$, with $\mathbf{n}_i$ a unit vector near the direction of motion of particle i. We will also define r light-cone directions $\bar{n}_i$ by reversing the sign of space components of n_i, i.e. by applying parity to n_i, $\bar{n}_i^\mu = (1, -\mathbf{n}_i)$. Note that $\bar{n}_i \cdot n_i = 2$. The momentum of any particle can be written as

$$p_i^\mu = \frac{1}{2} n_i^\mu (\bar{n}_i \cdot p_i) + \frac{1}{2} \bar{n}_i^\mu (n_i \cdot p_i) + p_{i,\perp}^\mu. \tag{3}$$

If $\mathbf{n}_i$ is chosen to be exactly along the direction of p_i, then $p_{i,\perp}^\mu = 0$. The particles are energetic, with $\bar{n}_i \cdot p_i \sim Q$. In the case of only two energetic particles, one can work in the Breit frame where the particles are back-to-back, with $\bar{n}_1 = n_2$ and $\bar{n}_2 = n_1$, so that one only deals with two null vectors n_1 and $\bar{n}_1$, conventionally called n and $\bar{n}$.

Consider a radiative correction graph to the tree-level process Fig. 1, such as the vertex correction shown in Fig. 2 in the full theory. The gauge boson exchanged between the two fermion lines still has virtuality of order Q^2, and so the diagram behaves like the graph in Fig. 3, with the highly virtual gauge boson shrunk to a point. As is well-known, there are several different momentum regions which contribute to the loop integral in Fig. 2. If the components of the gauge boson loop momentum are of order Q, then the gauge boson has virtuality of order Q^2. This contribution is not present in SCET, and is included in the one-loop matching coefficients at the scale Q. The other regions, which are included in SCET, are when the gauge boson is collinear to particle 1 (n_1-collinear gauge boson), to particle 2 (n_2-collinear gauge bosons), or is ultrasoft. The SCET theory thus contains n_i-collinear gauge bosons for each particle direction, $i = 1, \ldots, r$, with momenta scaling like p_i, denoted by A_{n_i,p_i} with labels, as well as ultrasoft gauge bosons denoted by A, with no labels, which couple to all the particles, analogous to the soft and ultrasoft fields introduced in NRQCD [28]. We work in the regime where

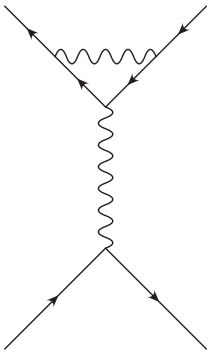

FIG. 2. Vertex correction to the scattering amplitude in the full theory.

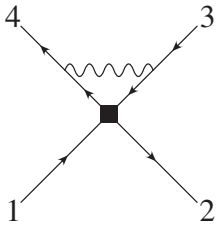

FIG. 3. Vertex correction in SCET.

the kinematic variables such as s, t are of order Q^2, and the invariant masses of the final states are much smaller than Q^2. The SCET power counting parameter is $\lambda = M/Q$. The formalism is valid for observables that can be constructed out of variables in the effective theory, for which the reduction to effective theory vertices such as in Fig. 3 is valid. In particular, it is valid for jet observables and top decay observables at the LHC.

Notation: We use the abbreviations

$$\begin{aligned}
&\mathsf{L}_M = \log\frac{M^2}{\mu^2}, \qquad \mathsf{L}_m = \log\frac{m^2}{\mu^2}, \qquad \mathsf{L}_Q = \log\frac{Q^2}{\mu^2}\\
&\mathsf{L}_s = \log\frac{-s}{\mu^2}, \qquad \mathsf{L}_t = \log\frac{-t}{\mu^2}, \qquad \mathsf{L}_u = \log\frac{-u}{\mu^2}\\
&\mathsf{L}_{s/t} = \log\frac{s}{t} = \log(-s) - \log(-t),\\
&\mathsf{L}_{t/u} = \log\frac{t}{u} = \log(-t) - \log(-u),\\
&\mathsf{L}_{ut/s^2} = \log\frac{ut}{s^2} = \log(-u) + \log(-t) - 2\log(-s).
\end{aligned} \tag{4}$$

For scattering kinematics, $s > 0$, $t < 0$, and $u < 0$. All logarithms arise in the form $\log(-x - i0^+)$ for $x = s, t. u$, so that $\log(-s - i0^+) = \log s - i\pi$. Similarly, $\mathsf{L}_{s/t} = \log(-s) - \log(-t) = \log(-s/t) - i\pi$, and $\mathsf{L}_{t/s} = \log(-t) - \log(-s) = \log(-t/s) + i\pi$. This procedure can be used to find the branch cut of logarithms with negative argument which occur in the subsequent formulas.

III. EXPONENTIATION AND LOG-COUNTING

The exponentiation properties of Sudakov logarithms, and the relation between the renormalization group results and those obtained by exponentiating fixed order computations was discussed in CGKM2. This section summarizes the results we need for our standard model calculation.

The scattering amplitude A has an expansion of the form[1]

$$\mathsf{A} = \begin{pmatrix} 1 & & & & \\ \alpha\mathsf{L}^2 & \alpha\mathsf{L} & \alpha & & \\ \alpha^2\mathsf{L}^4 & \alpha^2\mathsf{L}^3 & \alpha^2\mathsf{L}^2 & \alpha^2\mathsf{L} & \alpha^2 \\ \alpha^3\mathsf{L}^6 & & \cdots & & \\ \vdots & & & & \end{pmatrix} \tag{5}$$

where α represents a gauge coupling constant (α_1, α_2 or α_s), M is an electroweak gauge boson mass (M_W or M_Z) and $Q \gg M$ is of order the center of mass energy of the scattering process, and $\mathsf{L} = \log Q/M$ is the large logarithm. Each entry in Eq. (4) has a numerical coefficient, and the total amplitude is given by summing all the terms. The first row is the tree-level result, the second row is the one-loop contribution, etc. The α^n contribution has logarithms up to power L^{2n}.

The logarithm of the scattering amplitude has an expansion of the form [29–31]

$$\log\mathsf{A} = \begin{pmatrix} \alpha\mathsf{L}^2 & \alpha\mathsf{L} & \alpha & & \\ \alpha^2\mathsf{L}^3 & \alpha^2\mathsf{L}^2 & \alpha^2\mathsf{L} & \alpha^2 & \\ \alpha^3\mathsf{L}^4 & \alpha^3\mathsf{L}^3 & \alpha^3\mathsf{L}^2 & \alpha^3\mathsf{L} & \alpha^3 \\ \alpha^4\mathsf{L}^5 & & \cdots & & \\ \vdots & & & & \end{pmatrix} \tag{6}$$

where the α^n contribution now has logarithms only up to power L^{n+1}, and the amplitude has been normalized so that its tree-level value is unity. The nth row can be computing using perturbation theory at n loops. There are far fewer coefficients in Eq. (6) than Eq. (5), so the form Eq. (6) for $\log\mathsf{A}$ is highly nontrivial. Equation (6) is referred to as the exponentiated form of the amplitude, since A is given by exponentiating the right-hand side. The first column gives the leading-log (LL) series, the second gives the next-to-leading-log (NLL) series, etc.[2]

The EFT computation naturally gives the scattering amplitude in exponentiated form. In general, there are several possible gauge invariants that contribute to the scattering amplitude, so that A is a matrix. The EFT computation gives the proper matrix ordering to be used for the exponentiated form of A. The difference between different matrix orderings can be computed using the Baker-Cambell-Hausdorff theorem. If X and Y are matrices, then

$$\begin{aligned}
&e^Z = e^X e^Y\\
&Z = X + Y + [X, Y] + \frac{1}{12}[X,[X, Y]] + \frac{1}{12}[Y,[Y, X]]\\
&\qquad + \ldots
\end{aligned} \tag{7}$$

where all the higher order terms are multiple commutators of X and Y. If X and Y represent contribution to $\log\mathsf{A}$ of the form Eq. (6), then X and Y are of order $\alpha^{n_{X,Y}}\mathsf{L}^{m_{X,Y}}$ where

[1]For multiparticle scattering, A is actually a matrix of amplitudes, and matrix ordering is important. We discuss the simpler case of the Sudakov form factor, where A is a number. This is sufficient to study the exponentiating and log power-counting we need. The matrix case is discussed in Sec. VI.

[2]The LL, NLL, etc. counting used here is different from that used in fixed order calculations. The relation between the two is explained in CGKM2, and after Eq. (11) in this section.

$m_{X,Y} \leq n_{X,Y} + 1$. Thus one could in principle generate terms in $\log \mathsf{A}$ of the form $\alpha^n \mathsf{L}^m$ with $m > n + 1$ by reordering a matrix product using Eq. (7). This does not occur, because, as discussed in Sec. VI, the leading Sudakov series $\alpha^n \mathsf{L}^{n+1}$ is proportional to the unit matrix, and so drops out of the commutators in Eq. (7), so that the form Eq. (6) is preserved independent of the matrix ordering.

When L is large, fixed order perturbation theory breaks down, and one needs to sum the logarithmically enhanced higher order corrections. There are two interesting regimes relevant for the standard model, in which resummation is necessary. The first is the leading-log (LL) regime in which $\alpha\mathsf{L}$ is of order unity.[3] This is the regime in TeV scale scattering for strong interaction corrections, where $\alpha \to \alpha_s$. Using $\mathsf{L} \sim 1/\alpha$, the various terms in Eqs. (5) are of order

$$\mathsf{A} = \begin{pmatrix} 1 & & & & \\ \frac{1}{\alpha} & 1 & \alpha & & \\ \frac{1}{\alpha^2} & \frac{1}{\alpha} & 1 & \alpha & \alpha^2 \\ \frac{1}{\alpha^3} & & \cdots & & \\ \vdots & & & & \end{pmatrix}. \tag{8}$$

Clearly the fixed order perturbation expansion breaks down, and higher order terms grow with inverse powers of α. To obtain a reliable value for the amplitude requires summing all terms along and below the diagonal, i.e. all terms of order unity or larger. The first superdiagonal gives the order α correction, the second superdiagonal gives the order α^2 correction, etc.

The terms in the exponentiated form Eq. (6) are of order

$$\log \mathsf{A} = \begin{pmatrix} \frac{1}{\alpha} & 1 & \alpha & & \\ \frac{1}{\alpha} & 1 & \alpha & \alpha^2 & \\ \frac{1}{\alpha} & 1 & \alpha & \alpha^2 & \alpha^3 \\ \frac{1}{\alpha} & & \cdots & & \\ \vdots & & & & \end{pmatrix}. \tag{9}$$

The expression for $\log \mathsf{A}$ has already achieved a partial summation of higher order terms. The largest terms are order $1/\alpha$, and there are no terms with higher powers of $1/\alpha$. To obtain $\log \mathsf{A}$ requires summing the first column (the LL series) and the second column (the NLL series). The NNLL series gives order α corrections, the $\mathrm{N^3LL}$ series gives the order α^2 corrections, and so on. While the NLL series is suppressed by one power of α relative to the LL series, it cannot be considered as a correction to the scattering amplitude A, since we have to exponentiate $\log \mathsf{A}$. If we write f_n for the $\mathrm{N}^n\mathrm{LL}$ contribution to $\log \mathsf{A}$, then

$$\begin{aligned} \log \mathsf{A} &= \frac{1}{\alpha} f_0 + f_1 + \alpha f_2 + \ldots \\ &= \frac{1}{\alpha}[f_0 + \alpha f_1 + \alpha^2 f_2 + \ldots] \end{aligned} \tag{10}$$

so that f_1 and f_2 are corrections to $\log \mathsf{A}$. However,

$$\begin{aligned} \mathsf{A} &= \exp\left[\frac{1}{\alpha} f_0 + f_1 + \alpha f_2 + \ldots\right] \\ &= e^{(1/\alpha) f_0} \times e^{f_1} \times e^{\alpha f_2} \times \ldots \end{aligned} \tag{11}$$

and $\exp f_1$ can make a large change in A. Only f_2 and higher can be considered as corrections to A.

The counting discussed above is consistent with that used in renormalization group improved perturbation theory computations. In much of the literature, it is more common to use a different counting, which we denote by the subscript FO. The $\mathrm{LL_{FO}}$ terms are those in A (*not* $\log \mathsf{A}$) of the form $\alpha^n \mathsf{L}^{2n}$, the $\mathrm{NLL_{FO}}$ terms are those in A of the form $\alpha^n \mathsf{L}^{2n-1}$, and in general, the $\mathrm{N}^k\mathrm{LL_{FO}}$ terms are those in A of the form $\alpha^n \mathsf{L}^{2n-k}$. In terms of fixed-order counting, Eq. (6) can be written as

$$\log \mathsf{A} = \begin{pmatrix} \alpha\mathsf{L}^2 \sim \mathrm{LL_{FO}} & \alpha\mathsf{L} \sim \mathrm{NLL_{FO}} & \alpha \sim \mathrm{N^2LL_{FO}} & & \\ \alpha^2\mathsf{L}^3 \sim \mathrm{NLL_{FO}} & \alpha^2\mathsf{L}^2 \sim \mathrm{N^2LL_{FO}} & \alpha^2\mathsf{L} \sim \mathrm{N^3LL_{FO}} & \alpha^2 \sim \mathrm{N^4LL_{FO}} & \\ \alpha^3\mathsf{L}^4 \sim \mathrm{N^2LL_{FO}} & \alpha^3\mathsf{L}^3 \sim \mathrm{N^3LL_{FO}} & \alpha^3\mathsf{L}^2 \sim \mathrm{N^4LL_{FO}} & \alpha^3\mathsf{L} \sim \mathrm{N^5LL_{FO}} & \alpha^3 \sim \mathrm{N^6LL_{FO}} \\ \alpha^4\mathsf{L}^5 \sim \mathrm{N^3LL_{FO}} & & \cdots & & \\ \vdots & & & & \end{pmatrix} \tag{12}$$

and terms in A obtained by exponentiating are given by combining the powers of N.

Note that with this counting, terms of a given series grow at higher order in perturbation theory, e.g. the $\mathrm{N^3LL_{FO}}$ terms are $\alpha^2\mathsf{L}$, $\alpha^3\mathsf{L}^3$, $\alpha^4\mathsf{L}^5$, …, $\alpha^n\mathsf{L}^{2n-3}$, which in the leading-log regime are of order α, 1, $1/\alpha$, …, $1/\alpha^{n-3}$, and grow at higher orders. One can see this clearly from Eq. (11)—f_{k+1} is of order α^k, and is small for $k \geq 1$, as are all terms in the expansion of $\exp \alpha^k f_{k+1}$. However, the perturbation expansion for A contains the prefactor $\exp f_0/\alpha$, and the terms $(f_0/\alpha)^n$ in the expansion of this

[3]Including loop factors of 4π.

prefactor for $n > k$ mutiply the small terms in the expansion of $\exp\alpha^k f_{k+1}$ to produce terms which are larger than unity, with a series of large contributions of alternating sign (since f_0 is negative). The problem is that the tree-level value $\mathsf{A} = 1$ is not close to the true result for A; the leading contribution $\exp f_0/\alpha$ has an essential singularity at $\alpha = 0$ in the perturbation expansion. The second term $\exp f_1$ also is not small. Only after these two contributions are factored out and properly exponentiated does one have a reliable perturbation expansion. Summing all terms up to order $\mathrm{N}^k\mathrm{LL}_{\mathrm{FO}}$ does not give a reliable calculation, because $\mathrm{N}^{k+1}\mathrm{LL}_{\mathrm{FO}}$ terms at order α^r, $r \geq k+1$ are larger than unity. It is essential to properly exponentiate the f_0 and f_1 contributions to get a reliable expansion. Once this done, the higher order contributions are a small correction to the full amplitude A. The amplitude A can be very different from the tree-level amplitude (a factor of 100 in our problem), and still be reliably computed in perturbation theory.

The second regime we consider is the leading-log-squared (LL^2) regime in which $\alpha\mathsf{L}^2$ is of order unity. This is the regime in TeV scale scattering for electroweak corrections, with $\alpha \to \alpha_{1,2}$. Using $\mathsf{L} \sim 1/\alpha^{1/2}$, the various terms in Eq. (5) are of order

$$\mathsf{A} = \begin{pmatrix} 1 & & & & \\ 1 & \alpha^{1/2} & \alpha & & \\ 1 & \alpha^{1/2} & \alpha & \alpha^{3/2} & \alpha^2 \\ 1 & & \cdots & & \\ \vdots & & & & \end{pmatrix} \tag{13}$$

and in Eq. (6) are of order

$$\log \mathsf{A} = \begin{pmatrix} 1 & \alpha^{1/2} & \alpha & & \\ \alpha^{1/2} & \alpha & \alpha^{3/2} & \alpha^2 & \\ \alpha & \alpha^{3/2} & \alpha^2 & \alpha^{5/2} & \alpha^3 \\ \alpha^{3/2} & & \cdots & & \\ \vdots & & & & \end{pmatrix}. \tag{14}$$

The computation of A requires summing the first column, the Sudakov double-logs of order $\alpha^n\mathsf{L}^{2n}$. The remaining terms can be treated in a perturbative expansion. The second column gives the correction of order $\alpha^{1/2}$, the third column the order α correction, etc. The exponentiated form $\log \mathsf{A}$ can be computed to order unity from the $\alpha\mathsf{L}^2$ term. The first correction, of order $\alpha^{1/2}$, is from the $\alpha^2\mathsf{L}^3$ and $\alpha\mathsf{L}$ terms, the order α correction is from the $\alpha^3 L^4$, $\alpha^2 L^2$, and α terms, etc. We will refer to these as the LL^2 (leading-log-squared), NLL^2, NNLL^2, etc. contributions to $\log \mathsf{A}$.

The scattering amplitude in the EFT computation has the form [1,2]

$$\begin{aligned} \mathsf{A} = \exp\!\left[D_0(\alpha(M)) + D_1(\alpha(M)) \log\frac{Q^2}{M^2} \right] \\ \times \exp\!\left\{ -\int_M^Q \frac{\mathrm{d}\mu}{\mu} \left[A(\alpha(\mu)) \log\frac{\mu^2}{Q^2} + B(\alpha(\mu)) \right] \right\} \\ \times \exp C(\alpha(Q)) \end{aligned} \tag{15}$$

Here $\exp C(\alpha(Q))$ is the high scale matching coefficient at Q^2, $\gamma(\mu) = A(\alpha(\mu)) \log(\mu^2/Q^2) + B(\alpha(\mu))$ is the SCET anomalous dimension between Q and M, $\exp D(\alpha(M))$, $D(\alpha(M)) = D_0(\alpha(M)) + D_1(\alpha(M)) \log Q^2/M^2$ is the low scale matching coefficient at M, α the gauge coupling constant (α_1, α_2 or α_s), M is the electroweak gauge boson mass (M_W or M_Z) and $Q \gg M$ is of order the center of mass energy of the scattering process. A is called the cusp anomalous dimension, and is linear in $\log Q$ to all orders in perturbation theory [32,33]. The low-scale matching $\exp D$ has a single-log term D_1 to all orders in perturbation theory [1,2]. The LL series is given by the one-loop cusp anomalous dimension, the NLL series by the two-loop cusp anomalous dimension, the one-loop value of B and the one-loop value of D_1, the NNLL series by the three-loop cusp, two-loop B and D_1, and one-loop D_0 and C, and the $\mathrm{N}^n\mathrm{LL}$ series by the $n+1$ loop cusp, the n-loop B and D_1, and the $n-1$ loop D_0 and C. Equation (15) for the standard model, which we study in this paper, sums the QCD and electroweak corrections, including cross terms such as $\alpha_s\alpha_{1,2}$, $\alpha_s g_t^2$, or $\alpha_{1,2} g_t^2$ which depend on mixed products of the Yukawa, strong and electroweak coupling constants.

A. Absence of some terms in the Sudakov expansion

In Eq. (6), we wrote the generic expansion for $\log \mathsf{A}$. In the standard model, one gets the form Eq. (5) where α^n can be a product of the gauge or Yukawa couplings. It is interesting to note that not all possible terms are present. The leading Sudakov series in $\log \mathsf{A}$ of the form $\alpha^n\mathsf{L}^{n+1}$ is given by integrating the one-loop cusp anomalous dimension with the leading order β-function. The one-loop cusp anomalous dimension $\Gamma(\mu)$ is trivially a sum over the different gauge groups, since there can be no mixed terms like $\alpha_s\alpha_{1,2}$ at one-loop, and because there is no Yukawa contribution to the cusp anomalous dimension (see CGKM1). The one-loop gauge β-function also does not mix different gauge couplings. Thus the leading Sudakov series is a sum of independent terms for each gauge group, with no mixed contributions, i.e. there are terms of the form $\alpha_s^n\mathsf{L}^{2n}$, $\alpha_1^n\mathsf{L}^{2n}$ and $\alpha_2^n\mathsf{L}^{2n}$, but no terms of the form $\alpha_s^n\alpha_{1,2}^m\mathsf{L}^{2n+2m}$ for $n, m \neq 0$.

The first contribution to the cusp anomalous dimension which involves couplings from two-different gauge groups, and so cannot be written as the sum of contributions over individual groups, arises at four-loop order.[4] The two-loop β-function also has contributions from two different gauge couplings. Thus at LL, the running strong coupling α_s only gets modified by terms of the form $\alpha_s(\alpha_s\mathsf{L})^n$, but at NLL, one can have terms of the form $\alpha_s(\alpha_{1,2}\alpha_s\mathsf{L})(\alpha_s\mathsf{L})^n \times (\alpha_{1,2}\mathsf{L})^m$. The $(\alpha_{1,2}\alpha_s\mathsf{L})$ factor comes from one insertion

[4] i.e., $\Gamma(\alpha_s, \alpha_1, \alpha_2) = \Gamma_s(\alpha_s) + \Gamma_1(\alpha_1) + \Gamma_2(\alpha_2)$ up to three-loop order. We would like to thank Z. Bern and L. Dixon for helpful correspondence on this point.

of the two-loop β-function in the renormalization group integration, and the other factors come from using the leading-order β-functions for the remaining integration of α_s and $\alpha_{1,2}$.

Using the above, and noting that the matching conditions and non-cusp anomalous dimensions have all allowed terms, one finds that one can get all possible terms in Eq. (6) for the N^2LL and higher series (third column and beyond). For the LL series (first column), all terms have a single gauge coupling. For the NLL (second column), all terms can occur with the exception of the $\alpha^2\mathsf{L}^2$ contribution, which can only have a single gauge coupling, so that terms such as $\alpha_s\alpha_1\mathsf{L}^2$ are absent.

B. Terms included in the computation

In the standard model, the radiative corrections involve the strong coupling α_s and the electroweak couplings $\alpha_{1,2}$. For log-counting purposes, we assume that the strong coupling is in the leading-log regime, and the electroweak couplings are in the leading-log-squared regime. Let a be the log-counting parameter. Then $\mathsf{L}\sim 1/a$, $\alpha_{1,2}\sim a^2$, $\alpha_s\sim a$. The top-quark Yukawa coupling is also treated as the same order as the electroweak couplings, $g_t^2\sim\alpha_{1,2}\sim a^2$. The terms in $\log\mathsf{A}$ are given in Eq. (6), but now each α can be either a strong coupling α_s of order a or an electroweak coupling $\alpha_{1,2}$ of order a^2. The order of terms with all couplings equal to α_s are given by Eq. (9) with $\alpha\to a$, those with one coupling $\alpha_{1,2}$ and the rest α_s are given by Eq. (9) with $a\times(\alpha\to a)$, etc. The leading terms of order $1/a$ in $\log\mathsf{A}$ are given by summing the $\alpha_s^n\mathsf{L}^{n+1}$ terms, i.e. the leading-log QCD series. The order 1 terms are given by summing the $\alpha_s^n\mathsf{L}^n$ and $\alpha_{1,2}\alpha_s^{n-1}\mathsf{L}^{n+1}$ terms, i.e. the NLL QCD series and the LL series with one power of the electroweak coupling. The order a corrections are given by summing the $\alpha_s^n\mathsf{L}^{n-1}$, $\alpha_{1,2}\alpha_s^{n-1}\mathsf{L}^n$ and $\alpha_{1,2}^2\alpha_s^{n-2}\mathsf{L}^{n+1}$ terms, etc. In the exponentiated form Eq. (6), one only needs to include electroweak corrections at low orders, so that summing terms to order unity only require one-loop electroweak computations, to order a only requires two-loop electroweak corrections, etc. In contrast, the unexponentiated form Eq. (5) of fixed-order computations requires electroweak corrections of arbitrarily high order to sum all terms of order unity or larger.

In the numerical results of Sec. VIII, we include the one-loop QCD, electroweak and Higgs corrections, as well as the two-loop QCD anomalous dimension [34] and two-loop running of the gauge coupling constants. This includes the entire one-loop correction to the scattering amplitude, as well as all higher order corrections which are formally of order $1/a$ or a^0. The terms we neglect are order a or higher in the log counting, and at least second order in the gauge couplings constants $\alpha_{s,1,2}$. The error due to the neglected terms is numerically less than 1% in the rate.

In terms of the commonly used fixed-order counting, we have included all $\mathrm{LL_{FO}}$ and $\mathrm{NLL_{FO}}$ terms for both the QCD and electroweak corrections. In addition we have included all $\mathrm{NNLL_{FO}}$ of the form $\alpha_s^n\mathsf{L}^{2n-2}$ and $\alpha_s^{n-1}\alpha_{1,2}\mathsf{L}^{2n-2}$. Using the counting that $\alpha_s\sim a$ and $\alpha_{1,2}\sim a^2$, and counting $a^n\mathsf{L}^{2n-k}$ as $\mathrm{N^kLL_{FO}}$, we have summed all terms of order $\mathrm{N^3LL_{FO}}$. In terms of the exponentiated form Eq. (6), which is the form given by SCET and used for the numerics, we have included

$$\log\mathsf{A}=\begin{pmatrix}\surd & \surd & \surd & & \\ \surd & \text{not } \alpha_{1,2}^2\mathsf{L}^2 & \text{only } \alpha_s^2\mathsf{L} & \times & \\ \surd & \text{not } \alpha_{1,2}^3\mathsf{L}^3 & \times & \times & \times \\ \surd & \text{not } \alpha_{1,2}^4\mathsf{L}^4 & \cdots & & \\ \vdots & \vdots & & & \end{pmatrix}, \tag{16}$$

where $\surd$ means all terms have been included, $\times$ means no terms have been included. The largest terms omitted are $\alpha_{1,2}^2\mathsf{L}^2$, $\alpha_s^3\mathsf{L}^2$, and $\alpha_s\alpha_{1,2}\mathsf{L}$, and are estimated to be $(\alpha/(\pi\sin^2\theta_W))^2\mathsf{L}^2\sim 0.006$, $(\alpha_s/\pi)^3\mathsf{L}^2\sim 0.003$, and $\alpha_s\alpha/(\pi^2\sin^2\theta_W)\mathsf{L}\sim 0.003$ using $\mathsf{L}\sim\log(4\ \mathrm{TeV})^2/M_Z^2\sim 7$. This gives a sub-1% error. The $\alpha_{1,2}^2\mathsf{L}^2$ term arises from the two-loop electroweak cusp anomalous dimension, and the $\alpha_s^3\mathsf{L}^2$ term from the three-loop QCD cusp anomalous dimension. These are known, and could be easily included in the computation. We have checked that these change the rates by less than 1%.

IV. SCET FORMALISM AND WILSON LINES

In SCET, n_1 collinear gauge bosons can interact with particle 1, or with the other particles in the process. The coupling of n_1-collinear gauge bosons to particle 1 is included explicitly in the SCET Lagrangian. The particle-gauge interactions are identical to those in the full theory, and there is no simplification on making the transition to SCET. However, if an n_1-collinear gauge boson interacts with a particle other than 1 (pick particle 2 for definiteness), then particle 2 becomes off-shell by an amount of order Q, and the intermediate particle 2 propagators can integrated out, giving a Wilson line interaction in SCET. The form of these operators was derived in Ref. [22]. We will use the definitions

$$W_{n_1}^{(n_2)}=\left[\exp\left(-g\frac{1}{\bar{\mathcal{P}}}n_2\cdot A_{n_1,q}^A T^A\right)\right] \tag{17}$$

which is the expression given in Ref. [22] with the replacement $n\to n_1$, $\bar{n}\to n_2$. The gauge generators T^A are in the representation $\mathfrak{R}_2$ of particle 2. The subscript n_1 is a reminder that the Wilson line contains n_1-collinear gauge fields, and the superscript (n_2) is a reminder that the integration path is directed along n_2, and that the gauge generators are in the representation of particle 2.

$W_{n_1}^{(n_2)}$ is a $d_2 \times d_2$ matrix where d_2 is the dimension of $\Re_2$, and transforms under n_1-collinear gauge transformations as

$$[W_{n_1}^{(n_2)}]_{ab} \to U_{ac}^{(2)}[W_{n_1}^{(n_2)}]_{cb} \tag{18}$$

where $U^{(2)}$ is the gauge transformation matrix in the $\Re_2$ representation. One can similarly define $W_{n_i}^{(n_j)}$ for any pair ij of particles, with $i \neq j$. It is convenient to treat all gauge indices as incoming, i.e. an outgoing fermion line in the gauge representation $\Re$ will be treated as an incoming fermion in the representation $\bar{\Re}$.

A generic gauge invariant local operator in the full theory can be written as the gauge invariant product of fields,

$$\mathcal{O} = \sum_{\{a_i\}} c(\{a_i\}) \prod_i \chi_{i,a_i}(0), \tag{19}$$

where χ_{i,a_i} is ψ_{i,a_i} for incoming particles, $\chi_{i,a_i} = \psi_{i,a_i}^\dagger$ for outgoing particles, and c is a Clebsch-Gordan coefficient. χ_i transforms as $\Re_i$ for incoming particles, and as $\bar{\Re}_i$ for outgoing particles. The indices a_i are gauge indices, and $c(\{a_i\}) \equiv c(a_1, \ldots, a_r)$ is the Clebsch-Gordan coefficient for combining the product of fields into a gauge singlet. For n_1-collinear gauge couplings, the field χ_1 in Eq. (19) can be replaced by the SCET field ξ_{n_1,p_1}, and the other fields are replaced by Wilson lines. Collinear gauge invariance implies that the operator Eq. (19) in the effective theory is

$$\mathcal{O} = \sum_{\{a_i\}} c(\{a_i\}) \prod_i [W_{n_i}^{(\bar{n}_i)\dagger} \xi_{n_i,p_i}]_{a_i}, \tag{20}$$

which is gauge invariant under collinear gauge transformations. The sum of all graphs in the full theory with n_1-collinear gauge emission off any of the particles $1, \ldots, r$ in the full theory operator Eq. (19) is equivalent to n_1-collinear emission from ξ_{n_1,p_1}, or from the Wilson line $W_{n_1}^{\bar{n}_1}$ [22] in the operator Eq. (20).

The structure Eq. (20) is nontrivial, and requires combining terms with gluon emission from all the particles, and using the fact that the operator is a gauge singlet. The Feynman rules for multiple gauge emission of n_1-collinear gluons from particle i gives factors of the form

$$\frac{\epsilon \cdot n_i}{k \cdot n_i}. \tag{21}$$

The n_1-collinear gauge field has momentum k and polarization ϵ in the n_1-direction at leading order in SCET power counting, so the above expression can be replaced by

$$\frac{\epsilon \cdot n_i}{k \cdot n_i} \to \frac{n_1 \cdot n_i}{n_1 \cdot n_i} \frac{\epsilon \cdot \bar{n}_1}{k \cdot \bar{n}_1} = \frac{\epsilon \cdot \bar{n}_1}{k \cdot \bar{n}_1} \tag{22}$$

using the leading (first) term in Eq. (3) for the decomposition of both k and ϵ. This expression is independent of n_i. This means that one can change the direction n_i, provided $n_i \cdot n_1$ remains leading order in the power counting, i.e. n_i does not become almost parallel to n_1. One can thus move all the n_i labels so that they all point in a common direction, which can conveniently be chosen to be $\bar{n}_1$. *This choice only makes reference to particle 1, and has no information about the directions of the other particles.* This is the basis for soft-collinear factorization.

In this paper, we will use the analytic regulator [25,26] used in CGKM1, CGKM2. With analytic regularization, Eq. (22) becomes

$$\begin{aligned} \frac{\epsilon \cdot n_i}{(k \cdot n_i)^{1+\delta}} &\to \frac{n_1 \cdot n_i}{(n_1 \cdot n_i)^{1+\delta}} \frac{\epsilon \cdot \bar{n}_1}{(k \cdot \bar{n}_1)^{1+\delta}} \\ &= \frac{1}{(n_1 \cdot n_i)^{\delta}} \frac{\epsilon \cdot \bar{n}_1}{(k \cdot \bar{n}_1)^{1+\delta}} \end{aligned} \tag{23}$$

and the n_i dependence no longer cancels. Thus the identities which allowed one to combine all the n_1-collinear emissions into a single Wilson line in the $\bar{n}_1$ direction no longer hold. This is a big drawback of the analytic regulator. It is possible to use other regulators which do not have this problem [35], but then there are other subtleties which must be addressed, related to zero-bin subtractions [36], which are necessary for soft-collinear factorization [37–40]. With the analytic regulator, n_1-colllinear interactions cannot be encoded in a single Wilson line in the $\bar{n}_1$ direction; instead one needs to include Wilson lines along the directions of all the other particles. In the scattering case, this means that n_1-collinear interactions at one loop are given graphically by Fig. 4. This is equivalent to evaluating the collinear graphs in the full theory using the method of regions with an analytic regulator. We have followed this

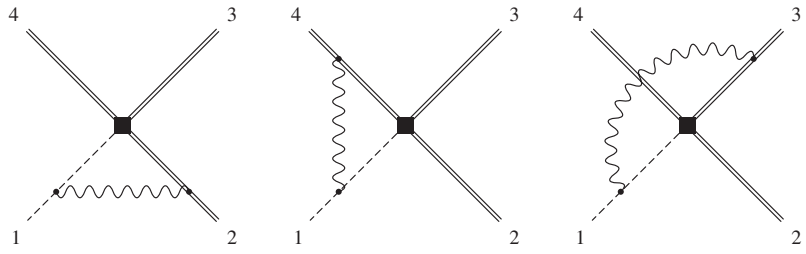

FIG. 4. Graphical representation of n_1-collinear interactions in SCET.

procedure because it allows for a direct comparison of our intermediate results with previous work.

V. SUDAKOV CORRECTIONS TO SCATTERING PROCESSES

In this section we use the toy model to calculate the amplitudes for $qq \to qq$, $q\bar{q} \to q\bar{q}$, $q\bar{q} \to t\bar{t}$, and $q\bar{q} \to \tilde{q}\tilde{q}^c$, where $\tilde{q}$ denotes a colored scalar particle such as a squark. We will call the gauge symmetry color and the particles quarks. The corresponding results in the standard model are given in Sec. VII.

An interesting result is that the SCET S-matrix elements are given by summing the results for the two-particle case, the on-shell Sudakov form-factor given in CGKM1, CGKM2, over all pairs of particles. We first compute the $q\bar{q} \to q\bar{q}$ amplitude explicitly by summing the diagrams, and show how the answer can be written as a sum over two-particle S-matrix elements. The general proof is given in Sec. V E.

In this section, as in CGKM2 we use the decomposition

$$C = C^{(0)} + \frac{\alpha}{4\pi} C^{(1)} \ldots \tag{24}$$

of coefficients and anomalous dimensions into their tree-level and one-loop values. In the next section on the standard model, we will explicitly include the $\alpha/(4\pi)$ factor in the definition of $C^{(1)}$, since there are several different gauge coupling constants.

A. Light quark production

We start with light quark pair-production, $q\bar{q} \to q'\bar{q}'$. The kinematics for $q\bar{q} \to q'\bar{q}'$ is illustrated schematically in Fig. 5 where the incoming and outgoing particles have momenta p_1, p_2 and p_3, p_4, respectively, and we work in the limit $s, t, u \gg M^2 \gg m_i^2$. The external particles are all on-shell ($p_i^2 = m_i^2$). The Mandelstam variables are $s = (p_1 + p_2)^2$, $t = (p_4 - p_1)^2$ and $u = (p_3 - p_1)^2$. We assume q and q' are different flavors, so that only the s-channel annihilation graphs contribute. Identical flavors are discussed in Appendix A.

At the scale $\mu \sim Q$ the full theory is matched onto SCET, and the full theory amplitude at leading order in the power counting is expressed as a sum of local operator matrix elements, as in Eq. (1). The gauge-invariant operators in the effective theory are

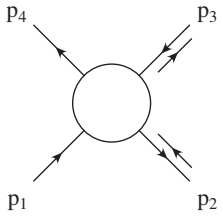

FIG. 5. Pair production $q(p_1) + \bar{q}(p_2) \to q'(p_4) + \bar{q}'(p_3)$. Time runs vertically.

$$\begin{aligned}\mathcal{O}_{1_{RR}^{LL}} &= [\bar{\xi}_4 W_4] t^a \gamma^\mu P_R^L [W_3^\dagger \xi_3][\bar{\xi}_2 W_2] t^a \gamma_\mu P_R^L [W_1^\dagger \xi_1] \\ \mathcal{O}_{2_{RR}^{LL}} &= [\bar{\xi}_4 W_4] \gamma^\mu P_R^L [W_3^\dagger \xi_3][\bar{\xi}_2 W_2] \gamma_\mu P_R^L [W_1^\dagger \xi_1].\end{aligned} \tag{25}$$

There are only two operators which contribute because the fermions are in the fundamental representation of the gauge group. For other representations, there can be more invariants which contribute, e.g., for isospin one fermions, there are three invariant amplitudes in the $I = 0, 1, 2$ channels.

At tree-level,

$$\begin{aligned}C_{1LL}^{(0)} &= C_{1LR}^{(0)} = C_{1RL}^{(0)} = C_{1RR}^{(0)} = \frac{4\pi\alpha}{s} \\ C_{2LL}^{(0)} &= C_{2LR}^{(0)} = C_{2RL}^{(0)} = C_{2RR}^{(0)} = 0\end{aligned} \tag{26}$$

from the graph in Fig. 1.

The one-loop corrections in the full theory are given by the diagrams in Fig. 6, as well as vacuum polarization and wave function graphs. The one-loop corrections in the effective theory are given by computing radiative corrections to the matrix elements of the 4 fermi operators $\mathcal{O}_i$ with tree-level coefficients, and the one-loop matching corrections $C_i^{(1)}$ are given by the difference of the two computations. The graphs in the effective theory vanish on-shell in dimensional regularization, so the one-loop matching coefficients are given by the full theory graphs computed on-shell [32,41,42]. In the full theory matching computation, infrared scales such as the gauge boson mass M and fermion masses m_i, which are all much smaller than Q, can be set to zero. Thus the coefficients C_i are given by the graphs in Fig. 6 with all masses set to zero. The computation is summarized in Appendix A, and agrees with previous calculations [9,43,44]. The one-loop coefficients are (removing an overall $\alpha/(4\pi)$, see Eq. (24)):

$$\begin{aligned}C_{1LL}^{(1)} &= C_{1RR}^{(1)} = \frac{4\pi\alpha}{s}\left[X(s,t) - \frac{(C_d + C_A)}{4}\tilde{f}(s,t)\right] \\ C_{2LL}^{(1)} &= C_{2RR}^{(1)} = -\frac{4\pi\alpha}{s}\tilde{f}(s,t) C_1 \\ C_{1LR}^{(1)} &= C_{1RL}^{(1)} = \frac{4\pi\alpha}{s}\left[X(s,u) + \frac{(C_d - C_A)}{4}\tilde{f}(s,u)\right] \\ C_{2LR}^{(1)} &= C_{2RL}^{(1)} = \frac{4\pi\alpha}{s}\tilde{f}(s,u) C_1\end{aligned} \tag{27}$$

where

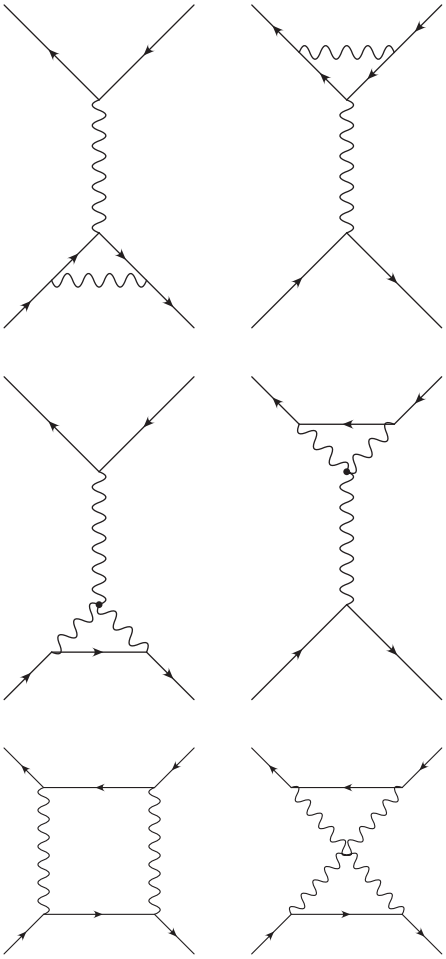

FIG. 6. One loop corrections to pair production in the full theory. Wave function and vacuum polarization graphs are not shown.

$$
\begin{aligned}
X(s,t) &= 2C_F\left(-\mathsf{L}_s^2 + 3\mathsf{L}_s + \frac{\pi^2}{6} - 8\right) \\
&\quad + C_A\left(2\mathsf{L}_s^2 - 2\mathsf{L}_{-s-t}\mathsf{L}_s - \frac{11}{3}\mathsf{L}_s + \pi^2 + \frac{85}{9}\right) \\
&\quad + \left(\frac{4}{3}\mathsf{L}_s - \frac{20}{9}\right)T_F n_F + \left(\frac{1}{3}\mathsf{L}_s - \frac{8}{9}\right)T_F n_s \\
\tilde{f}(s,t) &= -\frac{2s}{s+t}\mathsf{L}_{t/s} + \frac{s(s+2t)}{(s+t)^2}(\mathsf{L}_{t/s}^2 + \pi^2) \\
&\quad + 4\mathsf{L}_s\mathsf{L}_{t/(-s-t)}.
\end{aligned} \tag{28}
$$

Here n_F and n_S are the number of Dirac fermions and complex scalars. The group theory invariants C_d and C_1 are defined in Eq. (40) and (41) below. The high scale matching is the only piece of the computation which cannot be obtained by summing the Sudakov form-factor results over all pairs of particles.

If the initial and final quark flavors are identical, then there are also t-channel graphs which contribute to the matching (see Appendix A).

The next step is to compute the anomalous dimension in SCET between Q and M, and the matching corrections in SCET at M when the gauge bosons are integrated out. Both results can be obtained simultaneously by computing the on-shell matrix elements of $\mathcal{O}_i$ in SCET. The finite part of the graph gives the matching correction, and the infinite part gives the anomalous dimension. The SCET diagrams are n_i-collinear diagrams and ultrasoft graphs. As in CGKM1, CGKM2 the ultrasoft graphs vanish on-shell with the analytic regulator, so the only graphs which contribute are the collinear graphs.

The one-loop n_i-sector graphs are given in Fig. 4. Particle i is given by the field ξ_i, and the remaining particles are represented by Wilson lines. The computations are done using the same analytic regularization method used in CGKM1, CGKM2. The regulated n_i-collinear propagator denominator is

$$
\frac{1}{(p_i + k)^2} \to \frac{(-\nu_i^2)^{\delta_i}}{[(p_i + k)^2]^{1+\delta_i}}. \tag{29}
$$

The propagator denominator for particle j interacting with n_i-collinear gluons becomes

$$
\frac{1}{(p_j + k)^2} \to \frac{(-\nu_j^2)^{\delta_j}}{[(p_j + k)^2]^{1+\delta_j}} \to \frac{(-\nu_j^2)^{\delta_j}}{[2p_j \cdot k]^{1+\delta_j}}. \tag{30}
$$

At leading order in SCET power counting, p_i and k are n_i-collinear, so $p_i^\mu = n_i^\mu(\bar{n}_i \cdot p_i)/2$, $k^\mu = n_i^\mu(\bar{n}_i \cdot k)/2$ and

$$
\frac{1}{(p_j + k)^2} \to \frac{(-\nu_j^2)^{\delta_j}}{[\frac{1}{2}(\bar{n}_j \cdot p_j)(n_j \cdot n_i)]^{1+\delta_j}}. \tag{31}
$$

Thus the analytic continuation of the Wilson line propagator arising from particle j is

$$
\frac{1}{\bar{n}_i \cdot k} \to \frac{(-\nu_i^{(j)})^{\delta_j}}{(\bar{n}_i \cdot k)^{1+\delta_j}}, \qquad \nu_i^{(j)} = \frac{\nu_j^2}{[\frac{1}{2}(\bar{n}_j \cdot p_j)(n_j \cdot n_i)]}. \tag{32}
$$

The key observation is that the ν_j regulator parameter when particle j is the n_j-collinear field ξ_{n_j,p_j} is related to the $\nu_i^{(j)}$ regulator parameter when particle j interacts with n_i-collinear gluons as a Wilson line. This feature was already studied in CGKM1, CGKM2 and leads to a calculable logarithmic violation of factorization, as discussed further in Sec. VI.

The n_i collinear graph with the particle j Wilson line is then identical to the n_1 collinear graph interacting with the n_2 Wilson line result in CGKM1, CGKM2 with the replacement $\nu_1 \to \nu_i$ for the collinear particle regulator, and $\nu_2^+ \to \nu_i^{(j)}$ for the Wilson line regulator. The regulator variables ν_i, $\nu_i^{(j)}$ only appear in logarithms, and $\nu_i^{(j)}$ only appears in the boost-invariant combination

$$\frac{\nu_i^{(j)}}{\bar{n}_i\cdot p_i} = \frac{\nu_j^2}{\frac{1}{2}(\bar{n}_j\cdot p_j)(n_j\cdot n_i)(\bar{n}_i\cdot p_i)} = \frac{\nu_j^2}{2p_i\cdot p_j}. \quad (33)$$

In the Sudakov form-factor results in CGKM1, CGKM2 $2p_1\cdot p_2 = Q^2$, and Eq. (33) was the origin of the $\log Q^2$ terms in SCET. Here $2p_i\cdot p_j$ depends on the kinematic variables, and gives a dependence on $\log s$, $\log t$ and $\log u$.

In the Sudakov form-factor computation, there was a nontrivial cancellation between the n-collinear and $\bar{n}$-collinear graphs, so that the sum of the graphs was independent of the analytic regulator parameters ν_i. There is a similar cancellation here. There are two graphs which are related to each other: graphs with gauge boson exchange between i and j in which i is n_i-collinear and j is a Wilson line, and in which i is a Wilson line and j is n_j-collinear (see Fig. 7). These graphs have identical color factors. The regulator cancellation depended on two identities given in Appendix A in CGKM2. The corresponding relations here are

$$\begin{aligned}
&\left(\log\frac{\nu_i^{(j)}}{\bar{n}_i\cdot p_i} + \log\frac{\nu_i^2}{\mu^2}\right) - \left(\log\frac{\nu_j^{(i)}}{\bar{n}_j\cdot p_j} + \log\frac{\nu_j^2}{\mu^2}\right)\\
&\quad = \log\frac{2\nu_i^2\nu_j^2}{\mu^2(\bar{n}_j\cdot p_j)(\bar{n}_i\cdot p_i)(n_i\cdot n_j)} - (i\leftrightarrow j) = 0\\
&\left(\log\frac{\nu_i^{(j)}}{\bar{n}_i\cdot p_i} - \log\frac{\nu_i^2}{\mu^2}\right) + \left(\log\frac{\nu_j^{(i)}}{\bar{n}_j\cdot p_j} - \log\frac{\nu_j^2}{\mu^2}\right)\\
&\quad = \log\frac{2\mu^2\nu_j^2}{\nu_i^2(\bar{n}_j\cdot p_j)(\bar{n}_i\cdot p_i)(n_i\cdot n_j)} + (i\leftrightarrow j)\\
&\quad = 2\log\frac{\mu^2}{(\bar{n}_j\cdot p_j)(\bar{n}_i\cdot p_i)\frac{1}{2}(n_i\cdot n_j)} = 2\log\frac{\mu^2}{2p_i\cdot p_j}
\end{aligned} \quad (34)$$

which follow from Eq. (32), so the ν cancellation continues to hold. Thus the collinear graphs are obtained by the collinear graphs in the Sudakov form-factor case with the replacement $Q^2 \to 2p_i\cdot p_j$, and summing over pairs with the appropriate group theory factor. The ultrasoft graphs vanish on-shell, as in the Sudakov form-factor case, so the complete answer is given by adding the wave function renormalization graphs to the collinear contribution.

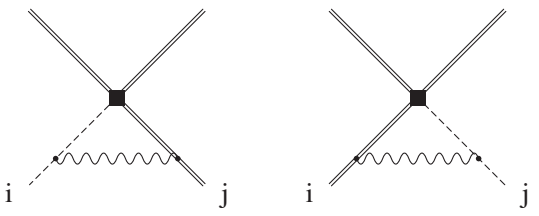

FIG. 7. Collinear graphs involving particles i and j which are related.

The terms which depend on $\log(p_i\cdot p_j)$ arise from the regularization of Wilson lines using the analytic regulator. They depend on the momenta of both particles, so it is clear that in n_i-collinear graphs, it is not possible to combine the Wilson lines for the other particles into a single Wilson line, as that would lose information on the p_j dependence.

Note that the r-particle result obtained by combining the Sudakov form-factors over all pairs of particles is valid even if all the momenta flowing into the operator do not add to zero, i.e. even if there is some momentum inserted at the vertex. In the case of 2-particle scattering, we are interested in operator insertions at zero momentum, and the six $p_i\cdot p_j$ invariants can be written in terms of two independent Mandelstam variables.

The SCET graphs do not change the Lorentz or chiral structure of the operators, and only cause rearrangements of the gauge indices. Thus $\mathcal{O}_{1LL}$ can mix only with $\mathcal{O}_{2LL}$. Furthermore, the mixing matrix for $\mathcal{O}_{1hh'}$, $\mathcal{O}_{2hh'}$ is independent of the chirality labels h, h'. To keep track of the gauge indices, it is convenient to denote $\mathcal{O}_{1hh'}$, $\mathcal{O}_{2hh'}$ by

$$\mathcal{O}_1 = t^a\otimes t^a, \qquad \mathcal{O}_2 = 1\otimes 1. \quad (35)$$

The SCET graphs are then a 2×2 matrix in $\mathcal{O}_{1,2}$ space, and a unit matrix in chirality (h, h') space.

The sum of the n-collinear and $\bar{n}$-collinear vertex graphs with the gauge factor C_F omitted is

$$\begin{aligned}
\Gamma(Q^2) = \frac{\alpha}{4\pi}\Big[&\frac{2}{\epsilon^2} + \frac{4}{\epsilon} - \frac{2}{\epsilon}\mathsf{L}_Q - \mathsf{L}_M^2 + 2\mathsf{L}_M\mathsf{L}_Q\\
&- 4\mathsf{L}_M + 4 - \frac{5\pi^2}{6}\Big].
\end{aligned} \quad (36)$$

The wave function renormalization, omitting group theory factors is[5]

$$\delta Z^{-1} = \frac{\alpha}{4\pi}\left[\frac{1}{\epsilon} - \mathsf{L}_M - \frac{1}{2}\right] \quad (37)$$

The sum of graphs in Fig. 7 which connect particles 1 and 2 is thus

$$\Gamma_{12}(-2p_1\cdot p_2)t^b t^a t^b\otimes t^a \quad (38)$$

if the operator at the vertex is $\mathcal{O}_1$, and

$$\Gamma_{12}(-2p_1\cdot p_2)t^b t^b\otimes 1 \quad (39)$$

if the operator at the vertex is $\mathcal{O}_2$. The minus signs relative to Eq. (36) arise because both momenta $p_{1,2}$ are incoming, whereas in Eq. (36) computed in CGKM2, p_1 was incoming, p_2 was outgoing, and $Q^2 = 2p_1\cdot p_2$. It is useful to add subscripts to Γ denoting the particles involved in the diagram.

[5]These are Eq. (43) with the wave function correction removed and Eq. (40) of CGKM2. Since we work on-shell, there is no need to introduce infrared modes whose virtuality is governed by the off-shellness [45].

The group theory factors can be simplified using

$$t^a t^a = C_F 1 \qquad t^a t^b t^a = \left(C_F - \frac{1}{2} C_A\right) t^b$$
$$t^a t^b \otimes t^a t^b = C_1 1 \otimes 1 + \frac{1}{4}(C_d - C_A) t^a \otimes t^a \tag{40}$$
$$t^a t^b \otimes t^b t^a = C_1 1 \otimes 1 + \frac{1}{4}(C_d + C_A) t^a \otimes t^a$$

in the notation of Ref. [46]. For an $SU(N)$ gauge theory,

$$C_A = N, \qquad C_F = \frac{N^2-1}{2N},$$
$$C_d = \frac{N^2-4}{N}, \qquad C_1 = \frac{N^2-1}{4N^2}, \tag{41}$$

so $C_F = 4/3$, $C_A = 3$, $C_d = 5/3$, $C_1 = 2/9$ for $SU(3)$ and $C_F = 3/4$, $C_A = 2$, $C_d = 0$, $C_1 = 3/16$ for $SU(2)$.

The matrix element of $\mathcal{O}_1$ is

$$\left(C_F - \frac{1}{2}C_A\right)(t^a \otimes t^a)\Gamma_{12}(-2p_1\cdot p_2) + \left(C_F - \frac{1}{2}C_A\right)(t^a \otimes t^a)\Gamma_{34}(-2p_3\cdot p_4) + \left(C_1 1\otimes 1 + \frac{1}{4}(C_d + C_A)t^a \otimes t^a\right)\Gamma_{14}(2p_1\cdot p_4)$$
$$+ \left(C_1 1\otimes 1 + \frac{1}{4}(C_d + C_A)t^a \otimes t^a\right)\Gamma_{23}(2p_2\cdot p_3) - \left(C_1 1\otimes 1 + \frac{1}{4}(C_d - C_A)t^a \otimes t^a\right)\Gamma_{13}(2p_1\cdot p_3)$$
$$- \left(C_1 1\otimes 1 + \frac{1}{4}(C_d - C_A)t^a \otimes t^a\right)\Gamma_{24}(2p_2\cdot p_4) - \frac{1}{2}(\delta Z_1^{-1} + \delta Z_2^{-1} + \delta Z_3^{-1} + \delta Z_4^{-1}) C_F (t^a \otimes t^a). \tag{42}$$

The terms are given by summing over the six possible choices of particle pairs, and including the wave function contribution for each particle. The terms from gluon exchange between 13 or 24 have minus signs, from charge conjugation, since both lines have color flowing into the vertex.[6]

For $\mathcal{O}_2$, one has instead

$$C_F(1\otimes 1)\Gamma_{12}(-2p_1\cdot p_2) + C_F(1\otimes 1)\Gamma_{34}(2p_3\cdot p_4) + (t^a\otimes t^a)\Gamma_{14}(-2p_1\cdot p_4) + (t^a\otimes t^a)\Gamma_{23}(2p_2\cdot p_3)$$
$$- (t^a\otimes t^a)\Gamma_{13}(2p_1\cdot p_3) - (t^a\otimes t^a)\Gamma_{24}(2p_2\cdot p_4) - \frac{1}{2}(\delta Z_1^{-1} + \delta Z_2^{-1} + \delta Z_3^{-1} + \delta Z_4^{-1}) C_F (1\otimes 1). \tag{43}$$

Equations. (42) and (43) can be written in matrix form, by defining the matrix

$$\mathcal{R} = \tilde{\mathcal{R}}\mathbb{1} + \mathcal{R}_S$$
$$\tilde{\mathcal{R}} = C_F\left[\Gamma_{12}(-2p_1\cdot p_2) - \frac{1}{2}\delta Z_1^{-1} - \frac{1}{2}\delta Z_2^{-1}\right] + C_F\left[\Gamma_{34}(-2p_3\cdot p_4) - \frac{1}{2}\delta Z_3^{-1} - \frac{1}{2}\delta Z_4^{-1}\right]$$
$$\mathcal{R}_S = \begin{bmatrix} \frac{1}{4}C_d r_1 + \frac{1}{4}C_A r_2 & r_1 \\ C_1 r_1 & 0 \end{bmatrix} \tag{44}$$
$$r_1 = \Gamma_{14}(2p_1\cdot p_4) + \Gamma_{23}(2p_2\cdot p_3) - \Gamma_{13}(2p_1\cdot p_3) - \Gamma_{24}(2p_2\cdot p_4)$$
$$r_2 = \Gamma_{14}(2p_1\cdot p_4) + \Gamma_{23}(2p_2\cdot p_3) + \Gamma_{13}(2p_1\cdot p_3) + \Gamma_{24}(2p_2\cdot p_4) - 2\Gamma_{12}(-2p_1\cdot p_2) - 2\Gamma_{34}(-2p_3\cdot p_4).$$

Equation (44) has an interesting structure—It has a diagonal piece $\tilde{\mathcal{R}}$, which is the sum of the on-shell Sudakov form factor graphs (including wave function factors) for $1 \to 2$ and $3 \to 4$, and a term $\mathcal{R}_S$, which depends on the amplitude linear combinations r_1 and r_2. $\mathcal{R}_S$ contains differences of Γ_{ij}. One can include wave function factors in $\mathcal{R}_S$ by the replacement

$$\Gamma_{ij} \to \mathcal{S}_{ij} \equiv \Gamma_{ij} - \frac{1}{2}\delta Z_i^{-1} - \frac{1}{2}\delta Z_j^{-1} \tag{45}$$

without changing r_1 and r_2. We will thus use Eq. (44) in the form

$$\mathcal{R} = \tilde{\mathcal{R}}\mathbb{1} + \mathcal{R}_S$$
$$\tilde{\mathcal{R}} = C_F\mathcal{S}_{12}(-2p_1\cdot p_2) + C_F\mathcal{S}_{34}(-2p_3\cdot p_4)$$
$$\mathcal{R}_S = \begin{bmatrix} \frac{1}{4}C_d r_1 + \frac{1}{4}C_A r_2 & r_1 \\ C_1 r_1 & 0 \end{bmatrix}$$
$$r_1 = \mathcal{S}_{14}(2p_1\cdot p_4) + \mathcal{S}_{23}(2p_2\cdot p_3) - \mathcal{S}_{13}(2p_1\cdot p_3) - \mathcal{S}_{24}(2p_2\cdot p_4)$$
$$r_2 = \mathcal{S}_{14}(2p_1\cdot p_4) + \mathcal{S}_{23}(2p_2\cdot p_3) + \mathcal{S}_{13}(2p_1\cdot p_3) + \mathcal{S}_{24}(2p_2\cdot p_4) - 2\mathcal{S}_{12}(-2p_1\cdot p_2) - 2\mathcal{S}_{34}(-2p_3\cdot p_4) \tag{46}$$

[6]Equation (42) is true even if there is nonzero momentum inserted at the operator vertex, so that $p_1 + p_2 \neq p_3 + p_4$.

where $\mathcal{S}$ is the on-shell Sudakov form-factor including wave function corrections, i.e. an S-matrix element, without any color factors. The r_1 and r_2 terms contain differences of Sudakov form factors, and so do not contain Sudakov double-logs, which are universal, do not depend on particle type, and cancel in the difference.

The on-shell matrix element of the effective Lagrangian $C_i\mathcal{O}_i$ including wave function factors is

$$\begin{bmatrix} \langle\mathcal{O}_1\rangle^{(0)} & \langle\mathcal{O}_2\rangle^{(0)} \end{bmatrix}(1+\mathcal{R})\begin{bmatrix} C_1 \\ C_2 \end{bmatrix} \tag{47}$$

where C_i are the operator coefficients and $\mathcal{O}^{(0)}$ are the tree-level matrix elements.

Equations. (46) and (47) are master equations we will use for our scattering computations. For example, to compute the matching correction when the massive gauge bosons are integrated out, we use

$$\begin{bmatrix} \tilde{C}_1 \\ \tilde{C}_2 \end{bmatrix} = (1+R)\begin{bmatrix} C_1 \\ C_2 \end{bmatrix} \tag{48}$$

where R is the finite part of $\mathcal{R}$, and C and $\tilde{C}$ are the coefficients in the high-energy theory with gauge bosons and the low-energy theory without gauge bosons, respectively. Similarly, the anomalous dimension matrix is

$$\mu\frac{\mathrm{d}}{\mathrm{d}\mu}\begin{bmatrix} C_1 \\ C_2 \end{bmatrix} = \gamma\begin{bmatrix} C_1 \\ C_2 \end{bmatrix} \tag{49}$$

where γ is the anomalous dimension computed using the $1/\epsilon$ terms in $\mathcal{R}$, i.e. -2 times the $1/\epsilon$ terms in $\mathcal{R}$ at one loop. The matching conditions and anomalous dimensions are given by Eq. (46) with $\mathcal{S}_{ij}$ replaced by the corresponding Sudakov form-factor matching correction and anomalous dimension computed in CGKM2 without any additional Feynman graph computations.

We now apply the master formula to the SCET anomalous dimension for $q\bar{q}\to q'\bar{q}'$ in the region $Q>\mu>M$, and to the matching condition at M. The anomalous dimension is given using Eq. (46) with $\mathcal{S}$ replaced by the SCET anomalous dimension for the Sudakov form factor, i.e. by $\gamma^{(1)}$ for the bifermion operators in Table I of CGKM2, $\mathcal{S}\to 4\mathsf{L}_Q-6$. The anomalous dimension matrix is

$$\begin{aligned} \gamma^{(1)} &= \tilde{\gamma}^{(1)}\mathbb{1}+\gamma_S^{(1)} \\ \tilde{\gamma}^{(1)} &= 2C_F\left(4\log\frac{-s}{\mu^2}-6\right) \\ \gamma_S^{(1)} &= \begin{bmatrix} 2C_d\log\frac{t}{u}+2C_A\log\frac{ut}{s^2} & 8\log\frac{t}{u} \\ 8C_1\log\frac{t}{u} & 0 \end{bmatrix} \end{aligned} \tag{50}$$

or using the notation defined in Eq. (4),

$$\begin{aligned} \gamma^{(1)} &= \tilde{\gamma}^{(1)}\mathbb{1}+\gamma_S^{(1)} \\ \tilde{\gamma}^{(1)} &= 2C_F(4\mathsf{L}_s-6) \\ \gamma_S^{(1)} &= \begin{bmatrix} 2C_d\mathsf{L}_{t/u}+2C_A\mathsf{L}_{ut/s^2} & 8\mathsf{L}_{t/u} \\ 8C_1\mathsf{L}_{t/u} & 0 \end{bmatrix}. \end{aligned} \tag{51}$$

All logarithms of negative argument are defined by the branch $\log(-s-i0^+)$, and $\log(ut/s^2)\equiv\log(-u-i0^+)+\log(-t-i0^+)-2\log(-s-i0^+)$, etc. as discussed earlier. The off-diagonal terms vanish at $t=u$, i.e. when the center-of-mass scattering angle is $\pi/2$. γ_S is called the soft anomalous dimension. We will see explicitly that the soft anomalous dimension and the soft-matching R_S are universal, and independent of the external states, i.e. they are the same for fermions and scalars, and independent of the particle masses. In our computation using the analytic regulator, γ_S arises from *collinear* graphs; the ultrasoft graphs all vanish.

The anomalous dimension $\tilde{\gamma}$ is twice the anomalous dimension for the Sudakov form-factor, and contains a $\log(-s/\mu^2)$ term which produces double logs in the amplitude on integration. The soft anomalous dimension γ_S does not contain any parameterically large logarithms, since s, t, u are all formally of order Q^2.

The matching matrix is given by replacing $\mathcal{S}$ by the matching $D^{(1)}$ for bifermion operators in Table I of CGKM2, $\mathcal{S}\to-\mathsf{L}_M^2+2\mathsf{L}_M\mathsf{L}_Q-3\mathsf{L}_M+9/2-5\pi^2/6$,

$$\begin{aligned} R^{(1)} &= \tilde{R}^{(1)}\mathbb{1}+R_S^{(1)}, \\ \tilde{R}^{(1)} &= 2C_F\left[-\mathsf{L}_M^2+2\mathsf{L}_M\mathsf{L}_s-3\mathsf{L}_M+\frac{9}{2}-\frac{5\pi^2}{6}\right], \\ R_S^{(1)} &= \mathsf{L}_M\begin{bmatrix} C_d\mathsf{L}_{t/u}+C_A\mathsf{L}_{ut/s^2} & 4\mathsf{L}_{t/u} \\ 4C_1\mathsf{L}_{t/u} & 0 \end{bmatrix}. \end{aligned} \tag{52}$$

Note that there is a nontrivial low-scale matching correction. At $\mu=M$, $\mathsf{L}_M=0$, and $R_S^{(1)}$ vanishes. This is an accident in the toy model at one-loop. In the standard model, $R_S^{(1)}$ does not vanish, and has terms of the form $\log M_W^2/M_Z^2$.

This completes the computation for quark production. The matching and anomalous dimensions are combined to give the final amplitude in the usual way, and give the exponentiated SCET form for the Sudakov logarithms discussed in CGKM2. The matrices γ_S and R_S are universal, and have the same values for heavy quark production and for squark production, as we see explicitly below.

B. Light quark scattering

The next process we consider is light quark production, $q(p_1)+q(p_3)\to q'(p_2)+q'(p_4)$ (see Fig. 8) with $q\neq q'$, which is related to quark scattering in Fig. 5 by crossing symmetry, with the replacements $p_2\to-p_2$, $p_3\to-p_3$. The Mandelstam variables for quark scattering are $s=(p_1+p_3)^2$, $t=(p_2-p_1)^2$ and $u=(p_4-p_1)^2$, so the

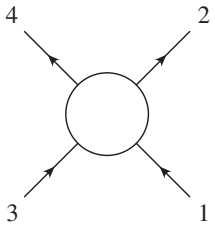

FIG. 8. Quark scattering $q(p_1) + q'(p_3) \to q(p_2) + q'(p_4)$. Time runs vertically.

amplitudes are obtained from those in the previous section by the replacement $s \to t$, $t \to u$, $u \to s$. Identical flavors are discussed in Appendix A.

The anomalous dimension matrix is

$$\begin{aligned}\gamma^{(1)} &= \tilde{\gamma}^{(1)}\mathbb{1} + \gamma_S^{(1)} \\ \tilde{\gamma}^{(1)} &= 2C_F(4\mathsf{L}_t - 6) \\ \gamma_S^{(1)} &= \begin{bmatrix} 2C_d\mathsf{L}_{u/s} + 2C_A\mathsf{L}_{us/t^2} & 8\mathsf{L}_{u/s} \\ 8C_1\mathsf{L}_{u/s} & 0 \end{bmatrix}\end{aligned} \tag{53}$$

and the matching matrix is

$$\begin{aligned}R^{(1)} &= \tilde{R}^{(1)}\mathbb{1} + R_S^{(1)} \\ \tilde{R}^{(1)} &= 2C_F\left[-\mathsf{L}_M^2 + 2\mathsf{L}_M\mathsf{L}_t - 3\mathsf{L}_M + \frac{9}{2} - \frac{5\pi^2}{6}\right] \\ R_S^{(1)} &= \mathsf{L}_M\begin{bmatrix} C_d\mathsf{L}_{u/s} + C_A\mathsf{L}_{us/t^2} & 4\mathsf{L}_{u/s} \\ 4C_1\mathsf{L}_{u/s} & 0 \end{bmatrix}.\end{aligned} \tag{54}$$

C. Heavy quark production

Consider the annihilation of a light-quark antiquark pair to produce a heavy quark-antiquark pair, suggestively labeled $t\bar{t}$, via the process $q(p_1) + \bar{q}(p_2) \to t(p_4) + \bar{t}(p_3)$. The kinematics and Mandelstam variables are the same as Sec. VA; the only difference is that the final particles have mass m which is not negligible compared with the gauge boson mass M, but is much smaller than Q, so that s, t, $u \sim Q^2 \gg m^2$, M^2.

The first step is to match the full theory onto SCET at $\mu \sim Q$. The fields ξ_{n_3} and ξ_{n_4} are now taken to have mass m [47,48]. The matching condition at Q can be computed by from the full theory graphs with all scales much smaller than Q set to zero, so the matching at Q is the same as for the light-quark case.

The second step is to run SCET operators in the effective theory from Q to m. The SCET anomalous dimension is independent of low mass scales and again gives the same result as in the massless case, Eq. (53).

The third step is to switch at the scale $\mu \sim m$ to an effective theory where the heavy quarks are described by heavy quark effective theory (HQET) fields t_{v_3} and t_{v_4} [49]. The four-fermi SCET operators of Eq. (25) are matched onto the SCET/HQET operators:

$$\begin{aligned}\mathcal{O}_1 \to \mathcal{O}_1' &= \bar{t}_{v_4}t^a\gamma^\mu P_{\frac{L}{R}}t_{v_3}[\bar{\xi}_{n_2}W_{n_2}]t^a\gamma_\mu P_{\frac{L}{R}}[W_{n_1}^\dagger\xi_{n_1}] \\ \mathcal{O}_2 \to \mathcal{O}_2' &= \bar{t}_{v_4}\gamma^\mu P_{\frac{L}{R}}t_{v_3}[\bar{\xi}_{n_2}W_{n_2}]\gamma_\mu P_{\frac{L}{R}}[W_{n_1}^\dagger\xi_{n_1}].\end{aligned} \tag{55}$$

The HQET fields do not transform under a collinear gauge transformation; therefore, there is no factor analogous to the $W_n^\dagger$ Wilson line that goes along with ξ_n. The heavy fields t_{v_i} still couple to ultrasoft gauge bosons.

The matching condition at $\mu \sim m$ is given by computing the difference of the graphs in the theory where particles 3 and 4 are described by SCET fields, and the same graphs computed when the two particles are described by HQET fields. Particles 1 and 2 continue to be described by SCET fields. The group theory and kinematic factors for each pair of particles remain unchanged as we switch from SCET to HQET, so the matching condition is given by Eqs. (46) with each Γ being replaced by the difference of the corresponding graph in the two theories. Thus one can use

$$\mathcal{S}_{12} \to 0, \quad \mathcal{S}_{34} \to R_{hh}, \quad \mathcal{S}_{ij}(x) \to R_{hl} \quad ij = 13, 14, 23, 24 \tag{56}$$

where R_{hh} is the matrix element for the Sudakov form-factor in going from two SCET to two HQET fields, and R_{hl} is the matrix element for the transition from two SCET fields to one SCET and one HQET field, dropping any overall group theory factors. The matching coefficients can be read off from Eq. (80) and Eq. (85) in CGKM2

$$\begin{aligned}&\mathcal{S}_{12} \to 0, \quad \mathcal{S}_{34} \to R + T, \quad \mathcal{S}_{ij}(x) \to R \quad ij = 13, 14, 23, 24 \\ &R = T = \frac{1}{2}\mathsf{L}_m^2 - \frac{1}{2}\mathsf{L}_m + \frac{\pi^2}{12} + 2,\end{aligned} \tag{57}$$

where we use the entries from the first rows of Tables II and IV of CGKM2. Thus

$$\begin{aligned}\mathcal{R}^{(1)} &= \tilde{\mathcal{R}}^{(1)}\mathbb{1} + \mathcal{R}_S^{(1)}, \\ \tilde{\mathcal{R}}^{(1)} &= C_F(R + T) = C_F\left(\mathsf{L}_m^2 - \mathsf{L}_m + \frac{\pi^2}{6} + 4\right), \\ \mathcal{R}_S^{(1)} &= 0,\end{aligned} \tag{58}$$

using Eq. (46) for the matching. $\mathcal{R}_S^{(1)}$ vanishes since $r_1 = 2R - 2R = 0$ and $r_2 = 4R - 2(R + T) = 0$.

The anomalous dimension below m is given by using Eq. (46) with the replacement analogous to Eq. (57) for the anomalous dimension,

$$\begin{aligned}\mathcal{S}_{12}(-2p_1 \cdot p_2) &\to \gamma_1(-s) \\ \mathcal{S}_{34}(-2p_3 \cdot p_4) &\to \gamma_3(-s) \\ \mathcal{S}_{13}(2p_1 \cdot p_3) &\to \gamma_2(-u) \\ \mathcal{S}_{14}(2p_1 \cdot p_4) &\to \gamma_2(-t) \\ \mathcal{S}_{23}(2p_2 \cdot p_3) &\to \gamma_2(-t) \\ \mathcal{S}_{24}(2p_2 \cdot p_4) &\to \gamma_2(-u)\end{aligned} \tag{59}$$

where $\gamma_{1,2,3}(Q^2)$ are the entries from the first rows of Tables I, II and IV of CGKM2. They are the anomalous dimensions for ll, hl and hh currents, respectively. The anomalous dimension matrix in the HQET/SCET theory is

$$\begin{aligned}
\gamma^{(1)} &= \tilde{\gamma}^{(1)}\mathbb{1} + \gamma_S^{(1)} \\
\tilde{\gamma}^{(1)} &= C_F(\gamma_1(-s) + \gamma_3(-s)) \\
r_1 &\to 2\gamma_2(-t) - 2\gamma_2(-u) \\
r_2 &\to 2\gamma_2(-t) + 2\gamma_2(-u) - 2\gamma_1(-s) - 2\gamma_3(-s) \\
\gamma_1(Q^2) &= 4\mathsf{L}_Q - 6 \\
\gamma_2(Q^2) &= 4\mathsf{L}_Q - 2\mathsf{L}_m - 5 \\
\gamma_3(Q^2) &= 4[wr(w) - 1] \\
r(w) &= \frac{\log(w + \sqrt{w^2-1})}{\sqrt{w^2-1}} \\
w &= 1 + \frac{Q^2}{2m^2}
\end{aligned} \tag{60}$$

Since we are working in the limit $Q^2 \gg m^2$, $wr(w) - 1 \to \log(2w) - 1 \to \log(Q^2/m^2) - 1$ up to power corrections. This gives

$$\begin{aligned}
\gamma^{(1)} &= \tilde{\gamma}^{(1)}\mathbb{1} + \gamma_S^{(1)} \\
\tilde{\gamma}^{(1)} &= C_F(8\mathsf{L}_s - 4\mathsf{L}_m - 10) \\
\gamma_S^{(1)} &= \begin{bmatrix} 2C_d\mathsf{L}_{t/u} + 2C_A\mathsf{L}_{ut/s^2} & 8\mathsf{L}_{t/u} \\ 8C_1\mathsf{L}_{t/u} & 0 \end{bmatrix}.
\end{aligned} \tag{61}$$

The last step is to integrate out the gauge boson at $\mu \sim M$ and transition to the theory with no gauge bosons. The matching is given by Eq. (46) where $\mathcal{S}_{ij}$ are replaced by the corresponding results for the Sudakov form-factor matching,

$$\begin{aligned}
&\mathcal{S}_{12}(-2p_1\cdot p_2) \to D(-s) \qquad \mathcal{S}_{34}(-2p_3\cdot p_4) \to U(-s) \\
&\mathcal{S}_{13}(2p_1\cdot p_3) \to S(-u) \qquad \mathcal{S}_{14}(2p_1\cdot p_4) \to S(-t) \\
&\mathcal{S}_{23}(2p_2\cdot p_3) \to S(-t) \qquad \mathcal{S}_{24}(2p_2\cdot p_4) \to S(-u)
\end{aligned} \tag{62}$$

where D, S, U are given in the first rows of Tables I, II and IV, respectively, of CGKM2. The matching is

$$\begin{aligned}
R^{(1)} &= \tilde{R}^{(1)}\mathbb{1} + R_S^{(1)} \\
\tilde{R}^{(1)} &= C_F(D(-s) + U(-s)) \\
r_1 &\to 2S(-t) - 2S(-u) \\
r_2 &\to 2S(-t) + 2S(-u) - 2D(-s) - 2U(-s)
\end{aligned} \tag{63}$$

so that

$$\begin{aligned}
R^{(1)} &= \tilde{R}^{(1)}\mathbb{1} + R_S^{(1)} \\
\tilde{R}^{(1)} &= C_F\left(-\mathsf{L}_M^2 + 4\mathsf{L}_M\mathsf{L}_s - 2\mathsf{L}_M\mathsf{L}_m - 5\mathsf{L}_M + \frac{9}{2} - \frac{5\pi^2}{6}\right) \\
R_S^{(1)} &= \mathsf{L}_M\begin{bmatrix} C_d\mathsf{L}_{t/u} + C_A\mathsf{L}_{ut/s^2} & 4\mathsf{L}_{t/u} \\ 4C_1\mathsf{L}_{t/u} & 0 \end{bmatrix}.
\end{aligned} \tag{64}$$

In summary, the computation proceeds as follows: (a) Match at $\mu \sim \sqrt{s}$ using Eq. (25) and (27) (b) Run between $\sqrt{s}$ and m using Eq. (50) (c) Matching at m using Eq. (58) (d) Run between m and M using Eq. (61) (e) Match at M using Eq. (64).

If the fermion mass is not much larger than M, as is the case for the top-quark, one can replace (c), (d) and (e) by a single step, (c') Integrate out the fermion and gauge bosons simultaneously at $\mu \sim m \sim M$, as in Secs. VIII D,G of CGKM2. In this case, the matching is given by Eq. (87) and (91) of CGKM2:

$$\begin{aligned}
&\mathcal{S}_{12}(-2p_1\cdot p_2) \to D(-s) \\
&\mathcal{S}_{34}(-2p_3\cdot p_4) \to D(-s) + 2f_F(z) - h_F(z) \\
&\mathcal{S}_{13}(2p_1\cdot p_3) \to D(-u) + f_F(z) - h_F(z)/2 \\
&\mathcal{S}_{14}(2p_1\cdot p_4) \to D(-t) + f_F(z) - h_F(z)/2 \\
&\mathcal{S}_{23}(2p_2\cdot p_3) \to D(-t) + f_F(z) - h_F(z)/2 \\
&\mathcal{S}_{24}(2p_2\cdot p_4) \to D(-u) + f_F(z) - h_F(z)/2 \\
&z = \frac{m^2}{M^2}
\end{aligned} \tag{65}$$

where the functions f_F and h_F are given in Appendix B of CGKM2. They are the change in the matching condition due to the quark mass. The matching matrix becomes

$$\begin{aligned}
R^{(1)} &= \tilde{R}^{(1)}\mathbb{1} + R_S^{(1)} \\
\tilde{R}^{(1)} &= C_F(2D(-s) + 2f_F(z) - h_F(z)) \\
&= 2C_F\left(-\mathsf{L}_M^2 + 2\mathsf{L}_M\mathsf{L}_s - 3\mathsf{L}_M + \frac{9}{2} - \frac{5\pi^2}{6}\right. \\
&\quad \left. + f_F(z) - h_F(z)/2\right) \\
R_S^{(1)} &= \mathsf{L}_M\begin{bmatrix} C_d\mathsf{L}_{t/u} + C_A\mathsf{L}_{ut/s^2} & 4\mathsf{L}_{t/u} \\ 4C_1\mathsf{L}_{t/u} & 0 \end{bmatrix}
\end{aligned} \tag{66}$$

The f_F and h_F terms cancel in R_S.

D. Squark pair production

As the final example, we consider heavy scalar (squark) pair production via $q(p_1) + \bar{q}(p_2) \to \tilde{t}(p_3) + \tilde{t}^*(p_4)$, where $\tilde{t}$, $\tilde{t}^*$ are the squark and antisquark. The squarks are taken to have mass $m \ll \sqrt{s}$. This example shows how one can use the scalar and scalar/fermion results in CGKM2 to compute squark production. The discussion parallels that for heavy quark production in the previous section. The only difference is that since some of the

particles are scalars, we need to use the $\bar{\psi}\phi$, $\phi^\dagger\psi$ and $\phi^\dagger\phi$ entries from the tables given in CGKM2.

The first step is to match onto SCET at the scale $\mu \sim \sqrt{s}$. The four-particle operators are

$$\begin{aligned}\mathcal{O}_1 &= [\Phi^\dagger_{n_4} W_{n_4}](it^a \mathcal{D}_3 + i\mathcal{D}_4 t^a)_\mu [W^\dagger_{n_3}\Phi_{n_3}] \\ &\quad \times [\bar{\xi}_{n_2} W_{n_2}] t^a \gamma^\mu [W^\dagger_{n_1}\xi_{n_1}] \\ \mathcal{O}_2 &= [\Phi^\dagger_{n_4} W_{n_4}](i\mathcal{D}_3 + i\mathcal{D}_4)_\mu [W^\dagger_{n_3}\Phi_{n_3}] \\ &\quad \times [\bar{\xi}^\dagger_{n_2} W_{n_2}] \gamma^\mu [W^\dagger_{n_1}\xi_{n_1}].\end{aligned} \tag{67}$$

where $i\mathcal{D}_3 = \mathcal{P} + g(\bar{n}_3 \cdot A_{n_3 q})(n_3/2)$, $i\mathcal{D}_4 = \mathcal{P} + g(\bar{n}_4 \cdot A_{n_4 q})(n_4/2)$ are the label covariant derivatives on particles 3 and 4, respectively.

The tree-level coefficients are

$$C_1^{(0)} = 4\pi\alpha/s \qquad C_2^{(0)} = 0 \tag{68}$$

from the graph in Fig. 9.

The anomalous dimension in SCET below the scale Q is given by using Eq. (46), and the values for the graphs in the region between Q and m given in CGKM2. For the anomalous dimension matrix, this means the replacements

$$\begin{aligned}\mathcal{S}_{12}(-2p_1\cdot p_2) &\to \gamma_{1\psi\psi}(-s) \\ \mathcal{S}_{34}(-2p_3\cdot p_4 &\to \gamma_{1\phi\phi}(-s) \\ \mathcal{S}_{13}(2p_1\cdot p_3) &\to \gamma_{1\psi\phi}(-u) \\ \mathcal{S}_{14}(2p_1\cdot p_4) &\to \gamma_{1\psi\phi}(-t) \\ \mathcal{S}_{23}(2p_2\cdot p_3) &\to \gamma_{1\psi\phi}(-t) \\ \mathcal{S}_{24}(2p_2\cdot p_4) &\to \gamma_{1\psi\phi}(-u).\end{aligned} \tag{69}$$

The anomalous dimensions are given in Table I of CGKM2. The subscript $\psi\psi$, $\psi\phi$ and $\phi\phi$ means we use the anomalous dimension for bi-fermion operators, fermion-scalar, and bi-scalar operators, respectively. The anomalous dimension is

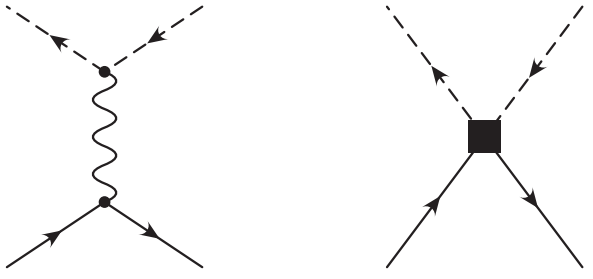

(a) (b)

FIG. 9. Tree level squark production in (a) the full theory and (b) the effective theory.

$$\begin{aligned}\gamma^{(1)} &= \tilde{\gamma}^{(1)}\mathbb{1} + \gamma_S^{(1)} \\ \tilde{\gamma}^{(1)} &= C_F(\gamma_{1\psi\psi}(-s) + \gamma_{1\phi\phi}(-s)) = 2C_F(4\mathsf{L}_s - 7) \\ r_1 &\to 2\gamma_{2\psi\phi}(-t) - 2\gamma_{2\psi\phi}(-u) = 8\log\frac{t}{u} \\ r_2 &\to 2\gamma_{2\psi\phi}(-t) + 2\gamma_{2\psi\phi}(-u) - 2\gamma_{1\psi\psi}(-s) \\ &\quad - 2\gamma_{1\phi\phi}(-s) = 8\log\frac{ut}{s^2} \\ \gamma_S^{(1)} &= \begin{bmatrix} 2C_d\mathsf{L}_{t/u} + 2C_A\mathsf{L}_{ut/s^2} & 8\mathsf{L}_{t/u} \\ 8C_1\mathsf{L}_{t/u} & 0 \end{bmatrix}.\end{aligned} \tag{70}$$

After running the operators down to $\mu \sim m$ using Eq. (70), one matches to an effective theory in which the scalars are replaced by HQET fields. This is given by using Eq. (56), where the scalar values of R_{hh} and R_{hl} are used. This means in Eq. (57), $R + T$ should be replaced by the bi-scalar value on the second rows of Tables III and IV, and for Γ_{ij}, R should be replaced by $R_{\phi_2^\dagger\psi_1}$, the entry on the fourth row of Table III for a bilinear with a heavy scalar and massless fermion:

$$\begin{aligned}\mathcal{R}^{(1)} &= \tilde{\mathcal{R}}^{(1)}\mathbb{1} + \mathcal{R}_S^{(1)} \\ \tilde{\mathcal{R}}^{(1)} &= C_F(R_{\phi\phi} + T_{\phi\phi}) = C_F\left(\mathsf{L}_m^2 - 2\mathsf{L}_m + \frac{\pi^2}{6} + 4\right) \\ r_1 &= 0 \\ r_2 &= 4R_{\phi_2^\dagger\psi_1} - 2R_{\phi\phi} - 2T_{\phi\phi} = 0 \Rightarrow \mathcal{R}_S^{(1)} = 0.\end{aligned} \tag{71}$$

The running in the HQET/SCET theory below m, and the matching at M is identical to Eq. (60) and (63) in the previous section, since it does not matter whether the HQET field is a scalar or a fermion.

In summary, the computation proceeds as follows: (a) Match at $\mu \sim \sqrt{s}$ using Eq. (67) (b) Run between $\sqrt{s}$ and m using Eq. (50) (c) Matching at m using Eq. (71) (d) Run between m and M using Eq. (60) (e) Match at M using Eq. (63).

If the squark mass is not much larger than M, one can replace (c), (d) and (e) by a single step, (c') Integrate out the squark and gauge bosons simultaneously at $\mu \sim m \sim M$, as in Sec. VIII G,D of CGKM2. In this case, the matching is given by

$$\begin{aligned}\mathcal{S}_{12}(-2p_1\cdot p_2) &\to D_{\psi\psi}(-s) \\ \mathcal{S}_{34}(-2p_3\cdot p_4) &\to D_{\phi\phi}(-s) + 2f_S(z) - h_S(z) \\ \mathcal{S}_{13}(2p_1\cdot p_3) &\to D_{\psi\phi}(-u) + f_S(z) - h_S(z)/2 \\ \mathcal{S}_{14}(2p_1\cdot p_4) &\to D_{\psi\phi}(-t) + f_S(z) - h_S(z)/2 \\ \mathcal{S}_{23}(2p_2\cdot p_3) &\to D_{\psi\phi}(-t) + f_S(z) - h_S(z)/2 \\ \mathcal{S}_{24}(2p_2\cdot p_4) &\to D_{\psi\phi}(-u) + f_S(z) - h_S(z)/2 \\ z &= \frac{m^2}{M^2}\end{aligned} \tag{72}$$

where the functions f_S and h_S are given in Appendix B of CGKM2. The matching matrix becomes

$$
\begin{aligned}
R^{(1)} &= \tilde{R}^{(1)}\mathbb{1} + R_S^{(1)} \\
\tilde{R}^{(1)} &= C_F(D_{\psi\psi}(-s) + D_{\phi\phi}(-s) + 2f_S(z) - h_S(z)) \\
&= 2C_F\bigg(-\mathsf{L}_M^2 + 2\mathsf{L}_M\mathsf{L}_s - \frac{3}{2}\mathsf{L}_M + 4 - \frac{5\pi^2}{6} \\
&\quad + f_S(z) - \frac{1}{2}h_S(z)\bigg) \\
r_1 &\to 2D_{\phi\phi}(-t) - 2D_{\phi\phi}(-u) = 4\mathsf{L}_M \log\frac{t}{u} \\
r_2 &\to 2D_{\phi\phi}(-t) + 2D_{\phi\phi}(-u) - 4D_{\phi\phi}(-s) = 4\mathsf{L}_M \log\frac{ut}{s^2} \\
R_S^{(1)} &= \mathsf{L}_M\begin{bmatrix} C_d\mathsf{L}_{t/u} + C_A\mathsf{L}_{ut/s^2} & 4\mathsf{L}_{t/u} \\ 4C_1\mathsf{L}_{t/u} & 0 \end{bmatrix}.
\end{aligned}
\tag{73}
$$

E. Extension to more particles

In the previous examples, we saw that the four-particle S-matrix elements could be obtained by summing the two-particle S-matrix elements over all pairs of particles. This result can be generalized to *gauge singlet* operators with an arbitrary of particles.

The SCET graphs do not depend on the Lorentz structure of the operators, the nontrivial dependence is on the gauge structure of the operators. We write the operators with all incoming fields. An outgoing particle can be represented as an incoming field in the complex conjugate representation. The incoming fields are combined into a net gauge singlet, and we have

$$\left(\sum_\alpha T_\alpha^a\right)\mathcal{O}_i = 0 \tag{74}$$

where T_α^a acts on the indices $\mathcal{O}_i$ associated with field α. To make the notation clear: Assume ψ and χ transform in the fundamental and antifundamental of $SU(N)$, and $\mathcal{O} = \chi^i\psi_i$. The action of T_ψ^a and T_χ^a on $\mathcal{O}$ are:

$$T_\psi^a\mathcal{O} = \chi^i(T^a)_i{}^j\psi_j \qquad T_\chi^a\mathcal{O} = (T^a)^i{}_j\chi^j\psi_i. \tag{75}$$

Here $(T^a)_i{}^j$ and $(T^a)^i{}_j$ are the representation matrices in the fundamental and antifundamental representations, so that

$$(T^a)^i{}_j = -(T^a)_j{}^i \tag{76}$$

from which it follows that

$$(T_\psi^a + T_\chi^a)\mathcal{O} = 0. \tag{77}$$

The sum of graphs with gauge boson exchange between particles α and β, without any gauge factors, will be denoted by $\Gamma_{\alpha\beta}(2p_\alpha\cdot p_\beta)$, as in the preceeding section. The graph is computed with momentum p_α incoming, and p_β outgoing. Treating all particles as incoming for both color and momentum flow means that the graph including color factors is $-\Gamma_{\alpha\beta}(-2p_\alpha\cdot p_\beta)T_\alpha^aT_\beta^a$. The minus sign of the argument takes care of the change in momentum labeling for β, and the overall minus sign is the charge conjugation minus sign from reversing the color flow of β.

The sum of graphs including gauge factors is then

$$\sum_{\langle\alpha\beta\rangle} -\Gamma_{\alpha\beta}(-2p_\alpha\cdot p_\beta)\langle T_\alpha^aT_\beta^a\mathcal{O}_i\rangle^{(0)} \tag{78}$$

where we sum over all pairs $\langle\alpha\beta\rangle$, and $\langle T_\alpha^aT_\beta^a\mathcal{O}_i\rangle^{(0)}$ is the tree-level matrix element of the operator after the action of the gauge operators.

The one-loop contribution to the on-shell matrix element is

$$
\begin{aligned}
\langle\mathcal{O}_j\rangle^{(0)}R_{ji} &= \sum_{\langle\alpha\beta\rangle} -\Gamma_{\alpha\beta}(-2p_\alpha\cdot p_\beta)\langle T_\alpha^aT_\beta^a\mathcal{O}_i\rangle^{(0)} \\
&\quad -\frac{1}{2}\sum_\alpha \delta Z_\alpha^{-1}\langle T_\alpha^aT_\alpha^a\mathcal{O}_i\rangle^{(0)}
\end{aligned}
\tag{79}
$$

including the wave function corrections for each external leg. This can be rewritten as

$$
\begin{aligned}
&\langle\mathcal{O}_j\rangle^{(0)}R_{ji} \\
&= \sum_{\langle\alpha\beta\rangle} -\left[\Gamma_{\alpha\beta}(-2p_\alpha\cdot p_\beta) - \frac{1}{2}\delta Z_\alpha^{-1} - \frac{1}{2}\delta Z_\beta^{-1}\right]\langle T_\alpha^aT_\beta^a\mathcal{O}_i\rangle^{(0)} \\
&\quad -\sum_{\langle\alpha\beta\rangle}\left[\frac{1}{2}\delta Z_\alpha^{-1} + \frac{1}{2}\delta Z_\beta^{-1}\right]\langle T_\alpha^aT_\beta^a\mathcal{O}_i\rangle^{(0)} \\
&\quad -\frac{1}{2}\sum_\alpha \delta Z_\alpha^{-1}\langle T_\alpha^aT_\alpha^a\mathcal{O}_i\rangle^{(0)}.
\end{aligned}
\tag{80}
$$

The first term in square brackets is the on-shell Sudakov form-factor for the two-particle case, including the wave function correction,

$$
\begin{aligned}
&\Gamma_{\alpha\beta}(-2p_\alpha\cdot p_\beta) - \frac{1}{2}\delta Z_\alpha^{-1} - \frac{1}{2}\delta Z_\beta^{-1} \\
&\quad = \mathcal{S}_{\alpha\beta}(-2p_\alpha\cdot p_\beta).
\end{aligned}
\tag{81}
$$

We can simplify the remaining terms using

$$
\begin{aligned}
0 &= \left(\sum_\alpha \delta Z_\alpha^{-1}T_\alpha^a\right)\left(\sum_\beta T_\beta^a\right)\mathcal{O}_i = \sum_{\alpha,\beta}\delta Z_\alpha^{-1}T_\alpha^aT_\beta^a\mathcal{O}_i \\
&= \sum_{\langle\alpha\beta\rangle}[\delta Z_\alpha^{-1} + \delta Z_\beta^{-1}]T_\alpha^aT_\beta^a\mathcal{O}_i + \sum_\alpha \delta Z_\alpha^{-1}T_\alpha^aT_\alpha^a\mathcal{O}_i
\end{aligned}
\tag{82}
$$

which follows from Eq. (74), and reduces Eq. (80) to

$$\langle\mathcal{O}_j\rangle^{(0)}R_{ji} = \sum_{\langle\alpha\beta\rangle} -\mathcal{S}_{\alpha\beta}(-2p_\alpha\cdot p_\beta)\langle T_\alpha^aT_\beta^a\mathcal{O}_i\rangle^{(0)}. \tag{83}$$

The final answer can be written directly in terms of the on-shell two-particle matrix elements, as we found in the previous section for the four-particle case. Equation (83) is valid even without a summation on the gauge index a,

and this will be useful in breaking up the electroweak corrections into the W, Z and γ contributions.

It is conventional to take the multiparticle scattering amplitude and divide it by the Sudakov form factors,

$$A \equiv \sqrt{\prod_\alpha F_\alpha(Q^2)} A_S \tag{84}$$

where A is the scattering amplitude, and $F_r(Q^2)$ is the Sudakov form factor for particle r at some reference momentum, e.g. $Q^2 = -s$. A_S is called the soft amplitude in the literature. With this definition, the soft amplitude has the form at one-loop

$$A_S = \sum_\alpha -\frac{1}{2}\mathcal{S}_{\alpha\alpha}(Q^2)\langle T_\alpha^a T_\alpha^a \mathcal{O}_i\rangle^{(0)} + \sum_{\langle\alpha\beta\rangle} -\mathcal{S}_{\alpha\beta}(-2p_\alpha\cdot p_\beta)\langle T_\alpha^a T_\beta^a \mathcal{O}_i\rangle^{(0)}, \tag{85}$$

since the one-loop Sudakov form factor for particle α is $T_\alpha^a T_\alpha^a \mathcal{S}_{\alpha\alpha}(Q^2)$.

The Sudakov form factor has the form at one-loop (see the next section)

$$\mathcal{S}_{\alpha\beta}(-2p_\alpha\cdot p_\beta) = A\log\frac{-2p_\alpha\cdot p_\beta}{\mu^2} + B_\alpha + B_\beta, \tag{86}$$

where A is a universal coefficient independent of particle type proportional to the cusp anomalous dimension which is known to be universal [50], plus one-particle terms B_α which depend on the particle type, but are independent of $p_\alpha\cdot p_\beta$.

Using Eq. (82) with $\delta Z_\alpha^{-1} \to B_\alpha$, and with $\delta Z_\alpha^{-1} \to 1$ shows that the soft amplitude is given by a sum of the cusp part of the Sudkaov form factors, with coefficients which add up to zero, i.e. it can be written as differences of A-terms. The B terms all cancel. We have seen this explicitly in Eq. (46). Thus the soft amplitude is universal, proportional to the cusp anomalous dimension, and formally has no large log terms since the differences of two A terms gives a logarithm whose argument is order unity in the power counting, e.g. $\log t/u = \log(-t) - \log(-u)$. This also implies that the soft anomalous dimension is proportional to the cusp anomalous dimension. While the above argument is at one-loop, we believe the general structure persists at higher loops. This property has been seen explicitly at two-loops in a very interesting recent computation [34].

VI. FACTORIZATION

There are strong constraints on the form of the scattering amplitude in SCET. We will discuss these in the context of the analytic regulator. The results hold for the S-matrix elements, and so are independent of any specific regulator. We have obtained the same results using a different regulator [35]. We study the case where there is only a single amplitude to avoid problems with matrix ordering. This is the case, for example, for scattering in a $U(1)$ gauge theory. If there are several gauge structures which can contribute, then the amplitude A is a matrix, and one has to worry about matrix ordering. For example in $SU(N)$ gauge theory, there are two gauge invariant four-particle operators, $T^a\otimes T^a$ and $\mathbf{1}\otimes\mathbf{1}$, so A is a 2×2 matrix. We briefly comment on the matrix ordering problem at the end of this section.

The r-particle scattering amplitudes are given by n_i-collinear sectors, $i = 1,\ldots,r$ and the ultrasoft graphs. With the analytic regulator, the on-shell ultrasoft graphs vanish, and we only have to consider the collinear sectors.[7]

The n_i-collinear graphs have the form Fig. 4, where particle i is given by the SCET field, and all the other particles are Wilson lines. The on-shell graph depends on the particle masses $\{m_k\}$, the renormalization scale μ, and the analytic regulator parameters. The particle masses are the masses of any particles given by n_i-collinear SCET fields, such as the gauge boson masses, and the mass of particle i. They can also include the masses of other particles which couple to particle i. For example, in the standard model, a graph with a final n_1-collinear t-quark can depend on m_t and m_b, since n-collinear W bosons couple t to b. The analytic regulator parameters for an n_i-collinear graph are ν_i^2 from the SCET field, and $\nu_i^{(j)}$, $j\neq i$ from the Wilson lines. Boost invariance requires $\nu_i^{(j)}$ to occur in the combination $\nu_i^{(j)}/(\bar n_i\cdot p_i) = \nu_j^2/(2p_i\cdot p_j)$, as noted in Sec. V. The analytic regulator parameters only occur in logarithms, and we use the abbreviations

$$\begin{aligned} &\mathsf{L}_i = \log\nu_i^2, \qquad &&\mathsf{P}_{ij} = \log(2p_i\cdot p_j) \qquad (i\neq j)\\ &\mathsf{P}_{ii}\equiv 0, &&\mathsf{P}_{ij}\equiv\mathsf{P}_{ji}. \end{aligned} \tag{87}$$

The total n_i-collinear amplitude has the form

$$\exp A_i(\{\mathsf{L}_j - \mathsf{P}_{ij}\}, \{m_k\}, \mu, \{\delta_k\}) \tag{88}$$

A_i depends on the momenta of all the particles in the process through its dependence on $2p_i\cdot p_j$ in L_{ij}. The total connected amplitude $\exp A$ is given by the product of the different collinear sectors, so that

$$A(\{p_k\},\{m_k\},\mu) = \sum_{i=1}^r A_i(\{\mathsf{L}_j - \mathsf{P}_{ij}\},\{m_k\},\mu,\{\delta_k\}). \tag{89}$$

The amplitudes A_i and A begin at order α. The tree-level amplitude is the 1 in the expansion of $\exp A$.

The individual terms A_i depend on the regulator parameters $\{\nu_k\}$ and $\{\delta_k\}$ and are singular as $\{\delta_k\}\to 0$, as can be seen explicitly in the one-loop results given in I and CGKM2. However, the sum A is finite as $\{\delta_k\}\to 0$ and independent of the analytic regulator parameters $\{\nu_k\}$. It can only depend on the particle masses (including internal

[7]With other regulators, the ultrasoft graphs can be nonzero.

particles), the external momenta, and μ, as written in Eq. (89).

The cancellation of the L_i dependence is a powerful constraint on the form of the SCET amplitudes. We showed in CGKM2 how it implied that the low-scale matching D when the massive gauge bosons were integrated out had to be at most linear in $\log Q^2$ to all orders in perturbation theory. In Eq. (89), the right-hand side depends on momenta only through the terms P_{ij}, which occur only in the combination $\mathsf{L}_j - \mathsf{P}_{ij}$ in A_i. The L_i cancellation implies that A_i and A can be at most linear in P_{ij}, to all orders in perturbation theory. The proof follows from a straightforward but tedious application of the principle of separation of variables used in partial differential equations—if $f(x) + g(y)$ is a constant, and x and y are independent variables, then $f(x)$ and $g(y)$ must both be constant.

The linearity of A in $\mathcal{P}_{ij}$ implies that the anomalous dimension and low-scale matching conditions D are linear in $\mathcal{P}_{ij}$, since they are determined by the infinite and finite parts of A, respectively. The only multiparticle dependence of A is through the $\mathcal{P}_{ij}$ dependence in the analytic regulator. Since A is linear in $\mathcal{P}_{ij}$, this leads to a two-particle dependence, plus one-particle terms, i.e. A has the form Eq. (86) to all orders. The A term is universal; it cannot depend on the properties of the particles such as masses, because it is generated from Wilson line vertices which are independent of m. The m-dependence must be in one-particle contributions.

If A is a matrix, then the analysis becomes more complicated, but the general features discussed above continue to hold. The SCET anomalous dimension still contains only a single logarithm to all orders in perturbation theory [32,33]. The amplitude Eq. (15) is now a matrix equation, and the anomalous dimension integration is path-ordered in μ. The L_Q terms in the anomalous dimension γ are proportional to the unit matrix $\mathbf{1}$, and can be pulled out as an overall multiplicative factor that commutes with the non-Abelian exponentiation of the integral of the rest of γ.

The high-scale matching need not be a square matrix, and one should replace $\exp C(Q) \to c(Q)$ in Eq. (15). There are no large logs in either $C(Q)$ or $c(Q)$. The low-scale matching D is also not a square matrix. It has the form

$$d_0(\alpha(M)) e^{D_1(\alpha(M)) \log Q^2/M^2} \tag{90}$$

where d_0 is a matrix, and D_1 is a number, i.e. it is proportional to the unit matrix. Thus our result that the low scale matching has the form $\exp D$, where D has a single log to all orders in perturbation theory still holds in the matrix case, in the form Eq. (90).

The structure of the amplitudes discussed in this and the previous section are a very powerful constraint. They follow from renormalization invariance of the effective theory and the universality of the cusp anomalous dimension. More extensive comments will be given elsewhere [35].

VII. APPLICATION TO THE STANDARD MODEL

In this section, we apply the methods developed so far to compute radiative corrections in the standard model. There are several major differences between the toy theory and the standard model. The standard model is a chiral theory and the couplings of the matter fields to the gauge fields are more complicated, with matter fields in several different representations of the gauge group. The gauge group is not simple and, we have to treat several different gauge interactions. After electroweak symmetry breaking, there is electroweak gauge boson mixing between the W_3 and B, which gives W and Z bosons with different masses, and a massless photon. Finally, there are also Higgs exchange corrections proportional to the fermion mass, which are relevant for the top quark. It is straightforward to obtain the results for the standard model, following the same procedure used for the toy model. We have already shown in CGKM2 how to obtain the Sudakov form-factor for the standard model including all these effects. In this section, we use the methods demonstrated in the previous section to calculate the radiative corrections to dijet, dilepton, top quark and squark production in the standard model. These calculation are a nontrival example of the techniques developed in the previous sections and in CGKM2. There are 80 independent amplitudes we need to compute, not including those related by crossing or flavor symmetry.

The left-handed quarks and right-handed quarks are in different representations of the unbroken gauge group of the standard model. The left-handed quark doublets will be denoted by $Q_L^{(i)}$, where $i = u, c, t$ is a flavor index, the right-handed charge $2/3$ quarks by $U_R^{(i)}$, the right-handed charge $-1/3$ quarks by $D_R^{(i)}$, the left-handed lepton doublets by $L_L^{(i)}$ and the right-handed lepton singlets by $E_R^{(i)}$.

Written in terms of $SU(2)$ components, $Q^{(i)}$ is

$$Q^{(i)} = \begin{pmatrix} U_L^{(i)} \\ D_L'^{(i)} \end{pmatrix} = \begin{pmatrix} U_L^{(i)} \\ V_{ij} D_L^{(j)} \end{pmatrix} \tag{91}$$

and $L^{(i)}$ is

$$L^{(i)} = \begin{pmatrix} \nu_L^{(i)} \\ E_L^{(i)} \end{pmatrix} \tag{92}$$

where the neutrinos are weak-eigenstates.

All the lepton and down-type quark masses can be neglected in our calculation, so we can work in the weak eigenstate basis, the CKM matrix V does not enter the SCET computation, and generation number is conserved. The only place where V enters is in the matrix element of SCET operators in the proton state, i.e. in computing the cross-section from the amplitude using the parton distribution functions, since these are given in terms of mass-eigenstate quarks.

A. Matching at Q

For scattering processes, we need to consider four-particle operators in $\mathrm{SCET}_{\mathrm{EW}}$ generated at the scale Q by the graphs in Figs. 1 and 6. The SCET fields corresponding to a standard model field will be given by the replacement $Q^{(i)} \to \xi_r(Q^{(i)})$, etc. We will drop the n, p labels on ξ, and instead use the subscript $r = 1, \ldots, 4$ to denote the particle label in the scattering process. Thus $\xi_1(u)$ described collinear u quarks with momentum p_1, etc.

At the scale Q, the effective Lagrangian is the sum of terms representing the scattering of the various particles. If the initial and final particles are both quark doublets, then the Lagrangian is

$$\begin{aligned}\mathcal{L}_{QQ} = {} & C_{QQ11,fi}[\bar\xi_4(Q^{(f)})W_4 T^A t^b \gamma_\mu W_3^\dagger \xi_3(Q^{(f)})]_L[\bar\xi_2(Q^{(i)})W_2 T^A t^b \gamma^\mu W_1^\dagger \xi_1(Q^{(i)})]_L \\ & + C_{QQ12,fi}[\bar\xi_4(Q^{(f)})W_4 t^a \gamma_\mu W_3^\dagger \xi_3(Q^{(f)})]_L[\bar\xi_2(Q^{(i)})W_2 t^a \gamma^\mu W_1^\dagger \xi_1(Q^{(i)})]_L \\ & + C_{QQ21,fi}[\bar\xi_4(Q^{(f)})W_4 T^A \gamma_\mu W_3^\dagger \xi_3(Q^{(f)})]_L[\bar\xi_2(Q^{(i)})W_2 T^A \gamma^\mu W_1^\dagger \xi_1(Q^{(i)})]_L \\ & + C_{QQ22,fi}[\bar\xi_4(Q^{(f)})W_4 \gamma_\mu W_3^\dagger \xi_3(Q^{(f)})]_L[\bar\xi_2(Q^{(i)})W_2 \gamma^\mu W_1^\dagger \xi_1(Q^{(i)})]_L. \end{aligned} \tag{93}$$

We will write this in the abbreviated form

$$\mathcal{L}_{QQ} = C_{QQ11,fi}[T^A t^a]_L \otimes [T^A t^a]_L + C_{QQ12,fi}[t^a]_L \otimes [t^a]_L + C_{QQ21,fi}[T^A]_L \otimes [T^A]_L + C_{QQ22,fi}[\mathbf{1}]_L \otimes [\mathbf{1}]_L. \tag{94}$$

The flavor quantum numbers are encoded in the subscripts on C. Recall that T^A are the $SU(3)$ generators, and t^a are the $SU(2)$ generators. The subscript 1 is used for $T^A \otimes T^A$ or $t^a \otimes t^a$, and the subscript 2 for $\mathbf{1} \otimes \mathbf{1}$. Similarly, one has the other terms

$$\begin{aligned}
\mathcal{L}_{QU} &= C_{QU1,fi}[T^A]_L \otimes [T^A]_R + C_{QU2,fi}[\mathbf{1}]_L \otimes [\mathbf{1}]_R & \mathcal{L}_{QD} &= C_{QD1,fi}[T^A]_L \otimes [T^A]_R + C_{QD2,fi}[\mathbf{1}]_L \otimes [\mathbf{1}]_R \\
\mathcal{L}_{QL} &= C_{QL1,fi}[t^a]_L \otimes [t^a]_L + C_{QL2,fi}[\mathbf{1}]_L \otimes [\mathbf{1}]_L & \mathcal{L}_{QE} &= C_{QE,fi}[\mathbf{1}]_L \otimes [\mathbf{1}]_R \\
\mathcal{L}_{UQ} &= C_{UQ1,fi}[T^A]_R \otimes [T^A]_L + C_{UQ2,fi}[\mathbf{1}]_R \otimes [\mathbf{1}]_L & \mathcal{L}_{UU} &= C_{UU1,fi}[T^A]_R \otimes [T^A]_R + C_{UU2,fi}[\mathbf{1}]_R \otimes [\mathbf{1}]_R \\
\mathcal{L}_{UD} &= C_{UD1,fi}[T^A]_R \otimes [T^A]_R + C_{UD2,fi}[\mathbf{1}]_R \otimes [\mathbf{1}]_R & \mathcal{L}_{UL} &= C_{UL,fi}[\mathbf{1}]_R \otimes [\mathbf{1}]_L \\
\mathcal{L}_{UE} &= C_{UE,fi}[\mathbf{1}]_R \otimes [\mathbf{1}]_R & \mathcal{L}_{DQ} &= C_{DQ1,fi}[T^A]_R \otimes [T^A]_L + C_{DQ2,fi}[\mathbf{1}]_R \otimes [\mathbf{1}]_L \\
\mathcal{L}_{DU} &= C_{DU1,fi}[T^A]_R \otimes [T^A]_R + C_{DU2,fi}[\mathbf{1}]_R \otimes [\mathbf{1}]_R & \mathcal{L}_{DD} &= C_{DD1,fi}[T^A]_R \otimes [T^A]_R + C_{DD2,fi}[\mathbf{1}]_R \otimes [\mathbf{1}]_R \\
\mathcal{L}_{DL} &= C_{DL,fi}[\mathbf{1}]_R \otimes [\mathbf{1}]_L & \mathcal{L}_{DE} &= C_{DE,fi}[\mathbf{1}]_R \otimes [\mathbf{1}]_R \\
\mathcal{L}_{LQ} &= C_{LQ1,fi}[t^a]_L \otimes [t^a]_L + C_{LQ2,fi}[\mathbf{1}]_L \otimes [\mathbf{1}]_L & \mathcal{L}_{LU} &= C_{LU,fi}[\mathbf{1}]_L \otimes [\mathbf{1}]_R \\
\mathcal{L}_{LD} &= C_{LD,fi}[\mathbf{1}]_L \otimes [\mathbf{1}]_R & \mathcal{L}_{LL} &= C_{LL1,fi}[t^a]_L \otimes [t^a]_L + C_{LL2,fi}[\mathbf{1}]_L \otimes [\mathbf{1}]_L \\
\mathcal{L}_{LE} &= C_{LE,fi}[\mathbf{1}]_L \otimes [\mathbf{1}]_R & \mathcal{L}_{EQ} &= C_{EQ,fi}[\mathbf{1}]_R \otimes [\mathbf{1}]_L \\
\mathcal{L}_{EU} &= C_{EU,fi}[\mathbf{1}]_R \otimes [\mathbf{1}]_R & \mathcal{L}_{ED} &= C_{ED,fi}[\mathbf{1}]_R \otimes [\mathbf{1}]_R \\
\mathcal{L}_{EL} &= C_{EL,fi}[\mathbf{1}]_R \otimes [\mathbf{1}]_R & \mathcal{L}_{EE} &= C_{EE,fi}[\mathbf{1}]_R \otimes [\mathbf{1}]_R.
\end{aligned} \tag{95}$$

The tree-level matching coefficients from the graph in Fig. 1 are ($f \neq i$)

$$\begin{aligned}
&C^{(0)}_{QQ11,fi} = 0, && sC^{(0)}_{QQ12,fi} = 4\pi\alpha_2, && sC^{(0)}_{QQ21,fi} = 4\pi\alpha_3, && sC^{(0)}_{QQ22,fi} = 4\pi\alpha_1 Y_Q^2, \\
&sC^{(0)}_{QU1,fi} = 4\pi\alpha_3, && sC^{(0)}_{QU2,fi} = 4\pi\alpha_1 Y_Q Y_U, && sC^{(0)}_{QL1,fi} = 4\pi\alpha_2, && sC^{(0)}_{QL2,fi} = 4\pi\alpha_1 Y_Q Y_L, \\
&sC^{(0)}_{QE,fi} = 4\pi\alpha_1 Y_Q Y_E, && sC^{(0)}_{UD1,fi} = 4\pi\alpha_3, && sC^{(0)}_{UD2,fi} = 4\pi\alpha_1 Y_U Y_D, && sC^{(0)}_{UL,fi} = 4\pi\alpha_1 Y_U Y_L, \\
&sC^{(0)}_{UE,fi} = 4\pi\alpha_1 Y_U Y_E, && sC_{LL1,fi} = 4\pi\alpha_2, && sC^{(0)}_{LL2,fi} = 4\pi\alpha_1 Y_L^2, && sC^{(0)}_{LE,fi} = 4\pi\alpha_1 Y_L Y_E, \\
&sC^{(0)}_{EE,fi} = 4\pi\alpha_1 Y_E^2,
\end{aligned} \tag{96}$$

and the one loop matching coefficients are

$$
\begin{aligned}
sC^{(1)}_{QQ11,fi} &= -2\alpha_2\alpha_3\tilde{f}(s,t)\\
sC^{(1)}_{QQ12,fi} &= \alpha_2^2\left[X_2(s,t) - \frac{(C_{d_2}+C_{A_2})}{4}\tilde{f}(s,t)\right] + 2[\alpha_1\alpha_2 Y_Q^2 + \alpha_2\alpha_3 C_{F_3}]W - 2\alpha_1\alpha_2 Y_Q^2\tilde{f}(s,t)\\
sC^{(1)}_{QQ21,fi} &= \alpha_3^2\left[X_3(s,t) - \frac{(C_{d_3}+C_{A_3})}{4}\tilde{f}(s,t)\right] + 2[\alpha_1\alpha_3 Y_Q^2 + \alpha_2\alpha_3 C_{F_2}]W - 2\alpha_1\alpha_3 Y_Q^2\tilde{f}(s,t)\\
sC^{(1)}_{QQ22,fi} &= -[\alpha_3^2 C_{1_3} + \alpha_2^2 C_{1_2} + \alpha_1^2 Y_Q^4]\tilde{f}(s,t) + \alpha_1^2 Y_Q^2\Pi_1 + 2[\alpha_1\alpha_3 Y_Q^2 C_{F_3} + \alpha_1\alpha_2 Y_Q^2 C_{F_2} + \alpha_1^2 Y_Q^4]W\\
sC^{(1)}_{QU1,fi} &= \alpha_3^2\left[X_3(s,u) + \frac{(C_{d_3}-C_{A_3})}{4}\tilde{f}(s,u)\right] + [\alpha_1\alpha_3(Y_Q^2+Y_U^2) + \alpha_2\alpha_3 C_{F_2}]W + 2\alpha_1\alpha_3 Y_Q Y_U\tilde{f}(s,u)\\
sC^{(1)}_{QU2,fi} &= [\alpha_3^2 C_{1_3} + \alpha_1^2 Y_Q^2 Y_U^2]\tilde{f}(s,u) + \alpha_1^2 Y_U Y_Q\Pi_1 + [\alpha_1\alpha_2 Y_U Y_Q C_{F_2} + 2\alpha_1\alpha_3 Y_U Y_Q C_{F_3} + \alpha_1^2(Y_Q^3 Y_U + Y_U^3 Y_Q)]W\\
sC^{(1)}_{QL1,fi} &= \alpha_2^2\left[X_2(s,t) - \frac{(C_{d_2}+C_{A_2})}{4}\tilde{f}(s,t)\right] + [\alpha_2\alpha_3 C_{F_3} + \alpha_1\alpha_2(Y_Q^2+Y_L^2)]W - 2\alpha_1\alpha_2 Y_L Y_Q\tilde{f}(s,t)\\
sC^{(1)}_{QL2,fi} &= -[\alpha_2^2 C_{1_2} + \alpha_1^2 Y_L^2 Y_Q^2]\tilde{f}(s,t) + \alpha_1^2 Y_L Y_Q\Pi_1 + [\alpha_1\alpha_3 Y_L Y_Q C_{F_3} + 2\alpha_1\alpha_2 Y_L Y_Q C_{F_2} + \alpha_1^2(Y_L^3 Y_Q + Y_Q^3 Y_L)]W\\
sC^{(1)}_{QE,fi} &= \alpha_1^2 Y_E^2 Y_Q^2\tilde{f}(s,u) + \alpha_1^2 Y_E Y_Q\Pi_1 + [\alpha_1\alpha_3 Y_E Y_Q C_{F_3} + \alpha_1\alpha_2 Y_E Y_Q C_{F_2} + \alpha_1^2(Y_E^3 Y_Q + Y_Q^3 Y_E)]W\\
sC^{(1)}_{UD1,fi} &= \alpha_3^2\left[X_3(s,t) - \frac{(C_{d_3}+C_{A_3})}{4}\tilde{f}(s,t)\right] - 2\alpha_1\alpha_3 Y_D Y_U\tilde{f}(s,t) + \alpha_1\alpha_3(Y_D^2+Y_U^2)W\\
sC^{(1)}_{UD2,fi} &= -[\alpha_3^2 C_{1_3} + \alpha_1^2 Y_U^2 Y_D^2]\tilde{f}(s,t) + \alpha_1^2 Y_U Y_D\Pi_1 + [2\alpha_1\alpha_3 Y_U Y_D C_{F_3} + \alpha_1^2(Y_D^3 Y_U + Y_U^3 Y_D)]W\\
sC^{(1)}_{UL,fi} &= \alpha_1^2 Y_L^2 Y_U^2\tilde{f}(s,u) + \alpha_1^2 Y_L Y_U\Pi_1 + [\alpha_1\alpha_3 Y_L Y_U C_{F_3} + \alpha_1\alpha_2 Y_L Y_U C_{F_2} + \alpha_1^2(Y_L^3 Y_U + Y_U^3 Y_L)]W\\
sC^{(1)}_{UE,fi} &= -\alpha_1^2 Y_E^2 Y_U^2\tilde{f}(s,t) + \alpha_1^2 Y_E Y_U\Pi_1 + [\alpha_1\alpha_3 Y_E Y_U C_{F_3} + \alpha_1^2(Y_E^3 Y_U + Y_U^3 Y_E)]W\\
sC_{LL1} &= \alpha_2^2[X_2(s,t) - \frac{(C_{d_2}+C_{A_2})}{4}\tilde{f}(s,t)] + 2\alpha_1\alpha_2 Y_L^2 W - 2\alpha_1\alpha_2 Y_L^2\tilde{f}(s,t)\\
sC^{(1)}_{LL2} &= -[\alpha_2^2 C_{1_2} + \alpha_1^2 Y_L^4]\tilde{f}(s,t) + \alpha_1^2 Y_L^2\Pi_1 + 2[\alpha_1\alpha_2 Y_L^2 C_{F_2} + \alpha_1^2 Y_L^4]W\\
sC^{(1)}_{LE,fi} &= \alpha_1^2 Y_E^2 Y_L^2\tilde{f}(s,u) + \alpha_1^2 Y_E Y_L\Pi_1 + [\alpha_1\alpha_2 Y_L Y_E C_{F_2} + \alpha_1^2(Y_L^3 Y_E + Y_E^3 Y_L)]W\\
sC^{(1)}_{EE,fi} &= -\alpha_1^2 Y_E^4\tilde{f}(s,t) + \alpha_1^2 Y_E^2\Pi_1 + 2\alpha_1^2 Y_E^4 W
\end{aligned}
\tag{97}
$$

where

$$
\begin{aligned}
X_N(s,t) &= 2C_{F_N}W + C_{A_N}\left(2\mathsf{L}_s^2 - 2\mathsf{L}_{-s-t}\mathsf{L}_s - \frac{11}{3}\mathsf{L}_s + \pi^2 + \frac{85}{9}\right) + \left(\frac{2}{3}\mathsf{L}_s - \frac{10}{9}\right)T_{F_N}n_{F_N} + \left(\frac{1}{3}\mathsf{L}_s - \frac{8}{9}\right)T_{F_N}n_{S_N}\\
W &= -\mathsf{L}_s^2 + 3\mathsf{L}_s + \frac{\pi^2}{6} - 8, \qquad \Pi_1 = \frac{41}{6}\mathsf{L}_s - \frac{104}{9}, \qquad \tilde{f}(s,t) = -\frac{2s}{s+t}\mathsf{L}_{t/s} + \frac{s(s+2t)}{(s+t)^2}(\mathsf{L}_{t/s}^2 + \pi^2) + 4\mathsf{L}_s\mathsf{L}_{t/(-s-t)},
\end{aligned}
\tag{98}
$$

for $N = 2,3$ for $SU(2)$ and $SU(3)$, respectively. $n_{F_N}(n_{S_N})$ denotes the number of Weyl fermions and complex scalars in the fundamental representation of $SU(N)$. The matching is symmetric between initial and final fermions, so that $C_{UQ,1} = C_{QU,1}$, etc. The coefficients $C_{QD,j}$ are given by $C_{QU,j}$ with $Y_U \to Y_D$, $C_{UU,j}$ by $C_{UD,j}$ with $Y_D \to Y_U$, $C_{DD,j}$ by $C_{UD,j}$ with $Y_U \to Y_D$, $C_{DL,j}$ by $C_{UL,j}$ with $Y_U \to Y_D$, and $C_{DE,j}$ by $C_{UE,j}$ with $Y_U \to Y_D$, and so have not been listed above. For identical particles (i.e. $C_{QQ,f=i}$, $C_{LL,f=i}$, etc.) there is also the crossed-channel contribution as discussed in Appendix A.

The above matching coefficients do not include Higgs exchange contributions. The Yukawa couplings are proportional to the fermion masses, and the only Yukawa coupling large enough to be relevant is the top quark Yukawa coupling. Higgs corrections only arise at one-loop for LHC processes, since the initial state is pp, and contains no t-quarks.[8] The Higgs contributions to the matching for operators containing $Q^{(t)}$ in the final state are

[8] One can always treat the proton as a hadron in QCD with all heavy flavors integrated out. Heavy quark distribution functions in the proton are calculable in terms of light-quark distribution functions; see e.g. Ref. [51].

$$
\begin{aligned}
\delta C_{QQ12,ti} &= \frac{g_t^2\alpha_2}{4\pi s}\left[\frac{3}{2}-\frac{1}{2}\mathsf{L}_s\right]\\
\delta C_{QQ21,ti} &= \frac{g_t^2\alpha_3}{4\pi s}\left[\frac{1}{2}-\frac{1}{2}\mathsf{L}_s\right]\\
\delta C_{QQ22,ti} &= \frac{g_t^2\alpha_1}{4\pi s}Y_{Q_u}\left[-\frac{5}{12}-\frac{1}{12}\mathsf{L}_s\right]\\
\delta C_{QU1,ti} &= \frac{g_t^2\alpha_3}{4\pi s}\left[\frac{1}{2}-\frac{1}{2}\mathsf{L}_s\right]\\
\delta C_{QU2,ti} &= \frac{g_t^2\alpha_1}{4\pi s}Y_U\left[-\frac{5}{12}-\frac{1}{12}\mathsf{L}_s\right]\\
\delta C_{QD1,ti} &= \frac{g_t^2\alpha_3}{4\pi s}\left[\frac{1}{2}-\frac{1}{2}\mathsf{L}_s\right]\\
\delta C_{QD2,ti} &= \frac{g_t^2\alpha_1}{4\pi s}Y_D\left[-\frac{5}{12}-\frac{1}{12}\mathsf{L}_s\right]\\
\delta C_{QL1,ti} &= \frac{g_t^2\alpha_2}{4\pi s}\left[\frac{3}{2}-\frac{1}{2}\mathsf{L}_s\right]\\
\delta C_{QL2,ti} &= \frac{g_t^2\alpha_1}{4\pi s}Y_L\left[-\frac{5}{12}-\frac{1}{12}\mathsf{L}_s\right]\\
\delta C_{QE,ti} &= \frac{g_t^2\alpha_1}{4\pi s}Y_E\left[-\frac{5}{12}-\frac{1}{12}\mathsf{L}_s\right],
\end{aligned}
\tag{99}
$$

whereas the contribution matching for operators containing $U^{(t)}$ in the final state are

$$
\begin{aligned}
\delta C_{UQ1,ti} &= \frac{g_t^2\alpha_3}{4\pi s}[1-\mathsf{L}_s]\\
\delta C_{UQ2,ti} &= \frac{g_t^2\alpha_1}{4\pi s}Y_Q\left[\frac{4}{3}-\frac{1}{3}\mathsf{L}_s\right]\\
\delta C_{UU1,ti} &= \frac{g_t^2\alpha_3}{4\pi s}\left[1-\mathsf{L}_s\right]\\
\delta C_{UU2,ti} &= \frac{g_t^2\alpha_1}{4\pi s}Y_U\left[-\frac{4}{3}-\frac{1}{3}\mathsf{L}_s\right]\\
\delta C_{UD1,ti} &= \frac{g_t^2\alpha_3}{4\pi s}[1-\mathsf{L}_s]\\
\delta C_{UD2,ti} &= \frac{g_t^2\alpha_1}{4\pi s}Y_D\left[\frac{4}{3}-\frac{1}{3}\mathsf{L}_s\right]\\
\delta C_{UL,ti} &= \frac{g_t^2\alpha_1}{4\pi s}Y_L\left[\frac{4}{3}-\frac{1}{3}\mathsf{L}_s\right]\\
\delta C_{UE,ti} &= \frac{g_t^2\alpha_1}{4\pi s}Y_E\left[\frac{4}{3}-\frac{1}{3}\mathsf{L}_s\right],
\end{aligned}
\tag{100}
$$

with $i = u, c$ for Q or U, and $i = d, s, b$ for D. The logarithmic terms for $\delta C_{QE,ti}$ and $\delta C_{UE,ti}$ agree with Ref. [52].

Once we match onto SCET, Higgs vertex corrections are power suppressed, as shown in Ref. [2], and the only Higgs contributions in SCET are wave function renormalization corrections.

B. Anomalous dimension below Q

The anomalous dimensions in SCET between Q and m are obtained using the results of Sec. V A. The anomalous dimension due to gluon exchange depends on the color quantum numbers of the initial and final fermions. If both are color triplets, then the operators have the color structure $C_1 T^A \otimes T^A + C_2 \mathbf{1}\otimes\mathbf{1}$. The anomalous dimension is given by Eq. (50) with group invariants replaced by their values for $N = 3$, and with the $\alpha/(4\pi)$ prefactor for QCD,

$$
\begin{aligned}
\gamma_{SU(3)} &= \tilde{\gamma}_{SU(3)}\mathbb{1} + \gamma_{S,SU(3)},\\
\tilde{\gamma}_{SU(3)} &= \frac{8}{3}\frac{\alpha_3}{4\pi}(4\mathsf{L}_s - 6),\\
\gamma_{S,SU(3)} &= \frac{\alpha_3}{4\pi}\begin{bmatrix} \frac{10}{3}\mathsf{L}_{t/u} + 6\mathsf{L}_{ut/s^2} & 8\mathsf{L}_{t/u}\\ \frac{16}{9}\mathsf{L}_{t/u} & 0\end{bmatrix}.
\end{aligned}
\tag{101}
$$

This 2×2 anomalous dimension matrix acts on operators with color structure $T^A\otimes T^A$ and $\mathbf{1}\otimes\mathbf{1}$, and does not mix different flavors, chiralities or $SU(2)$ quantum numbers. Thus the renormalization group equation has the form

$$
\mu\frac{\mathrm{d}}{\mathrm{d}\mu}\begin{bmatrix} C_1\\ C_2\end{bmatrix} = \gamma\begin{bmatrix} C_1\\ C_2\end{bmatrix}
\tag{102}
$$

where (C_1, C_2) are the pairs $(C_{QQ11,fi}, C_{QQ12,fi})$, $(C_{QQ21,fi}, C_{QQ22,fi})$, $(C_{QU1,fi}, C_{QU2,fi})$, $(C_{QD1,fi}, C_{QD2,fi})$, $(C_{UQ1,fi}, C_{UQ2,fi})$, $(C_{UU1,fi}, C_{UU2,fi})$, $(C_{UD1,fi}, C_{UD2,fi})$, $(C_{DQ1,fi}, C_{DQ2,fi})$, $(C_{DU1,fi}, C_{DU2,fi})$, and $(C_{DD1,fi}, C_{DD2,fi})$.

If one of the fermions is a color triplet and the other is a color singlet, the operator has the color structure $C\mathbf{1}\otimes\mathbf{1}$. The QCD anomalous dimension for C is identical to the Sudakov form-factor case,

$$
\gamma_{SU(3)} = \frac{4}{3}\frac{\alpha_3}{4\pi}(4\mathsf{L}_s - 6).
\tag{103}
$$

If both fermions are color singlets, then

$$
\gamma_{SU(3)} = 0.
\tag{104}
$$

The anomalous dimension due to $SU(2)$ gauge boson exchange is obtained similarly. If both fermions are doublets, the operator has the form $C_1 t^A\otimes t^A + C_2\mathbf{1}\otimes\mathbf{1}$, and the anomalous dimension matrix is

$$
\begin{aligned}
\gamma_{SU(2)} &= \tilde{\gamma}_{SU(2)}\mathbb{1} + \gamma_{S,SU(2)},\\
\tilde{\gamma}_{SU(2)} &= \frac{3}{2}\frac{\alpha_2}{4\pi}(4_s - 6),\\
\gamma_{S,SU(2)} &= \frac{\alpha_2}{4\pi}\begin{bmatrix} 4\mathsf{L}_{ut/s^2} & 8\mathsf{L}_{t/u}\\ \frac{3}{2}\mathsf{L}_{t/u} & 0\end{bmatrix},
\end{aligned}
\tag{105}
$$

where the (C_1, C_2) pairs are $(C_{QQ11,fi}, C_{QQ21,fi})$, $(C_{QQ12,fi}, C_{QQ22,fi})$, $(C_{QL1,fi}, C_{QL2,fi})$, $(C_{LQ1,fi}, C_{LQ2,fi})$, and $(C_{LL1,fi}, C_{LL2,fi})$.

If one of the fermions is a weak doublet and the other is a weak singlet, the operator has the structure $C\mathbf{1}\otimes\mathbf{1}$, and the $SU(2)$ anomalous dimension for C is identical to the Sudakov form-factor case,

$$\gamma_{SU(2)} = \frac{3}{4}\frac{\alpha_2}{4\pi}(4\mathsf{L}_s - 6). \tag{106}$$

If both fermions are weak singlets, then

$$\gamma_{SU(2)} = 0. \tag{107}$$

B exchange gives the diagonal contribution

$$\gamma_{U(1)} = \frac{\alpha_1}{4\pi}[(Y_i^2 + Y_f^2)(4\mathsf{L}_s - 6) + 8Y_iY_f\mathsf{L}_{t/u}] \tag{108}$$

where Y_i and Y_f are the hypercharges of the initial and final representations. Note that $Y(U_R) = 2/3$, $Y(D_R) = -1/3$ and $Y(E_R) = -1$.

The Higgs wave function graphs give the diagonal contribution

$$\gamma_H(Q^{(t)}) = \frac{g_t^2}{16\pi^2}\frac{1}{2}. \tag{109}$$

to an operator for each $Q^{(t)}$ field, and

$$\gamma_H(t_R) = \frac{g_t^2}{16\pi^2} \tag{110}$$

for each $t_R = U_R^{(t)}$ field. This term breaks the flavor symmetry in the anomalous dimension. The total anomalous dimension is the sum,

$$\gamma = \gamma_H + \gamma_{U(1)} + \gamma_{SU(2)} + \gamma_{SU(3)}, \tag{111}$$

and is used to run the operators from $\mu = s$ to $\mu \sim M_Z$.

C. Matching at the low scale to SCET$_\gamma$

At a low scale μ of order M_Z (or m_t) one matches from SCET$_{\rm EW}$ with dynamical gluons and electroweak bosons onto SCET$_\gamma$ with dynamical gluons and photons, by integrating out the W and Z bosons. The electroweak symmetry is broken in SCET$_\gamma$ so the operators in Eq. (95) must now be decomposed into separate $SU(2)$ component fields.

We start by considering the case where all particles have mass much smaller than m_t, i.e. for all particles except the t-quark. This includes all the operators in Eq. (95) except those that contain $Q_L^{(t)}$ and $U_R^{(t)}$. The photon and gluon graphs are the same in SCET$_{\rm EW}$ and SCET$_\gamma$ and do not contribute to the matching condition. The W contribution depends on whether the particles involved are $SU(2)$ doublets or singlets. For the case of two doublets, consider the operators

$$C_{QQ12,fi}[t^a]_L\otimes[t^a]_L + C_{QQ22,fi}[\mathbf{1}]_L\otimes[\mathbf{1}]_L \tag{112}$$

with $i \neq t$, $f \neq t$, which are two of the terms in Eq. (94). For definiteness, let $f = c$ and $i = u$. These operators match onto a linear combination of

$$\begin{aligned}
\hat{\mathcal{O}}_{12} &= [\bar{c}_{L4}\gamma_\mu c_{L3}][\bar{u}_{L2}\gamma^\mu u_{L1}]\\
\hat{\mathcal{O}}_{22} &= [\bar{c}_{L4}\gamma_\mu c_{L3}][\bar{d}'_{L2}\gamma^\mu d'_{L1}]\\
\hat{\mathcal{O}}_{32} &= [\bar{s}'_{L4}\gamma_\mu s'_{L3}][\bar{u}_{L2}\gamma^\mu u_{L1}]\\
\hat{\mathcal{O}}_{42} &= [\bar{s}'_{L4}\gamma_\mu s'_{L3}][\bar{d}'_{L2}\gamma^\mu d'_{L1}]\\
\hat{\mathcal{O}}_{52} &= [\bar{s}'_{L4}\gamma_\mu c_{L3}][\bar{u}_{L2}\gamma^\mu d'_{L1}]\\
\hat{\mathcal{O}}_{62} &= [\bar{c}_{L4}\gamma_\mu s'_{L3}][\bar{d}'_{L2}\gamma^\mu u_{L1}]
\end{aligned} \tag{113}$$

where the flavor label represents the SCET$_\gamma$ fields $W^\dagger\xi$.

The matching from Eq. (112) in SCET$_{\rm EW}$ onto Eq. (113) in SCET$_\gamma$ is computed as in Sec. V B. As shown in Sec. V E, the matching can be written as the sum of the Sudakov form-factor S-matrix elements, even though we are considering $W^\pm$ exchange, Z exchange and γ exchange separately, and not summing over all the $SU(2)$ gauge bosons. The matching matrix is

$$\begin{bmatrix}\hat{C}_{12}\\ \hat{C}_{22}\\ \hat{C}_{32}\\ \hat{C}_{42}\\ \hat{C}_{52}\\ \hat{C}_{62}\end{bmatrix} = R\begin{bmatrix}\hat{C}_{QQ12,cu}\\ \hat{C}_{QQ22,cu}\end{bmatrix} \tag{114}$$

where $\hat{C}_{i2}$ are the coefficients of $\hat{\mathcal{O}}_{i2}$. At tree-level R is

$$R^{(0)} = \begin{bmatrix}\frac{1}{4} & 1\\ -\frac{1}{4} & 1\\ -\frac{1}{4} & 1\\ \frac{1}{4} & 1\\ \frac{1}{2} & 0\\ \frac{1}{2} & 0\end{bmatrix}. \tag{115}$$

At one-loop

$$\begin{aligned}
R_W^{(1)} = \frac{\alpha_{\rm em}}{4\pi\sin^2\theta_W}\frac{1}{2}\Bigg\{&2F_g(-s, M_W^2, \mu^2)R^{(0)}\\
&+ 2\log\frac{M_W^2}{\mu^2}\begin{bmatrix}\log\frac{t}{s} & 0\\ -\log\frac{u}{s} & 0\\ -\log\frac{u}{s} & 0\\ \log\frac{t}{s} & 0\\ \frac{1}{2}\log\frac{ut}{s^2} & 2\log\frac{t}{u}\\ \frac{1}{2}\log\frac{ut}{s^2} & 2\log\frac{t}{u}\end{bmatrix}\Bigg\}
\end{aligned} \tag{116}$$

where

$$F_g(Q^2, M^2, \mu^2) = -\log^2\frac{M^2}{\mu^2} + 2\log\frac{M^2}{\mu^2}\log\frac{Q^2}{\mu^2} - 3\log\frac{M^2}{\mu^2} + \frac{9}{2} - \frac{5\pi^2}{6}. \tag{117}$$

The Z exchange contribution is

$$R_Z^{(1)} = \frac{\alpha_{\rm em}}{4\pi\sin^2\theta_W\cos^2\theta_W}\begin{bmatrix} \frac{1}{4}r_1 & r_1 \\ -\frac{1}{4}r_2 & r_2 \\ -\frac{1}{4}r_3 & r_3 \\ \frac{1}{4}r_4 & r_4 \\ \frac{1}{2}r_5 & 0 \\ \frac{1}{2}r_5 & 0 \end{bmatrix} \tag{118}$$

$$\begin{aligned}
r_1 &= (g_{Lc}^2 + g_{Lu}^2)F_g(-s, M_Z^2, \mu^2) + 4g_{Lc}g_{Lu}\log\frac{M_Z^2}{\mu^2}\log\frac{t}{u} \\
r_2 &= (g_{Lc}^2 + g_{Ld}^2)F_g(-s, M_Z^2, \mu^2) + 4g_{Lc}g_{Ld}\log\frac{M_Z^2}{\mu^2}\log\frac{t}{u} \\
r_3 &= (g_{Lu}^2 + g_{Ls}^2)F_g(-s, M_Z^2, \mu^2) + 4g_{Lu}g_{Ls}\log\frac{M_Z^2}{\mu^2}\log\frac{t}{u} \\
r_4 &= (g_{Ld}^2 + g_{Ls}^2)F_g(-s, M_Z^2, \mu^2) + 4g_{Ld}g_{Ls}\log\frac{M_Z^2}{\mu^2}\log\frac{t}{u} \\
r_5 &= \frac{1}{2}(g_{Lc}^2 + g_{Ls}^2 + g_{Lu}^2 + g_{Ld}^2)F_g(-s, M_Z^2, \mu^2) \\
&\quad + 2(g_{Lu}g_{Lc} + g_{Ld}g_{Ls})\log\frac{M_Z^2}{\mu^2}\log\frac{t}{s} \\
&\quad - 2(g_{Lu}g_{Ls} + g_{Ld}g_{Lc})\log\frac{M_Z^2}{\mu^2}\log\frac{u}{s}
\end{aligned} \tag{119}$$

where

$$\begin{aligned}
g_{Lc} &= g_{Lu} = \frac{1}{2} - \frac{2}{3}\sin^2\theta_W \\
g_{Ls} &= g_{Ld} = -\frac{1}{2} + \frac{1}{3}\sin^2\theta_W
\end{aligned} \tag{120}$$

are the couplings to the Z. The total one-loop matching is $R_W^{(1)} + R_Z^{(1)}$.

The remaining two operators in $\mathcal{L}_{QQ}$,

$$\mathcal{L}_{QQ} = C_{QQ11,fi}[T^A t^a]_L \otimes [T^A t^a]_L + C_{QQ21,fi}[T^A]_L \otimes [T^A]_L \tag{121}$$

match onto

$$\begin{aligned}
\hat{\mathcal{O}}_{11} &= [\bar{c}_{L4}T^A\gamma_\mu c_{L3}][\bar{u}_{L2}T^A\gamma^\mu u_{L1}] \\
\hat{\mathcal{O}}_{21} &= [\bar{c}_{L4}T^A\gamma_\mu c_{L3}][\bar{d}'_{L2}T^A\gamma^\mu d'_{L1}] \\
\hat{\mathcal{O}}_{31} &= [\bar{s}'_{L4}T^A\gamma_\mu s'_{L3}][\bar{u}_{L2}T^A\gamma^\mu u_{L1}] \\
\hat{\mathcal{O}}_{41} &= [\bar{s}'_{L4}T^A\gamma_\mu s'_{L3}][\bar{d}'_{L2}T^A\gamma^\mu d'_{L1}] \\
\hat{\mathcal{O}}_{51} &= [\bar{s}'_{L4}T^A\gamma_\mu c_{L3}][\bar{u}_{L2}T^A\gamma^\mu d'_{L1}] \\
\hat{\mathcal{O}}_{61} &= [\bar{c}_{L4}T^A\gamma_\mu s'_{L3}][\bar{d}'_{L2}T^A\gamma^\mu u_{L1}].
\end{aligned} \tag{122}$$

Since W exchange leaves the color indices unaffected, the matching matrix is identical to Eq. (115), (116), and (118), and the matching relation is given by Eq. (114) with the replacement $\hat{C}_{i2} \to \hat{C}_{i1}$, $\hat{C}_{QQi2,cu} \to \hat{C}_{QQi1,cu}$. The results Eq. (115) and (116) hold for all cases where both fermions are doublets. If the final quark doublet is replaced by a lepton doublet, the coupling constants in Eq. (119) have the obvious replacement $g_{Lc} \to g_{L\nu}$, $g_{Ls} \to g_{Le}$ with

$$g_{L\nu} = \frac{1}{2}, \qquad g_{Le} = -\frac{1}{2} + \sin^2\theta_W \tag{123}$$

and similarly if the initial doublet is a lepton doublet, or both doublets are lepton doublets.

The second case is where one fermion is a doublet and the other is a singlet. As an example, consider $C_{QU2,fi}[\mathbf{1}]_L \otimes [\mathbf{1}]_R$ with $f = c$ and $i = u$. This matches onto a linear combination of

$$\begin{aligned}
\hat{\mathcal{O}}_{12} &= [\bar{c}_{L4}\gamma_\mu c_{L3}][\bar{u}_{R2}\gamma^\mu u_{R1}] \\
\hat{\mathcal{O}}_{22} &= [\bar{s}'_{L4}\gamma_\mu s'_{L3}][\bar{u}_{R2}\gamma^\mu u_{R1}].
\end{aligned} \tag{124}$$

The matching matrix is

$$\begin{bmatrix} \hat{C}_{12} \\ \hat{C}_{22} \end{bmatrix} = R\hat{C}_{QU2,cu} \tag{125}$$

where $\hat{C}_{i2}$ are the coefficients of $\hat{\mathcal{O}}_{i2}$. At tree-level R is

$$R^{(0)} = \begin{bmatrix} 1 \\ 1 \end{bmatrix}. \tag{126}$$

At one-loop

$$\begin{aligned}
R_W^{(1)} &= \frac{\alpha_{\rm em}}{4\pi\sin^2\theta_W}\frac{1}{2}F_g(-s, M_W^2, \mu^2)R^{(0)} \\
R_Z^{(1)} &= \frac{\alpha_{\rm em}}{4\pi\sin^2\theta_W\cos^2\theta_W}\left\{F_g(-s, M_Z^2, \mu^2)\begin{bmatrix} g_{Lc}^2 + g_{Ru}^2 \\ g_{Ls}^2 + g_{Ru}^2 \end{bmatrix}\right. \\
&\quad \left. + 4\log\frac{M_Z^2}{\mu^2}\log\frac{t}{u}\begin{bmatrix} g_{Lc}g_{Ru} \\ g_{Ls}g_{Ru} \end{bmatrix}\right\}
\end{aligned} \tag{127}$$

where F_g is given in Eq. (117). The singlet fermion Z couplings are

$$\begin{aligned}
g_{Ru} &= -\frac{2}{3}\sin^2\theta_W, \qquad g_{Rd} = \frac{1}{3}\sin^2\theta_W, \\
g_{Re} &= \sin^2\theta_W.
\end{aligned} \tag{128}$$

Equations. (125)–(127) apply to all cases where one fermion is weak doublet, and the other is a weak singlet, with the obvious replacement of the Z charges for lepton doublets. Since electroweak exchange does not affect the color indices, the same matching matrix applies, for example, to the transition from $C_{QU1,fi}[T^A]_L \otimes [T^A]_R$ to

$$\begin{aligned}\hat{\mathcal{O}}_{11} &= [\bar{c}_{L4} T^A \gamma_\mu c_{L3}][\bar{u}_{R2} T^A \gamma^\mu u_{R1}] \\ \hat{\mathcal{O}}_{21} &= [\bar{s}'_{L4} T^A \gamma_\mu s'_{L3}][\bar{u}_{R2} T^A \gamma^\mu u_{R1}].\end{aligned} \tag{129}$$

The last case is if both fermions are weak singlets—take $C_{UU2,fi}[\mathbf{1}]_R \otimes [\mathbf{1}]_R$ as an example with $f = c$ and $i = u$. The operator matches to

$$\hat{\mathcal{O}} = [\bar{c}_{R4} \gamma_\mu c_{R3}][\bar{u}_{R2} \gamma^\mu u_{R1}]. \tag{130}$$

The one-loop matching condition is $\hat{C} = (1 + R_W^{(1)} + R_Z^{(1)}) C_{UU2,cu}$ with

$$\begin{aligned}R_W^{(1)} &= 0 \\ R_Z^{(1)} &= \frac{\alpha_{\rm em}}{4\pi \sin^2\theta_W \cos^2\theta_W}\Big\{(g_{Rc}^2 + g_{Ru}^2) F_g(-s, M_Z^2, \mu^2) \\ &\quad + 4 g_{Rc} g_{Ru} \log\frac{M_Z^2}{\mu^2} \log\frac{t}{u}\Big\}.\end{aligned} \tag{131}$$

Again, the same matching coefficient holds for the matching between $C_{UU1,fi}[T^A]_R \otimes [T^A]_R$ and $[\bar{c}_{R4} T^A \gamma_\mu c_{R3}][\bar{u}_{R2} T^A \gamma^\mu u_{R1}]$, and the equations hold with an obvious substitution of Z charges if the quarks are replaced by leptons.

Anomalous dimensions in SCET$_\gamma$

Finally, one computes the anomalous dimension of the operator in SCET$_\gamma$ between $\mu \sim M_Z$ and some low scale μ_0, at which point one takes operator matrix elements to compute the desired observables. The matrix elements of the initial state SCET fields in the proton are the usual parton distribution functions, and the final state fields are used to construct jet observables. The scale μ_0 is chosen to minimize logarithms in the matrix element computation. For LHC jet observables, it is of order the typical invariant mass of a single jet.

The QCD anomalous dimensions given in Eq. (101), (103), and (113) continue to hold for the case of two quarks, one quark and one lepton, or two leptons, respectively. The QED anomalous dimension is

$$\begin{aligned}\gamma_{\rm em} = \frac{\alpha_{\rm em}}{4\pi}\Big[&\frac{1}{2}(q_1^2 + q_2^2 + q_3^2 + q_4^2)\Big(4\log\frac{-s}{\mu^2} - 6\Big) \\ &+ 4(q_1 q_4 + q_2 q_3)\log\frac{t}{s} - 4(q_1 q_3 + q_2 q_4)\log\frac{u}{s}\Big]\end{aligned} \tag{132}$$

where q_{1-4} are the charges of the four fields, and $q_1 + q_3 = q_2 + q_4$. The initial particle charges are q_1 and $-q_2$, and the final particle charges are $-q_3$ and q_4.

D. t-quark production

In processes involving the t-quark, $m_t^2/M_{W,Z}^2$ terms must be included in the loop graphs, as discussed in CGKM2. At a scale μ, we transition to an effective theory in which the t-quark is represented by an HQET field, whereas the light quarks are still represented by SCET fields. Since m_t is not much larger than M_W and M_Z, it is convenient to make this transition at the same time that the W, Z and Higgs bosons are integrated out of the theory in the transition from SCET$_{\rm EW}$ to SCET$_\gamma$. This method was used in CGKM2 for the Sudakov form-factor of the t-quark, and allows one to include the complete $m_t^2/M_{W,Z}^2$ dependence in the matching computation. Here we apply the same procedure to the operators relevant for t-quark production—the operators in Eqs. (94) and (95) which contain either $Q_L^{(t)}$ or t_R fields. The initial state in proton-proton collisions contains only light quarks, so we will only look at operators with top-quarks in the final state and light quarks in the initial state.

The matching at Q and the anomalous dimension below Q are mass independent, and identical to those for light quarks. The m_t dependent terms give an additive correction to the low-scale matching matrices $R_{W,Z}^{(1)}$ of the previous section. There are also contributions $R_{\gamma,g}^{(1)}$ to low-scale matching from the photon and gluon, because of the transition to an HQET field for the t-quark. The graphs in SCET$_{\rm EW}$ use a SCET field for the t-quark, and those in SCET$_\gamma$ use a HQET field for the t-quark, so there is a matching correction even for massless gauge bosons, as computed in CGKM2.

The Higgs only contributes through wave function renormalization in SCET. The matching contribution from the Higgs is

$$\begin{aligned}H(t_L) &= -\frac{1}{2}\frac{y_t^2}{16\pi^2}\Big[\frac{1}{2}F_h(M_H^2, m_t^2) + \frac{1}{2}F_h(M_Z^2, m_t^2) \\ &\quad + \frac{1}{2}\tilde{a}(h_t, h_t) + \frac{1}{2}\tilde{a}(z_t, z_t) + \tilde{c}(h_t, h_t) + \tilde{c}(z_t, z_t) \\ &\quad + \tilde{c}(w_t, 0) - \tilde{b}(h_t, h_t) + \tilde{b}(z_t, z_t)\Big] \\ H(t_R) &= H(t_L) - \frac{1}{2}\frac{y_t^2}{16\pi^2}(F_h(M_W^2, m_t^2) + \tilde{a}(w_t, 0)) \\ H(b'_L) &= -\frac{1}{2}\frac{y_t^2}{16\pi^2}[F_h(M_W^2, m_t^2) + \tilde{a}(0, w_t)], \\ F_h(M^2, \mu^2) &= \frac{1}{4} - \frac{1}{2}\mathsf{L}_M \\ h_t &= \frac{m_t^2}{M_H^2}, \quad w_t = \frac{m_t^2}{M_W^2}, \quad z_t = \frac{m_t^2}{M_Z^2}\end{aligned} \tag{133}$$

where the functions are tabulated in Appendix B. For each t_L, t_R or b_L field, one adds $H(t_L)$, $H(t_R)$ or $H(b'_L)$ to the matching matrix. For example the operator $\bar{t}_L \gamma^\mu t_L \bar{b}'_L \gamma_\mu b'_L$ gets the Higgs matching contribution $2H(t_L) + 2H(b'_L)$.

The matching for operators containing $Q^{(t)}$ and a light quark doublet, Eq. (112) with $f = t$ and $i = u, c$, is given by Eq. (116), with the additional additive contribution

$$\delta R_H^{(1)} = \begin{bmatrix} \frac{1}{2}H(t_L) & 2H(t_L) \\ -\frac{1}{2}H(t_L) & 2H(t_L) \\ -\frac{1}{2}H(b'_L) & 2H(b'_L) \\ \frac{1}{2}H(b'_L) & 2H(b'_L) \\ \frac{1}{2}H(t_L)+\frac{1}{2}H(b'_L) & 0 \\ \frac{1}{2}H(t_L)+\frac{1}{2}H(b'_L) & 0 \end{bmatrix} \tag{134}$$

from the Higgs,

$$\delta R_W^{(1)} = \frac{\alpha_{\rm em}}{4\pi \sin^2\theta_W}\frac{1}{2}\begin{bmatrix} \frac{1}{2}W_1 & 2W_1 \\ -\frac{1}{2}W_1 & 2W_1 \\ -\frac{1}{2}W_2 & 2W_2 \\ \frac{1}{2}W_2 & 2W_2 \\ \frac{1}{2}W_1+\frac{1}{2}W_2 & 0 \\ \frac{1}{2}W_1+\frac{1}{2}W_2 & 0 \end{bmatrix} \tag{135}$$

from the W,

$$\delta R_Z^{(1)} = \frac{\alpha_{\rm em}}{4\pi \sin^2\theta_W \cos^2\theta_W} U_1 \begin{bmatrix} \frac{1}{2} & 2 \\ -\frac{1}{2} & 2 \\ 0 & 0 \\ 0 & 0 \\ \frac{1}{2} & 0 \\ \frac{1}{2} & 0 \end{bmatrix} \tag{136}$$

from the Z,

$$\delta R_\gamma^{(1)} = \frac{\alpha_{\rm em}}{4\pi} q_t^2 \left(\frac{\pi^2}{12}+2\right)\begin{bmatrix} \frac{1}{2} & 2 \\ -\frac{1}{2} & 2 \\ 0 & 0 \\ 0 & 0 \\ \frac{1}{2} & 0 \\ \frac{1}{2} & 0 \end{bmatrix} \tag{137}$$

from the photon, where $q_t = 2/3$ is the t-quark charge, and

$$\delta R_g^{(1)} = \frac{\alpha_s}{4\pi}\frac{4}{3}\left(\frac{\pi^2}{12}+2\right)\begin{bmatrix} \frac{1}{2} & 2 \\ -\frac{1}{2} & 2 \\ 0 & 0 \\ 0 & 0 \\ \frac{1}{2} & 0 \\ \frac{1}{2} & 0 \end{bmatrix} \tag{138}$$

from the gluon where

$$\begin{aligned} W_1 &= f_F(w_t, 0) - \frac{1}{2}a(w_t, 0) - \frac{1}{2}c(w_t, 0) \\ W_2 &= f_F(0, w_t) - \frac{1}{2}a(0, w_t) \\ U_1 &= g_{Lt}^2 f_F(z_t, z_t) - \frac{1}{2}g_{Lt}^2 a(z_t, z_t) - \frac{1}{2}(g_{Lt}^2 + g_{Rt}^2)c(z_t, z_t) \\ &\quad + g_{Lt}g_{Rt}b(z_t, z_t) \\ U_2 &= g_{Rt}^2 f_F(z_t, z_t) - \frac{1}{2}g_{Rt}^2 a(z_t, z_t) - \frac{1}{2}(g_{Lt}^2 + g_{Rt}^2)c(z_t, z_t) \\ &\quad + g_{Lt}g_{Rt}b(z_t, z_t) \end{aligned} \tag{139}$$

and the functions f_F, a, b and c are tabulated in Appendix B. The matching matrix multiplied by $(C_{QQ1l,tq}, C_{QQ2l,tq})$ gives the coefficients $\hat{C}_{kl}$, $k = 1, \ldots, 6$, $l = 1, 2$ of the operators in SCET$_\gamma$ listed in Eq. (113) and (122) with $c \to t$ and $s \to b'$ for the final state quarks, and the initial state flavors replaced by the two members of the light quark doublet q, $(u, d') \to (c, s')$, or $(u, d') \to (u, d')$. Note that $\mathcal{O}_{51}$, $\mathcal{O}_{52}$, $\mathcal{O}_{61}$, $\mathcal{O}_{62}$ are relevant for single-top production.

The gluon matching $\delta R_g^{(1)}$ is diagonal in color space, and does not mix the $\mathbf{1} \otimes \mathbf{1}$ and $T^A \otimes T^A$ operators. This follows from Eq. (46) and the additive nature of the mass corrections to the amplitudes.

The matching for operators containing $Q^{(t)}$ and a light quark singlet are given by Eq. (127) with the additional terms

$$\begin{aligned} \delta R_H^{(1)} &= \begin{bmatrix} 2H(t_L) \\ 2H(b'_L) \end{bmatrix} \\ \delta R_W^{(1)} &= \frac{\alpha_{\rm em}}{4\pi \sin^2\theta_W}\frac{1}{2}\begin{bmatrix} 2W_1 \\ 2W_2 \end{bmatrix} \\ \delta R_Z^{(1)} &= \frac{\alpha_{\rm em}}{4\pi \sin^2\theta_W \cos^2\theta_W}\begin{bmatrix} 2U_1 \\ 0 \end{bmatrix} \\ \delta R_\gamma^{(1)} &= \frac{\alpha_{\rm em}}{4\pi} q_t^2 \left(\frac{\pi^2}{6}+4\right)\begin{bmatrix} 1 \\ 0 \end{bmatrix} \\ \delta R_g^{(1)} &= \frac{\alpha_s}{4\pi}\frac{4}{3}\left(\frac{\pi^2}{6}+4\right)\begin{bmatrix} 1 \\ 0 \end{bmatrix}. \end{aligned} \tag{140}$$

with $X_{1,2}$ and U_1 given in Eq. (139).

The matching for operators containing t_R and a light quark doublet are given by Eq. (127) with the additional terms

$$\begin{aligned} \delta R_H^{(1)} &= \begin{bmatrix} 2H(t_R) \\ 2H(t_R) \end{bmatrix} \\ \delta R_W^{(1)} &= \frac{\alpha_{\rm em}}{4\pi \sin^2\theta_W}\frac{1}{2}\begin{bmatrix} -c(w_t, 0) \\ -c(w_t, 0) \end{bmatrix} \\ \delta R_Z^{(1)} &= \frac{\alpha_{\rm em}}{4\pi \sin^2\theta_W \cos^2\theta_W}\begin{bmatrix} 2U_2 \\ 2U_2 \end{bmatrix} \\ \delta R_\gamma^{(1)} &= \frac{\alpha_{\rm em}}{4\pi} q_t^2 \left(\frac{\pi^2}{6}+4\right)\begin{bmatrix} 1 \\ 1 \end{bmatrix} \\ \delta R_g^{(1)} &= \frac{\alpha_s}{4\pi}\frac{4}{3}\left(\frac{\pi^2}{6}+4\right)\begin{bmatrix} 1 \\ 1 \end{bmatrix}. \end{aligned} \tag{141}$$

The matching for operators containing t_R and singlet light quarks is given by Eq. (131) with the additional terms

$$\begin{aligned}
\delta R_H^{(1)} &= 2H(t_R) \\
\delta R_W^{(1)} &= \frac{\alpha_{\rm em}}{4\pi \sin^2\theta_W}\frac{1}{2}(-c(w_t,0)) \\
\delta R_Z^{(1)} &= \frac{\alpha_{\rm em}}{4\pi \sin^2\theta_W \cos^2\theta_W} 2U_2 \\
\delta R_\gamma^{(1)} &= \frac{\alpha_{\rm em}}{4\pi} q_t^2\left(\frac{\pi^2}{6}+4\right) \\
\delta R_g^{(1)} &= \frac{\alpha_s}{4\pi}\frac{4}{3}\left(\frac{\pi^2}{6}+4\right).
\end{aligned} \tag{142}$$

Anomalous dimension in $\mathbf{SCET}_\gamma$

The anomalous dimension in SCET_γ after integrating out the electroweak gauge bosons and switching to HQET for the top quarks, is given by gluon and photon exchange. For t pair production, particles 3 and 4 are HQET t-quarks, and γ can be obtained from Eq. (44), using the heavy-heavy anomalous dimension (γ_1 of CGKM2) for exchange between (3, 4), the heavy-light anomalous dimension (γ_2 of CGKM2) for exchange between (3, 4) and (1, 2) and the light-light anomalous dimension (γ_3 of CGKM2) for exchange between (1, 2). This gives Eq. (61) for the QCD part of the anomalous dimension, with $\alpha \to \alpha_s$, and group theory factors replaced by their $SU(3)$ values,

$$\begin{aligned}
\gamma^{(1)} &= \tilde{\gamma}^{(1)}\mathbb{1} + \gamma_S^{(1)}, \\
\tilde{\gamma}^{(1)} &= \frac{\alpha_s}{4\pi}\frac{4}{3}(8\mathsf{L}_s - 4\mathsf{L}_{m_t} - 10), \\
\gamma_S^{(1)} &= \frac{\alpha_s}{4\pi}\begin{bmatrix} \frac{10}{3}\mathsf{L}_{t/u} + 6\mathsf{L}_{ut/s^2} & 8\mathsf{L}_{t/u} \\ \frac{16}{9}\mathsf{L}_{t/u} & 0 \end{bmatrix}.
\end{aligned} \tag{143}$$

The QED anomalous dimension is

$$\gamma = \frac{\alpha_{\rm em}}{4\pi}\left[q_l^2\left(4\log\frac{-s}{\mu^2}-6\right) + q_t^2\left(4\log\frac{-s}{m_t^2}-4\right) + 8q_l q_t \log\frac{t}{u}\right] \tag{144}$$

where $q_t = 2/3$ and $q_l = 2/3, -1/3$ is the charge of the light quark.

For single-top production from the operators $\hat{O}_{51}$, $\hat{O}_{61}$, $\hat{O}_{52}$, $\hat{O}_{62}$, there is only one heavy quark in the final state, and

$$\begin{aligned}
\gamma &= \tilde{\gamma}^{(1)}\mathbb{1} + \gamma_S^{(1)}, \\
\tilde{\gamma}^{(1)} &= \frac{\alpha_s}{4\pi}\frac{4}{3}\left(8\mathsf{L}_s - 11 - 2\log\frac{m_t^2}{\mu^2}\right), \\
\gamma_S^{(1)} &= \frac{\alpha_s}{4\pi}\begin{bmatrix} \frac{10}{3}\mathsf{L}_{t/u} + 6\mathsf{L}_{ut/s^2} & 8\mathsf{L}_{t/u} \\ \frac{16}{9}\mathsf{L}_{t/u} & 0 \end{bmatrix},
\end{aligned} \tag{145}$$

and the QED anomalous dimension

$$\gamma = \frac{\alpha_{\rm em}}{4\pi}\left[(q_u^2+q_d^2)\left(8\log\frac{-s}{\mu^2} - 11 - 2\log\frac{m_t^2}{\mu^2}\right) + 8q_u q_d \log\frac{s}{u}\right] \tag{146}$$

where $q_u = 2/3$ and $q_d = -1/3$ are the charges of the up-type and down-type quarks, respectively.

This completes the computation of radiative corrections in the standard model. The formulas derived in this section will be used for the numerical computations in the next section. The only case we have not treated is when both initial and final particles are top quarks. This can be obtained from the case we have analyzed, with a heavy quark in the final state, by also adding heavy quark corrections terms for the initial quark.

E. $gg \to q\bar{q}$, $gq \to gq$ and $g\bar{q} \to g\bar{q}$

The computations in this paper have been restricted to those involving external matter fields. In top-quark production and in jet production, processes involving external gluons are also important. Consider, for definiteness, the case $gg \to q\bar{q}$. At the high-scale Q, the tree-graphs which contribute to $gg \to q\bar{q}$ are shown in Fig. 10. In the EFT, one generates a local operator which involves the fields q, $\bar{q}$, and two collinear-gluon field strength tensors, shown graphically in Fig. 11. The QCD corrections involve studying operators with gauge field strength tensors, and will be discussed elsewhere. The QCD corrections are known from existing fixed-order computations [53]. The new feature discussed in this article is the electroweak correction. If we restrict ourselves to the electroweak corrections alone, then we can compute these using the results in CGKM2. The gluon field strength tensor is an electroweak singlet, and so the $ggq\bar{q}$ operator in the EFT is equivalent to the electroweak singlet currents $\bar{q}\gamma^\mu P_{L,R} q$ studied in CGKM2 and the running and matching corrections in the effective the-

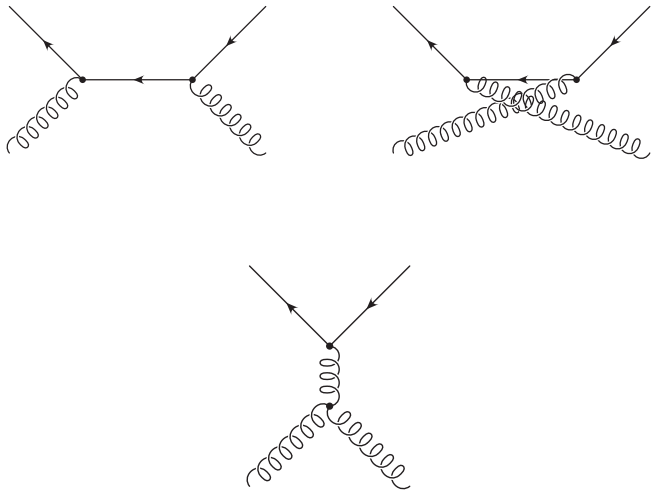

FIG. 10. Graphs contributing to $gg \to q\bar{q}$ in the full theory.

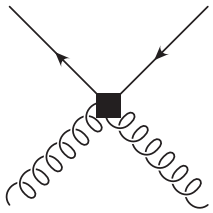

FIG. 11. Operator contributing to $gg \to q\bar{q}$ in the EFT.

ory are identical, with the identification $-Q^2 \to s$. Thus the total radiative corrections are given by combining the known QCD corrections, with the electroweak corrections for the current given in CGKM1, CGKM2. The other important parton subprocesses which contributes to dijet production are $gq \to gq$, $g\bar{q} \to g\bar{q}$, and $gg \to gg$. For gluon-quark or gluon-antiquark scattering, the EFT operator is a $ggq\bar{q}$ operator, and the electroweak corrections are the same as those for the Sudakov form-factor, with $Q^2 \to -t$. For gg scattering, there are no electroweak corrections to the order we are working, since the gluons do not couple to the electroweak gauge bosons, and the radiative corrections can be computed using the known QCD corrections.

F. Squark production

The techniques developed in the previous sections can be used to calculate the radiative corrections in a theory involving scalar particles in the final state such as SUSY. To perform a high precision computation requires specifying a particular supersymmetric theory, and computing the matching conditions and radiative corrections using the given SUSY particle spectrum. This is beyond the scope of the present work.

To estimate the size of electroweak Sudakov corrections in squark production, we will compute the $SU(2)$ corrections in the toy model of Sec. V D, assuming the squark is a doublet, and $\alpha \to \alpha_2$, the weak interaction coupling constant. This gives the expected size of electroweak Sudakov corrections in squark production.

VIII. NUMERICS

The formulas for the EFT computation of standard model scattering processes have been given in Sec. VII. As discussed in Sec. III, the anomalous dimensions are integrated using the two-loop β-functions, and we also include the known two-loop QCD anomalous dimensions [34] in addition to the one-loop results of Sec. VII. The corrections have a very small dependence on the Higgs mass (much less than 1%). In the numerics, we use a Higgs mass of 200 GeV. The EFT coefficients should be run down to a scale μ_0 of order a typical jet invariant mass. We have chosen to use $\mu_0 = 30$ GeV. The electroweak corrections are insensitive to this scale, because the only electroweak correction below M_Z is due to photon exchange.

The matching corrections at the high scale Q are about 2%, and dominated by the QCD contribution. The low-scale matching due to integrating out the W and Z is about 2%. Both matching corrections are not very strongly dependent on Q. The largest corrections are from the anomalous dimension running. These corrections grow rapidly with energy. The one-loop QCD corrections are very large, and reduce the rate by factors of 3–30 in the range $\sqrt{\hat{s}}$ between 1 and 5 TeV. The two-loop QCD cusp anomalous dimension reduces the rate by about 10% at $\sqrt{\hat{s}} = 5$ TeV. This is smaller than the electroweak corrections, but not negligible. The two-loop noncusp QCD anomalous dimension (the B term in Eq. (15)) increases the rate by about 2%. We have included the QCD two-loop cusp and noncusp terms in the numerical results. The two-loop cusp anomalous dimension has been shown to be proportional to the one-loop result [34], and we use their K factor to determine the two-loop cusp anomalous dimension (the A term in Eq. (15)). The two-loop noncusp anomalous dimension was determined in CGKM2 by comparing the EFT result with the two-loop results of Jantzen and Smirnov [17]. The two-loop cusp anomalous dimension also determines the two-loop contribution to the soft anomalous dimension matrix γ_S. The noncusp contribution vanishes, since γ_S depends on differences of anomalous dimensions. The three-loop QCD cusp anomalous dimension contribution [54] is less than 0.1%, and can be omitted. The one-loop electroweak anomalous dimension corrections are significant, ranging from 5% at 1 TeV to around 30% at 5 TeV. Higher order electroweak corrections, such as the two-loop electroweak cusp anomalous dimension are smaller than 0.1%. The numerical results are accurate at the one-percent level, so that the error in LHC cross-sections is dominated by other uncertainties, such as in the parton distribution functions.

The EFT analysis neglected power corrections of the form $M^2/\hat{s}$, $M^2/\hat{t}$ and $M^2/\hat{u}$. The dominant power corrections arise from one-loop QCD graphs, so we use the estimate $(\alpha_s M^2/\pi) \times 1/(\hat{s}, \hat{t}, \hat{u})$ since the graphs have a color factor of (roughly) $4C_F\alpha_s/(4\pi)$. To keep the power corrections below 1% requires $\sqrt{\hat{s}, |\hat{t}|, |\hat{u}|}$ to be larger than about 200 GeV for light-quark processes, where the largest M is M_Z, and larger than about 350 GeV for processes involving the top-quark. Note that we have included all power corrections that depend on ratios such as M_Z/m_t or M_Z/M_H, and not expanded in these ratios. There are tree-level power corrections due to gauge boson mass effects in the propagators, e.g. the s-channel propagator $\hat{s} - M_Z^2$ is approximated as $\hat{s}$. These trivial effects cancel in our results, because we normalize all amplitudes to their tree-level values.

The LHC cross-sections are given by using the coefficients computed earlier to compute the parton scattering cross-sections, and then convoluting them with parton distribution functions. For processes involving four-quark

operators, the effective interaction at the low-scale is a linear combination of two color structures,

$$\mathcal{O} = C_1(T^a \otimes T^a) + C_2(\mathbf{1} \otimes \mathbf{1}). \tag{147}$$

Color-averaging over initial particles and color summing over final particles lead to a contribution to the cross-section which is proportional to an effective coefficient C, with

$$|C|^2 = \frac{2}{9}|C_1|^2 + |C_2|^2. \tag{148}$$

For $q\bar{q} \to q'\bar{q}'$, e.g. $u\bar{u} \to b\bar{b}$, the parton scattering cross-section is

$$\frac{\mathrm{d}\hat{\sigma}}{\mathrm{d}\hat{t}} = \frac{1}{16\pi\hat{s}^2}[(|C_{LL}|^2_{s,t} + |C_{RR}|^2_{s,t})\hat{u}^2 + (|C_{LR}|^2_{s,t} + |C_{RL}|^2_{s,t})\hat{t}^2] \tag{149}$$

where C_{LL}, etc. are the coefficients of the LL, etc. operators. The $\hat{}$ denote partonic variables. The subscript s, t is a reminder that one uses the coefficients as computed in Sec. VII with annihilation channel kinematics. From this, one can compute hadronic cross-sections. For example, the dijet invariant mass distribution from the partonic subprocess $u\bar{u} \to d\bar{d}$ is given by

$$M^2\frac{\mathrm{d}^2\sigma}{\mathrm{d}M^2\mathrm{d}E_T} = 2E_T\sqrt{\frac{\hat{s}}{\hat{s}-4E_T^2}}\frac{\mathrm{d}\hat{\sigma}}{\mathrm{d}\hat{t}}\bigg|_{\hat{s}=\tau s}\tau\frac{\mathrm{d}L_{u\bar{u}}}{\mathrm{d}\tau} \tag{150}$$

where M^2 is the dijet invariant mass, E_T is the transverse energy of the jet, $\tau = M^2/s$, $\sqrt{s} = 14$ TeV is the LHC center of mass energy, and the parton luminosity function L_{ij} is defined by

$$\frac{\mathrm{d}L_{ij}}{\mathrm{d}\tau} = \frac{1}{1+\delta_{ij}}\int_\tau^1\frac{\mathrm{d}x}{x}[f_i^{(1)}(x)f_j^{(2)}(\tau/x) + f_j^{(1)}(x)f_i^{(2)}(\tau/x)] \tag{151}$$

where $f_i^{(1,2)}$ are the distribution functions for parton i in beams 1 and 2.[9] For the LHC, both are proton distribution functions. The $1+\delta_{ij}$ is the symmetry factor for identical partons in the initial state. For the case $q = q'$, e.g. $u\bar{u} \to u\bar{u}$, Eq. (149) still holds, and the coefficients $C_{LL,RR}$ get contributions from both the direct and crossed graphs.

For identical particles, e.g. $u\bar{u} \to u\bar{u}$, the partonic cross-section has the schematic form

$$\frac{\mathrm{d}\hat{\sigma}}{\mathrm{d}\hat{t}} = \frac{1}{16\pi\hat{s}^2}[(|C_{LL}+\tilde{C}_{LL}|^2_{s,t} + |C_{RR}+\tilde{C}_{LL}|^2_{s,t})\hat{u}^2 + (|C_{LR}|^2_{s,t} + |C_{RL}|^2_{s,t})\hat{t}^2 + (|C_{LR}|^2_{t,s} + |C_{RL}|^2_{t,s})\hat{s}^2]. \tag{152}$$

There is the direct channel as well as the crossed-channel with $s \leftrightarrow t$. For LL and RR, the crossed-channel amplitudes have the same fermion chiralities as the direct channel, and are included as $\tilde{C}$, which includes both $s \leftrightarrow t$ and the crossing matrix. One has to add the amplitudes in the two channels before squaring. For LR and RL, the crossed diagrams do not interfere because the initial and final chiralities do not match, and one adds the probabilities.

For qq' scattering processes not involving identical particles the cross-section is

$$\frac{\mathrm{d}\hat{\sigma}}{\mathrm{d}\hat{t}} = \frac{1}{16\pi\hat{s}^2}[(|C_{LL}|^2_{t,u} + |C_{RR}|^2_{t,u})\hat{s}^2 + (|C_{LR}|^2_{t,u} + |C_{RL}|^2_{t,u})\hat{u}^2] \tag{153}$$

and for $q\bar{q}'$ scattering

$$\frac{\mathrm{d}\hat{\sigma}}{\mathrm{d}\hat{t}} = \frac{1}{16\pi\hat{s}^2}[(|C_{LL}|^2_{t,s} + |C_{RR}|^2_{t,s})\hat{u}^2 + (|C_{LR}|^2_{t,s} + |C_{RL}|^2_{t,s})\hat{s}^2] \tag{154}$$

The subscripts t, u, etc. are a reminder the one has to use the amplitudes of Sec. VII with the replacements $s \to t$, $t \to u$, etc.

For identical quark scattering, $qq \to qq$, e.g. $uu \to uu$, the cross-section is

$$\frac{\mathrm{d}\hat{\sigma}}{\mathrm{d}\hat{t}} = \frac{1}{16\pi\hat{s}^2}\left[\frac{1}{2}(|C_{LL}+\tilde{C}_{LL}|^2_{t,u} + |C_{RR}+\tilde{C}_{LL}|^2_{t,u})\hat{s}^2 + 2|C_{LR}|^2_{t,u}\hat{u}^2 + 2|C_{LR}|^2_{u,t}\hat{t}^2\right]. \tag{155}$$

The $1/2$ is from final state phase space for identical particles. The initial state $1/2$ is included in the parton luminosity function.

There are 72 four-fermion amplitudes that have been computed in Sec. VII in the s-channel, not including those which are identical by flavor symmetry, and another 72 amplitudes in the t-channel, and we cannot plot them all here. We will choose some representative examples to illustrate the size of the radiative corrections in high energy LHC processes. Rather than plot the hadronic cross-sections, which involve convolutions over rapidly falling parton luminosities, we have chosen to plot the ratio of the partonic cross-sections $\mathrm{d}\hat{\sigma}/\mathrm{d}\hat{t}$ to their tree-level values. From Eq. (150), it follows that this also gives the ratio of the hadronic cross-section to its tree-level value. We will also neglect the CKM matrix in the plots, since the flavor dependence of the electroweak corrections is small, and the CKM factors enter as off-diagonal CKM matrix elements multiplied by the difference of electroweak corrections between d' and s', and d' and b'.

[9] $2E_T = \sqrt{\hat{s}}\sin\theta$ and $\hat{t} = -\hat{s}\sin^2\theta/2$, where θ is the center of mass scattering angle. Thus in Eq. (150), a given E_T values gets contributions from two values of $\hat{t}$, or equivalently, one should symmetrize $\mathrm{d}\hat{\sigma}/\mathrm{d}\hat{t}$ under $\hat{t} \leftrightarrow \hat{u}$. We will plot $\mathrm{d}\hat{\sigma}/\mathrm{d}\hat{t}$ before symmetrizing.

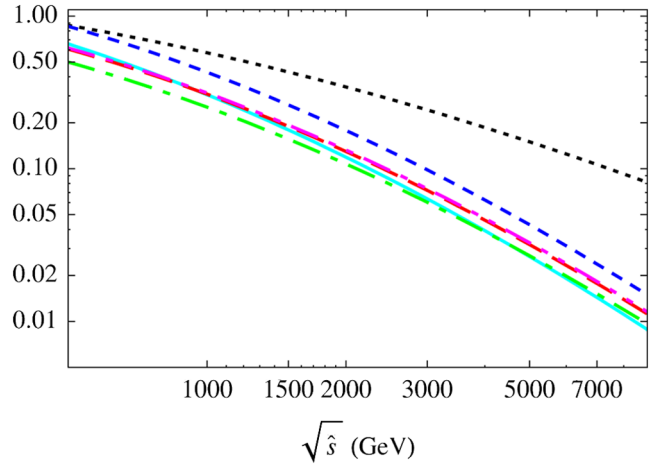

FIG. 12 (color online). Rates for $u\bar{u} \to \mu^+\mu^-$ (dotted black), $u\bar{u} \to u\bar{u}$ (solid cyan), $u\bar{u} \to c\bar{c}$ (long-dashed red), $u\bar{u} \to t\bar{t}$ (short-dashed blue), $u\bar{u} \to d\bar{d}$ (dot-dashed green) and $u\bar{u} \to b\bar{b}$ (double-dot-dashed magenta) as a function of $\sqrt{\hat{s}}$ in GeV at $\theta = 90°$, normalized to their tree-level values without any electroweak corrections. Note the logarithmic scale.

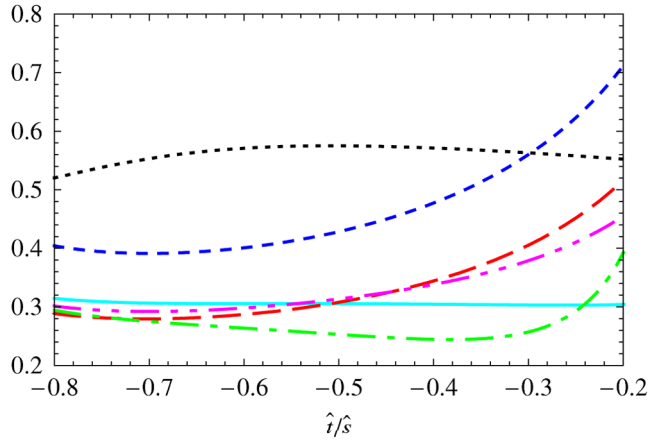

FIG. 13 (color online). Rates for $u\bar{u} \to \mu^+\mu^-$ (dotted black), $u\bar{u} \to u\bar{u}$ (solid cyan), $u\bar{u} \to c\bar{c}$ (long-dashed red), $u\bar{u} \to t\bar{t}$ (short-dashed blue), $u\bar{u} \to d\bar{d}$ (dot-dashed green) and $u\bar{u} \to b\bar{b}$ (double-dot-dashed magenta) as a function of $\hat{t}/\hat{s}$ for $\sqrt{\hat{s}} = 1$ TeV, normalized to their tree-level values without any electroweak corrections.

Plots

Figure 12 show the ratio $\mathrm{d}\hat{\sigma}/\mathrm{d}\hat{t}$ to its tree-level value for $u\bar{u} \to \mu^+\mu^-$, $u\bar{u}$, $c\bar{c}$, $t\bar{t}$ and $b\bar{b}$ as a function of $\sqrt{\hat{s}}$ for 90° scattering, $\hat{t} = -\hat{s}/2$, including QCD and electroweak corrections. The radiative corrections are enormous, and reduce the cross-sections by 1.15–2 at $\sqrt{\hat{s}} = 500$ GeV to a factor of 7–38 at $\sqrt{\hat{s}} = 5$ TeV compared to the tree-level value, depending on the process.[10] The bulk of the correction is due to QCD effects. Some of the QCD corrections are included in parton shower Monte-Carlos, because gluon radiation from tree-level branching is related to the LL Sudakov series. However, the electroweak corrections, and some of the QCD corrections are not included in the shower algorithms, so the Monte-Carlo results can have substantial ($\sim 50\%$) corrections.

The $u\bar{u}$ rate differs from $c\bar{c}$ because of the crossed-channel graph for identical particles. The difference between $c\bar{c}$ and $t\bar{t}$, and between $s\bar{s}$ (not shown) and $b\bar{b}$ is due to top-quark mass effects. The $u\bar{u} \to \mu^+\mu^-$ rate has smaller QCD corrections, since the final state is a color singlet. The anomalous dimension $\tilde{\gamma}$ is proportional to $4\mathsf{L}_s - 6$. At large values of $\hat{s}$, the $4\mathsf{L}_s$ term dominates, and produces the large Sudakov (double-log) suppression. At smaller values of $\hat{s}$, the -6 can compensate the $4\mathsf{L}_s$ term, leading to an enhancement of the cross-section. This leads to a flattening of the curves at the smallest values of $\hat{s}$. The cross-sections will decrease slightly if we continue the plot to even smaller values of $\hat{s}$. This effect can also be seen in the plots of Ref. [9]. Figure 13 show the radiative corrections to the angular distribution for $u\bar{u} \to \mu^+\mu^-$, $u\bar{u}$, $c\bar{c}$, $t\bar{t}$ and $b\bar{b}$ at $\sqrt{\hat{s}} = 1$ TeV. There is about a factor of 2 variation in the radiative correction over the range $-0.8 \le \hat{t}/\hat{s} \le -0.2$.

Figures 14 and 15 show the ratios $\mathrm{d}\hat{\sigma}(u\bar{u} \to t\bar{t})/\mathrm{d}\hat{t}/\mathrm{d}\hat{\sigma}(u\bar{u} \to c\bar{c})/\mathrm{d}\hat{t}$ and $\mathrm{d}\hat{\sigma}(u\bar{u} \to b\bar{b})/\mathrm{d}\hat{t}/\mathrm{d}\hat{\sigma}(u\bar{u} \to s\bar{s})/\mathrm{d}\hat{t}$ as a function of $\sqrt{\hat{s}}$ for different values of $\hat{t}$ (i.e. the scattering angle θ), including QCD and electroweak corrections. These ratios are unity in the absence of top-quark mass effects. There is a $\sim$40% increase in the $t\bar{t}$ rate due to the top-quark mass. About -4% is from the Higgs contribution, -2% from mass effects in the low-scale electroweak matching, and the rest from mass effects in the QCD matching at m_t and running below m_t. There is a

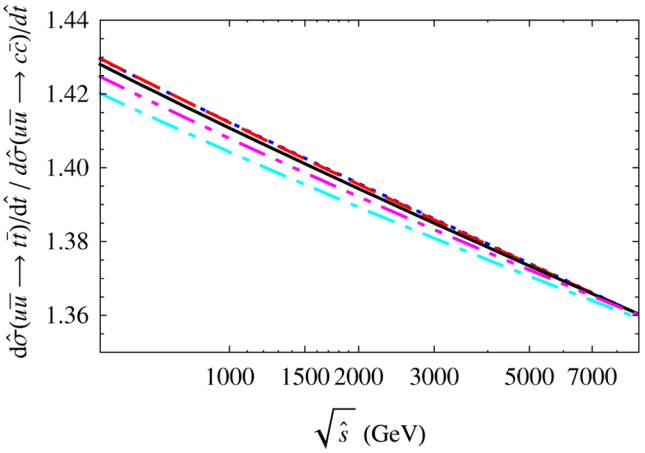

FIG. 14 (color online). The ratio $(u\bar{u} \to t\bar{t})/(u\bar{u} \to c\bar{c})$ at $\hat{t} = -0.2\hat{s}$, (dotted blue), $\hat{t} = -0.35\hat{s}$ (long-dashed red), $\hat{t} = -0.5\hat{s}$ (solid black), $\hat{t} = -0.65\hat{s}$ (double-dot-dashed magenta) and $\hat{t} = -0.8\hat{s}$ (dot-dashed cyan) as a function of $\sqrt{\hat{s}}$ in GeV.

[10]Note that the parton luminosity is falling by about 4 orders of magnitude over the same range.

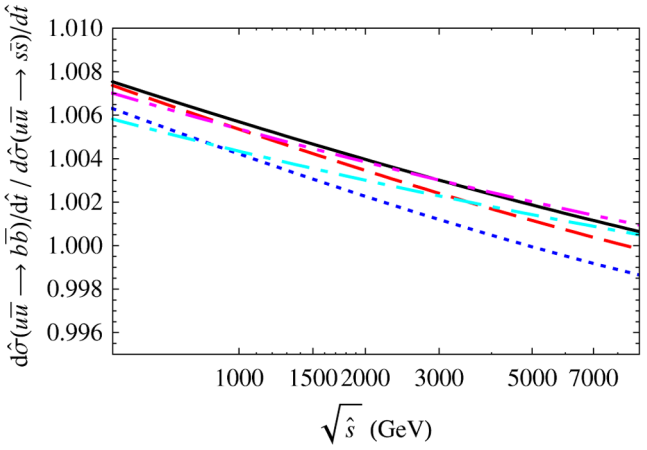

FIG. 15 (color online). The ratio $(u\bar{u} \to b\bar{b})/(u\bar{u} \to s\bar{s})$ at $\hat{t} = -0.2\hat{s}$, (dotted blue), $\hat{t} = -0.35\hat{s}$ (long-dashed red), $\hat{t} = -0.5\hat{s}$ (solid black), $\hat{t} = -0.65\hat{s}$ (double-dot-dashed magenta) and $\hat{t} = -0.8\hat{s}$ (dot-dashed cyan) as a function of $\sqrt{\hat{s}}$ in GeV.

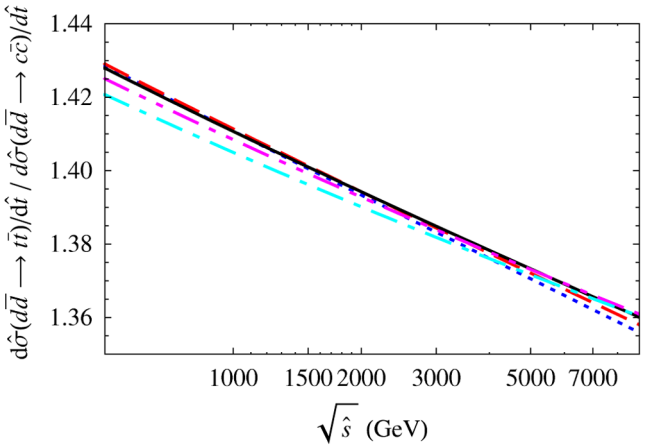

FIG. 16 (color online). The ratio $(d\bar{d} \to t\bar{t})/(d\bar{d} \to c\bar{c})$ at $\hat{t} = -0.2\hat{s}$, (dotted blue), $\hat{t} = -0.35\hat{s}$ (long-dashed red), $\hat{t} = -0.5\hat{s}$ (solid black), $\hat{t} = -0.65\hat{s}$ (double-dot-dashed magenta) and $\hat{t} = -0.8\hat{s}$ (dot-dashed cyan) as a function of $\sqrt{\hat{s}}$ in GeV.

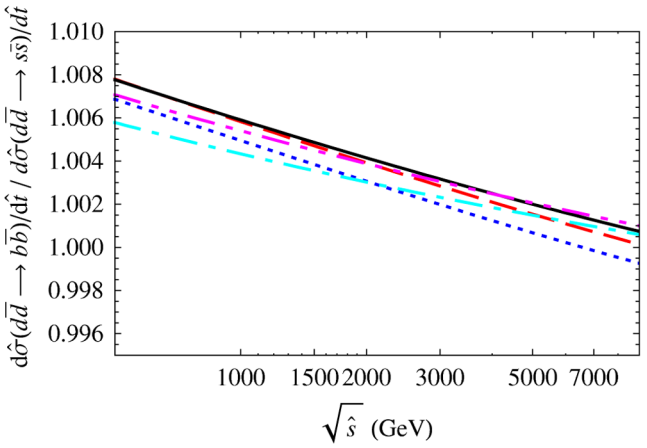

FIG. 17 (color online). The ratio of $(d\bar{d} \to b\bar{b})/(d\bar{d} \to s\bar{s})$ at $\hat{t} = -0.2\hat{s}$, (dotted blue), $\hat{t} = -0.35\hat{s}$ (long-dashed red), $\hat{t} = -0.5\hat{s}$ (solid black), $\hat{t} = -0.65\hat{s}$ (double-dot-dashed magenta) and $\hat{t} = -0.8\hat{s}$ (dot-dashed cyan) as a function of $\sqrt{\hat{s}}$ in GeV.

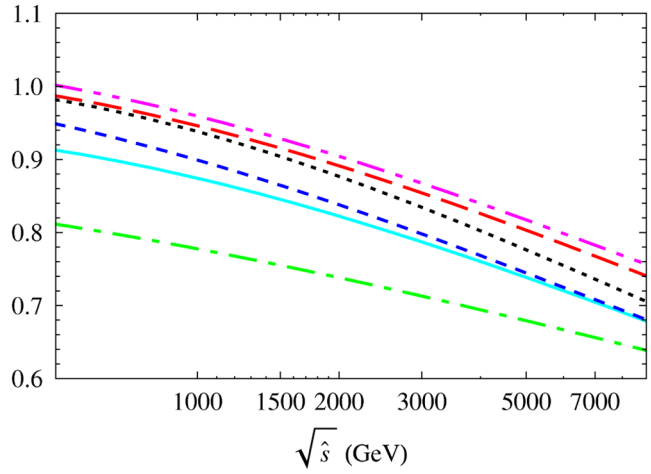

FIG. 18 (color online). Electroweak corrections to $u\bar{u} \to \mu^+\mu^-$ (dotted black), $u\bar{u} \to u\bar{u}$ (solid cyan), $u\bar{u} \to c\bar{c}$ (long-dashed red), $u\bar{u} \to t\bar{t}$ (short-dashed blue), $u\bar{u} \to d\bar{d}$ (dot-dashed green) and $u\bar{u} \to b\bar{b}$ (double-dot-dashed magenta) as a function of $\sqrt{\hat{s}}$ in GeV at $\theta = 90°$. The large corrections for $u\bar{u} \to d\bar{d}$ arise from the t-channel W exchange graph.

much smaller enhancement of $d\hat{\sigma}(u\bar{u} \to b\bar{b})/d\hat{t}/d\hat{\sigma}(u\bar{u} \to s\bar{s})/d\hat{t}$ due to virtual top-quark effects in the b-sector.[11] Figures 16 and 17 show the corresponding results for $d\bar{d} \to t\bar{t}, b\bar{b}$.

The plots discussed above include QCD and electroweak corrections. To show the importance of electroweak corrections, we show in Fig. 18, the same processes as in Fig. 12, but instead of plotting the ratio of the partonic cross-section to the tree-level value, we plot the ratio of the cross-section to the value including only QCD corrections, i.e. with $\alpha_{1,2} \to 0$.[12] This ratio shows the additional effect of electroweak corrections beyond the QCD corrections, which have been computed previously. The electroweak corrections are significant, increasing from (-4)–$(-22)\%$ at 1 TeV to (-18)–$(-32)\%$ at 5 TeV, depending on the process. The electroweak corrections to the angular distribution are shown in Fig. 19. There are 10–30% variations in the corrections in the range $-0.8 \le \hat{t}/\hat{s} \le -0.2$ for $\sqrt{s} = 1$ TeV.

The electroweak corrections alone (defined as just discussed) for lepton pair production from u-quark and d-quark annihilation are shown in Figs. 20 and 21 for different values of $\hat{t}$. At $\sqrt{\hat{s}} = 1$ TeV, the corrections range from (0.4)–$(-14)\%$, increasing to (-13)–$(-32)\%$ at $\sqrt{\hat{s}} = 5$ TeV. The electroweak corrections also change the angular distribution of the lepton pairs. Figures 22 and 23 show

[11]Even though our individual radiative corrections have corrections under 1%, ratios such as $d\hat{\sigma}(u\bar{u} \to b\bar{b})/d\hat{t}/d\hat{\sigma}(u\bar{u} \to s\bar{s})/d\hat{t}$ have much smaller errors, so that the deviation from unity in Fig. 15 is a real effect.

[12]In $q\bar{q} \to \mu^+\mu^-$, we include tree-level electroweak exchange, and keep $\alpha_s\alpha_{1,2}$ terms in the one-loop matching, but drop order $\alpha_{1,2}^2$ terms.

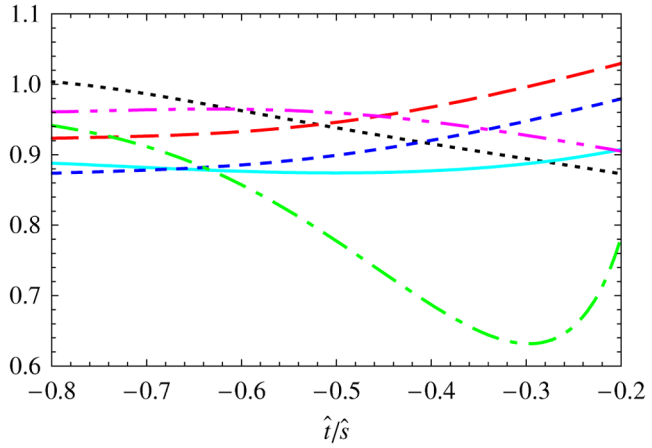

FIG. 19 (color online). Electroweak corrections to $u\bar{u} \to \mu^+\mu^-$ (dotted black), $u\bar{u} \to u\bar{u}$ (solid cyan), $u\bar{u} \to c\bar{c}$ (long-dashed red), $u\bar{u} \to t\bar{t}$ (short-dashed blue), $u\bar{u} \to d\bar{d}$ (dot-dashed green) and $u\bar{u} \to b\bar{b}$ (double-dot-dashed magenta) as a function of $\hat{t}/\hat{s}$ for $\sqrt{\hat{s}} = 1$ TeV. The large corrections for $u\bar{u} \to d\bar{d}$ arise from the t-channel W exchange graph.

the $\hat{t}$ dependence of the cross-section for different values of $\hat{s}$. The angular dependence is approximately independent of $\hat{s}$. The reason is that the dominant $\hat{t}$ dependence arises from the soft anomalous dimension γ_S, which is a function only of the dimensionless ratio $\hat{t}/\hat{s}$. The angular dependence of the electroweak corrections differ for $u\bar{u} \to \mu^+\mu^-$ and $d\bar{d} \to \mu^+\mu^-$.

The electroweak corrections to heavy quark production via u and d quark annihilation are shown in Figs. 24–27 for t-quark production, and Figs. 28–31 for b-quark production. Electroweak corrections to heavy quark production have been computed previously [55–63]. We find the same qualitative behavior—the electroweak corrections give a

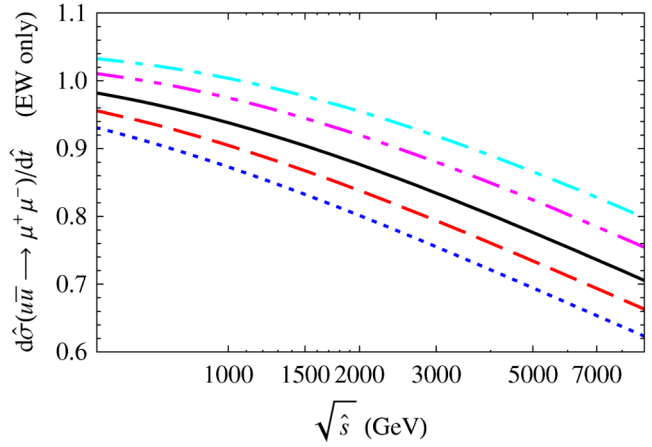

FIG. 20 (color online). Electroweak corrections to $u\bar{u} \to \mu^+\mu^-$ at $\hat{t} = -0.2\hat{s}$, (dotted blue), $\hat{t} = -0.35\hat{s}$ (long-dashed red), $\hat{t} = -0.5\hat{s}$ (solid black), $\hat{t} = -0.65\hat{s}$ (double-dot-dashed magenta) and $\hat{t} = -0.8\hat{s}$ (dot-dashed cyan) as a function of $\sqrt{\hat{s}}$ in GeV.

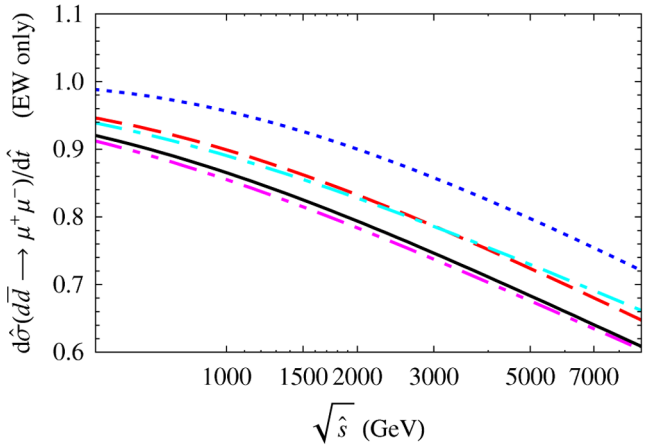

FIG. 21 (color online). Electroweak corrections to $d\bar{d} \to \mu^+\mu^-$ at $\hat{t} = -0.2\hat{s}$, (dotted blue), $\hat{t} = -0.35\hat{s}$ (long-dashed red), $\hat{t} = -0.5\hat{s}$ (solid black), $\hat{t} = -0.65\hat{s}$ (double-dot-dashed magenta) and $\hat{t} = -0.8\hat{s}$ (dot-dashed cyan) as a function of $\sqrt{\hat{s}}$ in GeV.

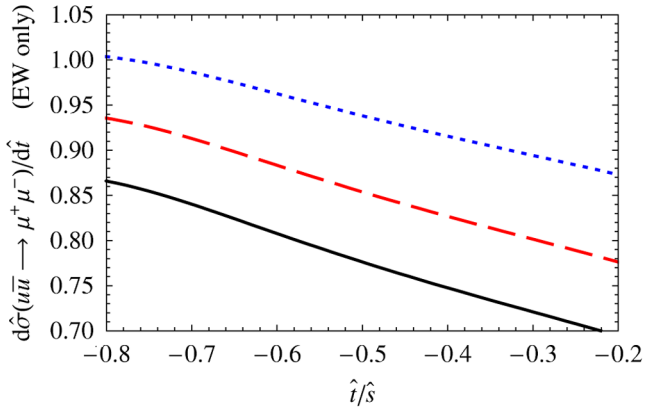

FIG. 22 (color online). Electroweak corrections to $u\bar{u} \to \mu^+\mu^-$ at $\sqrt{\hat{s}} = 1$ TeV, (dotted blue), $\sqrt{\hat{s}} = 2.5$ TeV (long-dashed red) and $\sqrt{\hat{s}} = 5$ TeV (solid black) as a function of $\hat{t}/\hat{s}$.

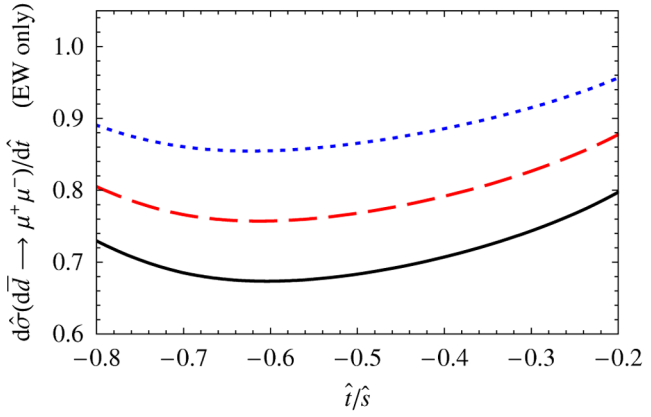

FIG. 23 (color online). Electroweak corrections to $d\bar{d} \to \mu^+\mu^-$ at $\sqrt{\hat{s}} = 1$ TeV, (dotted blue), $\sqrt{\hat{s}} = 2.5$ TeV (long-dashed red) and $\sqrt{\hat{s}} = 5$ TeV (solid black) as a function of $\hat{t}/\hat{s}$.

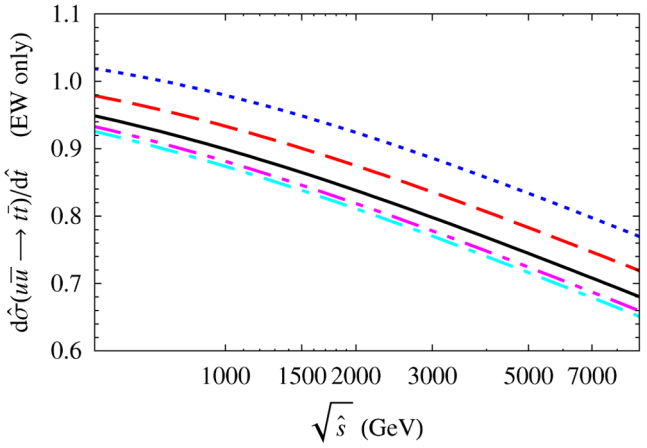

FIG. 24 (color online). Electroweak corrections to $u\bar{u} \to t\bar{t}$ at $\hat{t} = -0.2\hat{s}$, (dotted blue), $\hat{t} = -0.35\hat{s}$ (long-dashed red), $\hat{t} = -0.5\hat{s}$ (solid black), $\hat{t} = -0.65\hat{s}$ (double-dot-dashed magenta) and $\hat{t} = -0.8\hat{s}$ (dot-dashed cyan) as a function of $\sqrt{\hat{s}}$ in GeV.

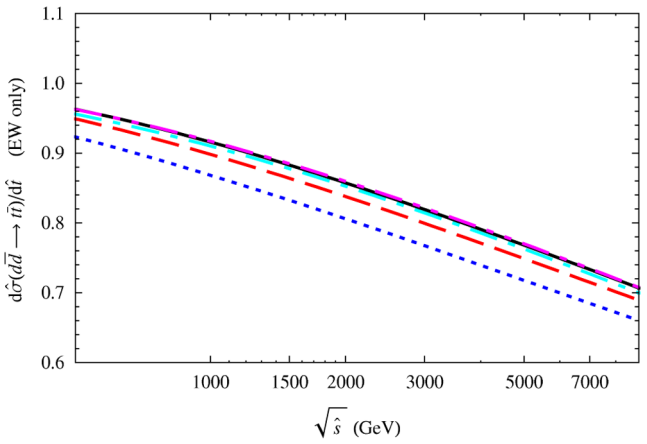

FIG. 25 (color online). Electroweak corrections to $d\bar{d} \to t\bar{t}$ at $\hat{t} = -0.2\hat{s}$, (dotted blue), $\hat{t} = -0.35\hat{s}$ (long-dashed red), $\hat{t} = -0.5\hat{s}$ (solid black), $\hat{t} = -0.65\hat{s}$ (double-dot-dashed magenta) and $\hat{t} = -0.8\hat{s}$ (dot-dashed cyan) as a function of $\sqrt{\hat{s}}$ in GeV.

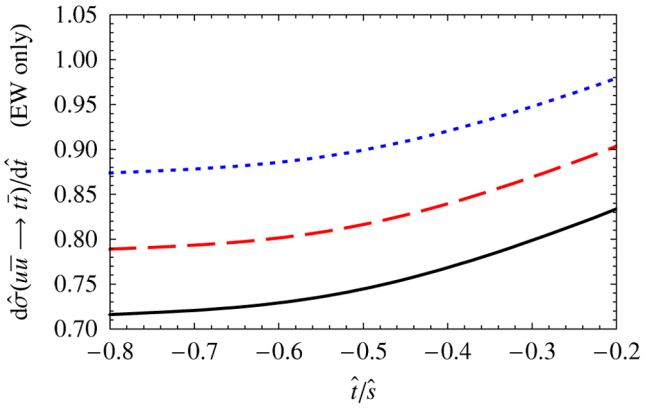

FIG. 26 (color online). Electroweak corrections to $u\bar{u} \to t\bar{t}$ at $\sqrt{\hat{s}} = 1$ TeV, (dotted blue), $\sqrt{\hat{s}} = 2.5$ TeV (long-dashed red) and $\sqrt{\hat{s}} = 5$ TeV (solid black) as a function of $\hat{t}/\hat{s}$.

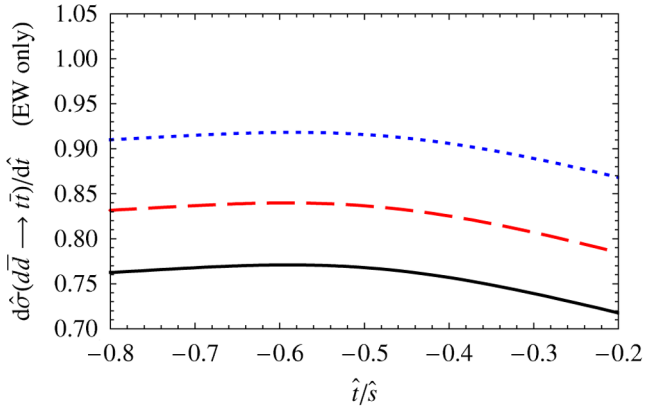

FIG. 27 (color online). Electroweak corrections to $d\bar{d} \to t\bar{t}$ at $\sqrt{\hat{s}} = 1$ TeV, (dotted blue), $\sqrt{\hat{s}} = 2.5$ TeV (long-dashed red) and $\sqrt{\hat{s}} = 5$ TeV (solid black) as a function of $\hat{t}/\hat{s}$.

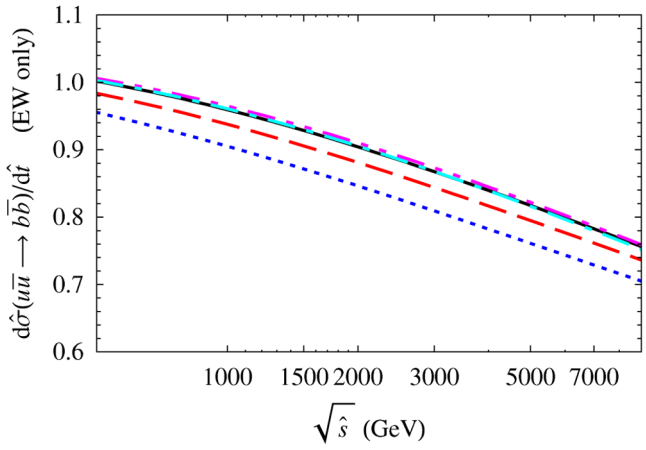

FIG. 28 (color online). Electroweak corrections to $u\bar{u} \to b\bar{b}$ at $\hat{t} = -0.2\hat{s}$, (dotted blue), $\hat{t} = -0.35\hat{s}$ (long-dashed red), $\hat{t} = -0.5\hat{s}$ (solid black), $\hat{t} = -0.65\hat{s}$ (double-dot-dashed magenta) and $\hat{t} = -0.8\hat{s}$ (dot-dashed cyan) as a function of $\sqrt{\hat{s}}$ in GeV.

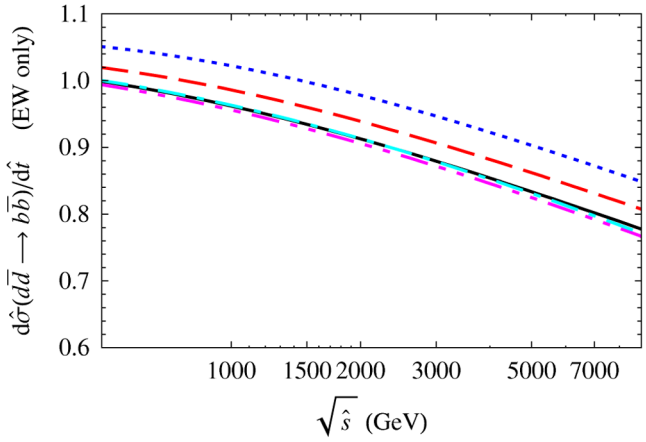

FIG. 29 (color online). Electroweak corrections to $d\bar{d} \to b\bar{b}$ at $\hat{t} = -0.2\hat{s}$, (dotted blue), $\hat{t} = -0.35\hat{s}$ (long-dashed red), $\hat{t} = -0.5\hat{s}$ (solid black), $\hat{t} = -0.65\hat{s}$ (double-dot-dashed magenta) and $\hat{t} = -0.8\hat{s}$ (dot-dashed cyan) as a function of $\sqrt{\hat{s}}$ in GeV.

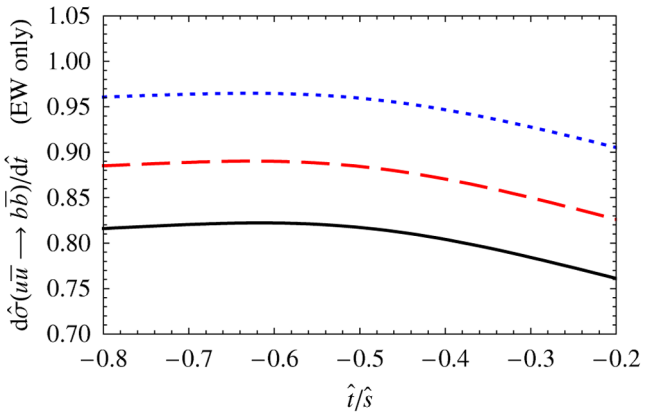

FIG. 30 (color online). Electroweak corrections to $u\bar{u} \to b\bar{b}$ at $\sqrt{\hat{s}} = 1$ TeV, (dotted blue), $\sqrt{\hat{s}} = 2.5$ TeV (long-dashed red) and $\sqrt{\hat{s}} = 5$ TeV (solid black) as a function of $\hat{t}/\hat{s}$.

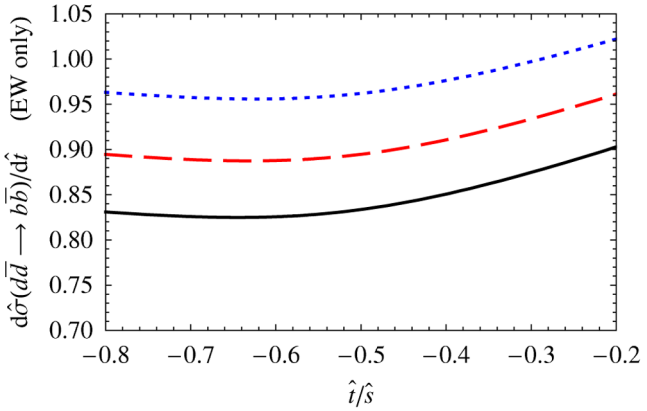

FIG. 31 (color online). Electroweak corrections to $d\bar{d} \to b\bar{b}$ at $\sqrt{\hat{s}} = 1$ TeV, (dotted blue), $\sqrt{\hat{s}} = 2.5$ TeV (long-dashed red) and $\sqrt{\hat{s}} = 5$ TeV (solid black) as a function of $\hat{t}/\hat{s}$.

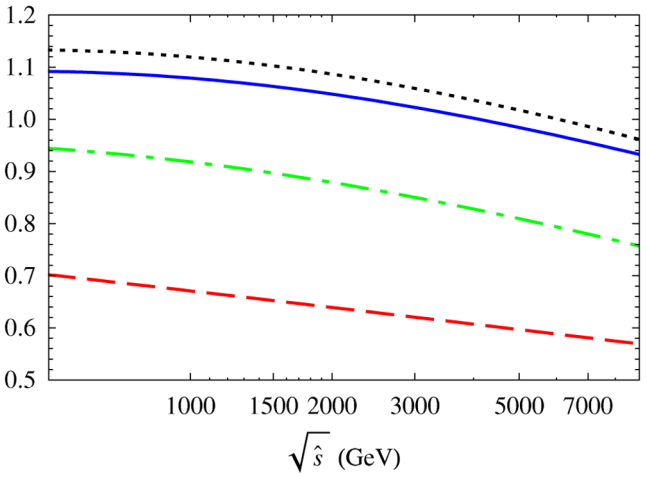

FIG. 32 (color online). Electroweak corrections to $uu \to uu$ (dotted black), $ud \to ud$ (long-dashed red), $dd \to dd$ (solid blue) and $u\bar{d} \to u\bar{d}$, $d\bar{u} \to d\bar{u}$ (dot-dashed green) as a function of $\sqrt{\hat{s}}$ in GeV at $\theta = 90°$.

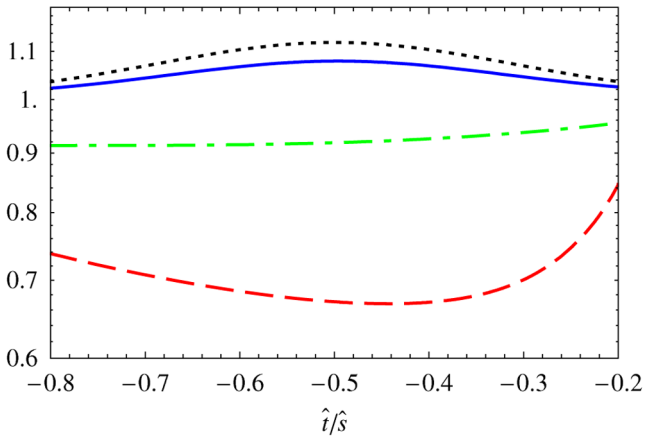

FIG. 33 (color online). Electroweak corrections to $uu \to uu$ (dotted black), $ud \to ud$ (long-dashed red), $dd \to dd$ (solid blue) and $u\bar{d} \to u\bar{d}$, $d\bar{u} \to d\bar{u}$ (dot-dashed green) as a function $\hat{t}/\hat{s}$ at $\sqrt{\hat{s}} = 1$ TeV.

small ($\sim -6\%$) suppression, and the QCD corrections give a large ($\sim 50\%$) enhancement.

The above plots have been for s-channel processes. There are also t-channel parton subprocesses that contribute to dijet production. Rather than go through these in detail, we show two illustrative plots: Fig. 32 shows the electroweak corrections to $uu \to uu$, $ud \to ud$, $dd \to dd$ and $u\bar{d} \to u\bar{d}$ (which is equal to $d\bar{u} \to d\bar{u}$) as a function of $\sqrt{\hat{s}}$ for 90° scattering, and Fig. 33 shows the angular dependence of the electroweak corrections at $\sqrt{s} = 1$ TeV.

There are also scattering processes involving external gluons. For $gg \to q\bar{q}$, $gq \to gq$, and $g\bar{q} \to g\bar{q}$, we have only computed the electroweak part of the correction, which is equal to that for the Sudakov form-factor. For the s-channel process $gg \to q\bar{q}$, the electroweak correction

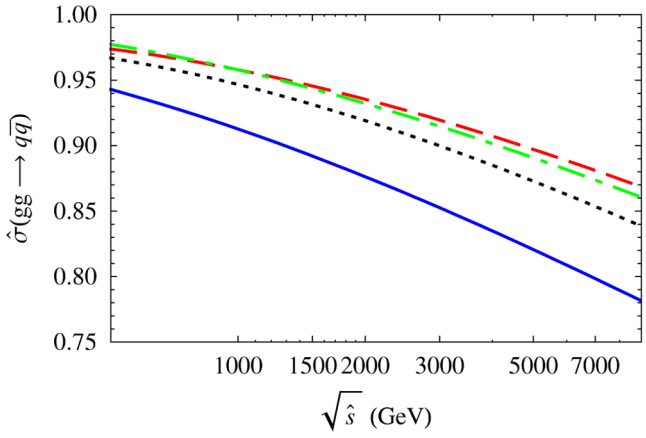

FIG. 34 (color online). Electroweak corrections to $gg \to u\bar{u}$, $c\bar{c}$ (dotted black), $gg \to d\bar{d}$, $s\bar{s}$ (long-dashed red), $gg \to t\bar{t}$ (solid blue) and $gg \to b\bar{b}$ (dot-dashed green) as a function of $\sqrt{\hat{s}}$ in GeV. The electroweak corrections are independent of $\hat{t}$ to the order we are working. The same plot also gives the electroweak corrections to $gq \to gq$ and $g\bar{q} \to g\bar{q}$, as a function of $\sqrt{-\hat{t}}$.

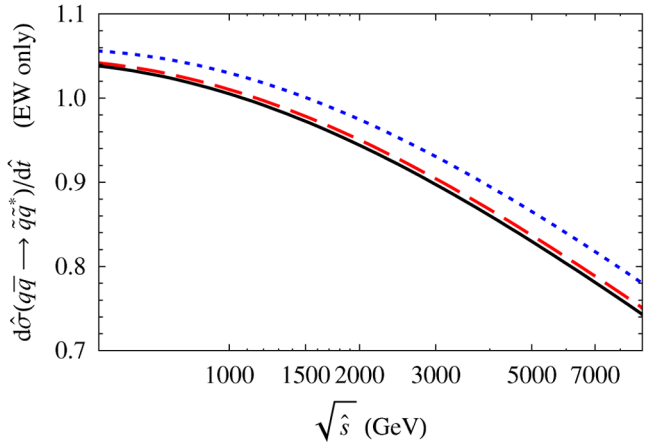

FIG. 35 (color online). Electroweak corrections to $q\bar{q} \to \tilde{q}\tilde{q}^*$ in the toy theory at $\hat{t} = -0.2\hat{s}$, (dotted blue), $\hat{t} = -0.35\hat{s}$ (long-dashed red), $\hat{t} = -0.5\hat{s}$ (solid black) as a function of $\sqrt{\hat{s}}$ in GeV. The rate is symmetric under $\theta \to 180^\circ - \theta$.

only depends on $\sqrt{\hat{s}}$, and is shown in Fig. 34. The same plot also gives the electroweak correction to the t-channel scattering processes $gq \to gq$ and $g\bar{q} \to g\bar{q}$ as a function of $\sqrt{-\hat{t}}$, by crossing symmetry. The imaginary parts from the logarithmic branch cuts in the s-channel amplitude do not change the absolute value of the amplitude.

Finally, we show the electroweak corrections for squark production. As discussed earlier, we use the electroweak correction for squark production in the toy theory, with the gauge coupling constant set equal to α_2 of the standard model. This gives an indication of the size of electroweak corrections to squark production in supersymmetric extensions of the standard model. A more precise computation depends on the specific scenario. The electroweak correction to squark production is shown in Fig. 35 for a squark mass of 250 GeV. The radiative correction to the angular distribution is shown in Fig 36. For discovering squarks,

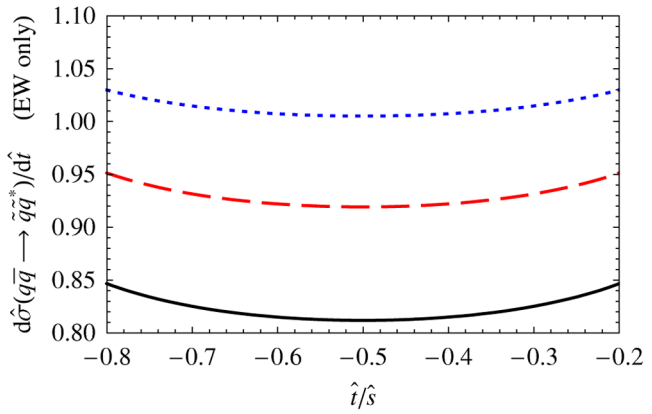

FIG. 36 (color online). Electroweak corrections to $q\bar{q} \to \tilde{q}\tilde{q}^*$ in the toy theory at $\sqrt{\hat{s}} = 1$ TeV as a function of $-\hat{t}/\hat{s}$ at $\sqrt{\hat{s}} =$ 1 TeV (black), $\sqrt{\hat{s}} = 2.5$ TeV (long-dashed red) and $\sqrt{\hat{s}} =$ 5 TeV (dotted blue).

the only correction which matters is that at threshold, $\sqrt{\hat{s}} = 2m_{\tilde{q}}$ since the parton luminosity falls steeply with $\hat{s}$. The electroweak corrections give a small (5%) enhancement of the rate for $\hat{s}$ near threshold.

IX. CONCLUSIONS

This paper extends the analysis of two previous publications [1,2], and gives detailed numerical results for radiative corrections to high energy scattering processes in the standard model. The electroweak and QCD corrections have been computed using EFT methods, and the Sudakov logarithms have been summed using renormalization group methods. The EFT also properly sums mixed higher order logarithms that depend on both α_s and $\alpha_{1,2}$, as well as those that depend on the top-quark Yukawa coupling. We have checked that our results agree with previous results when expanded in powers of α.

The electroweak corrections can be important for LHC processes, particularly in searches for new physics that look for deviations from the standard model. The corrections vary in size from about (0.4)–(−14)% at 1 TeV to about (−13)–(−32)% at 5 TeV, and need to be included to obtain LHC cross-sections with accuracies under 10%.

We have also shown that the radiative corrections to four-quark operators are given in terms of those for two-quark operators by summing over pairs of particles. The relation between this and factorization, and with the two-loop soft anomalous dimension of Aybat *et al.* [34] was discussed in Sec. VI. Further work on this important topic is in progress.

ACKNOWLEDGMENTS

We would like to thank F. Golf for his contributions during an early stage of this work. We would also like to thank A. H. Hoang, F. Würthwein and A. Yagil for helpful discussions. R. K. acknowledges support from the LHC Theory Initiative of the National Science Foundation.

APPENDIX A: MATCHING AT Q INCLUDING THE CASE OF IDENTICAL PARTICLES

In this appendix, we summarize the matching computation at scale Q, including the case of identical particles. We start with the case of an $SU(N)$ gauge theory with left-handed fermions in the fundamental representation.

The tree-graph in Fig. 37 gives

$$A^{(s)} = \frac{4\pi\alpha}{s}[\bar{u}_4\gamma^\mu T^a v_3]_L[\bar{v}_2\gamma^\mu T^a u_1]_L \qquad \text{(A1)}$$

which is written as

$$A^{(s)} = \frac{4\pi\alpha}{s}A_{LL}(T^a \otimes T^a)$$
$$A_{LL} = [\bar{u}_4\gamma^\mu v_3]_L[\bar{v}_2\gamma^\mu u_1]_L \qquad \text{(A2)}$$

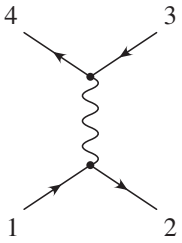

FIG. 37. s-channel tree level diagram.

factoring out the color structure from the spinor structure of the graph. The left T^a is contracted with the color indices of particles 4 and 3, and the right T^a with those of particles 2 and 1.

If the initial and final particles are identical, there is also the t-channel graph in Fig. 38 which gives

$$A^{(t)} = -\frac{4\pi\alpha}{t}[\bar{u}_4\gamma^\mu T^a u_1]_L[\bar{v}_2\gamma^\mu T^a v_3]_L = -\frac{4\pi\alpha}{t}[\bar{u}_4\gamma^\mu u_1]_L[\bar{v}_2\gamma^\mu v_3]_L(T^a\otimes T^a)_c \quad \text{(A3)}$$

and the relative minus sign is from Wick's theorem. The subscript c indicates that the color structure is in the crossed t-channel. The left T^a is contracted with the color indices of particles 4 and 1, and the right T^a with those of particles 2 and 3.

It is convenient to convert the t-channel graph to the standard basis used in the paper. The t-channel color structure can be converted to the s-channel using the $SU(N)$ color crossing matrix

$$\big[(T^a\otimes T^a)_c \quad (\mathbf{1}\otimes\mathbf{1})_c\big] = \big[(T^a\otimes T^a) \quad (\mathbf{1}\otimes\mathbf{1})\big]M_N. \quad \text{(A4)}$$

The color Fierz identity

$$(T^a)^i{}_j(T^a)^k{}_l = \frac{1}{2}\delta^i_l\delta^k_j - \frac{1}{2N}\delta^i_j\delta^k_l \quad \text{(A5)}$$

can be written as

$$(T^a\otimes T^a) = \frac{1}{2}(\mathbf{1}\otimes\mathbf{1})_c - \frac{1}{2N}(\mathbf{1}\otimes\mathbf{1}). \quad \text{(A6)}$$

Using this and the same equation with direct and crossed channels exchanged, one finds

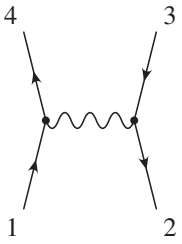

FIG. 38. t-channel tree level diagram.

$$M_N = \begin{bmatrix} -\frac{1}{N} & 2 \\ \frac{1}{2} - \frac{1}{2N^2} & \frac{1}{N} \end{bmatrix} \quad \text{(A7)}$$

with $M_N^2 = \mathbf{1}$. There is no color crossing matrix required for a $U(1)$ gauge theory. For $SU(2)$ and $SU(3)$,

$$M_2 = \begin{bmatrix} -\frac{1}{2} & 2 \\ \frac{3}{8} & \frac{1}{2} \end{bmatrix}, \qquad M_3 = \begin{bmatrix} -\frac{1}{3} & 2 \\ \frac{4}{9} & \frac{1}{3} \end{bmatrix}. \quad \text{(A8)}$$

The spinor Fierz is

$$[\bar{u}_4\gamma^\mu u_1]_L[\bar{v}_2\gamma^\mu v_3]_L = -[\bar{u}_4\gamma^\mu v_3]_L[\bar{v}_2\gamma^\mu u_1]_L \quad \text{(A9)}$$

so Eq. (A3) is

$$A = \frac{4\pi\alpha}{t}A_{LL}\left[-\frac{1}{N}T^a\otimes T^a + \left(\frac{1}{2} - \frac{1}{2N^2}\right)\mathbf{1}\otimes\mathbf{1}\right]. \quad \text{(A10)}$$

Comparing with Eq. (25) in Sec. V, we see that the s-channel contribution to the matching coefficient is

$$C^{(s)}_{1LL}(s,t) = \frac{4\pi\alpha}{s}, \qquad C^{(s)}_{2LL}(s,t) = 0 \quad \text{(A11)}$$

and the t-channel contribution is

$$\begin{bmatrix} C^{(t)}_{1LL}(s,t) \\ C^{(t)}_{2LL}(s,t) \end{bmatrix} = M_N \begin{bmatrix} C^{(s)}_{1LL}(t,s) \\ C^{(s)}_{2LL}(t,s) \end{bmatrix}. \quad \text{(A12)}$$

The total contribution is

$$C_{1LL} = C^{(s)}_{1LL}(s,t) + C^{(t)}_{1LL}(s,t) = \frac{4\pi\alpha}{s} - \frac{4\pi\alpha}{Nt}$$
$$C_{2LL} = C^{(s)}_{2LL}(s,t) + C^{(t)}_{2LL}(s,t) = \left(\frac{1}{2} - \frac{1}{2N^2}\right)\frac{4\pi\alpha}{t} \quad \text{(A13)}$$

where the t-channel pieces should only be included for identical particles.

This sets up the notation and procedure to be used for the one-loop matching computation. The full theory diagrams of Fig. 6 were computed in order to match the full gauge theory onto SCET at $\mu = Q$. Dimensional regularization was used to regulate both the infrared and ultraviolet divergences, which are distinguished by subscripts on $1/\epsilon$. The diagrams are computed with all masses set to zero. The logarithms are expressed using the short hand notation

$$x = \log\frac{-x}{\mu^2}, \qquad \mathsf{L}_{x/y} = \log\frac{x}{y} \quad \text{(A14)}$$

for $x, y = s, t, u$.

The first two vertex graphs of Fig. 6 each give a contribution of

$$V_v = \frac{\alpha^2}{s}A_{LL}\left(C_F - \frac{1}{2}C_A\right)\left[\frac{1}{\epsilon_{\rm UV}} - \frac{2}{\epsilon^2_{\rm IR}} - \frac{4}{\epsilon_{\rm IR}} + \frac{2}{\epsilon_{\rm IR}}\mathsf{L}_s - \mathsf{L}_s^2 + 3\mathsf{L}_s - 8 + \frac{\pi^2}{6}\right]. \quad \text{(A15)}$$

The next two vertex graphs in Fig. 6 each involve a triple gauge boson coupling, and give

$$V_g = \frac{\alpha^2}{s} A_{LL} \frac{C_A}{2}\left[\frac{3}{\epsilon_{\rm UV}} - \frac{4}{\epsilon_{\rm IR}} - 2 + \mathsf{L}_s\right]. \tag{A16}$$

The s-channel box graph in Fig. 39 with all fermions left-handed gives

$$\begin{aligned} V_b &= \alpha^2 I_2(s,t) A_{LL}\left[C_1 1\otimes 1 + \frac{1}{4}(C_d + C_A) T^a \otimes T^a\right] \\ &= \alpha^2 I_2(s,t) A_{LL}\left[\frac{N^2-1}{4N^2} 1\otimes 1 + \frac{N^2-2}{2N} T^a \otimes T^a\right] \end{aligned} \tag{A17}$$

where

$$\begin{aligned} I_2(s,t) &= I_1(s,t) - \frac{1}{s} f(s,t) \\ I_1(s,t) &= \frac{4}{s}\left(-\frac{1}{\epsilon_{\rm IR}^2} + \frac{1}{\epsilon_{\rm IR}}\mathsf{L}_t - \frac{1}{2}\mathsf{L}_t^2 + \frac{\pi^2}{12}\right) + \frac{2}{s}(\mathsf{L}_{s/t}^2 + \pi^2) \\ f(s,t) &= \frac{s(s+2t)}{(s+t)^2}(\mathsf{L}_{t/s}^2 + \pi^2) - \frac{2s}{s+t}\mathsf{L}_{t/s} \end{aligned} \tag{A18}$$

The s-channel crossed-box graph in Fig. 40 with all fermions left-handed gives

$$\begin{aligned} V_c &= -\alpha^2 I_1(s,u) A_{LL}\left[C_1 1\otimes 1 + \frac{1}{4}(C_d - C_A) T^a \otimes T^a\right] \\ &= -\alpha^2 I_1(s,u) A_{LL}\left[\frac{N^2-1}{4N^2} 1\otimes 1 - \frac{1}{N} T^a \otimes T^a\right]. \end{aligned} \tag{A19}$$

The gauge boson self-energy graphs combine to give a contribution of

$$\begin{aligned} V_s = \frac{\alpha^2}{s} A_{LL}\Big\{ & C_A\left[\frac{5}{3\epsilon_{\rm UV}} + \frac{31}{9} - \frac{5}{3}\mathsf{L}_s\right] + T_F n_F\left[-\frac{4}{3\epsilon_{\rm UV}}\right. \\ & \left. - \frac{20}{9} + \frac{4}{3}\mathsf{L}_s\right] + T_F n_S\left[-\frac{1}{3\epsilon_{\rm UV}} - \frac{8}{9} + \frac{1}{3}\mathsf{L}_s\right]\Big\} \end{aligned} \tag{A20}$$

and the wave function graph is

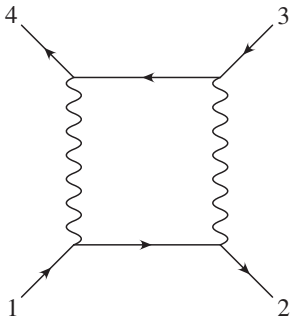

FIG. 39. Box diagram.

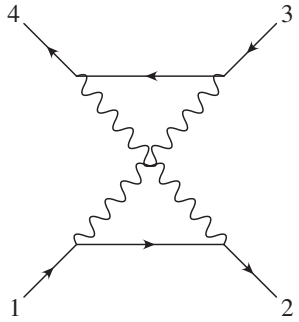

FIG. 40. Crossed-box diagram.

$$V_w = \frac{\alpha^2}{s} C_F A_{LL}\left[-\frac{1}{2\epsilon_{\rm UV}} + \frac{1}{2\epsilon_{\rm IR}}\right]. \tag{A21}$$

The sum of all of the diagrams of Fig. 6 including the gauge boson self-energy graphs and the wave function graphs is

$$V_{\rm total} = 2V_v + 2V_g + V_b + V_c + V_s + 4V_w \tag{A22}$$

and gives

$$\begin{aligned} A_{1LL} = \frac{\alpha^2}{s}\Big\{ & 2C_F\left[-\frac{2}{\epsilon_{\rm IR}^2} - \frac{3}{\epsilon_{\rm IR}} + \frac{2}{\epsilon_{\rm IR}}\mathsf{L}_s - \mathsf{L}_s^2 + 3\mathsf{L}_s - 8 + \frac{\pi^2}{6}\right] \\ & + C_A\left[\frac{2}{\epsilon_{\rm IR}}\mathsf{L}_{u/s} + 2\mathsf{L}_s^2 - 2\mathsf{L}_u\mathsf{L}_s - \frac{11}{3}\mathsf{L}_s + \pi^2 + \frac{85}{9}\right] \\ & + T_F n_F\left[-\frac{20}{9} + \frac{4}{3}\mathsf{L}_s\right] + T_F n_S\left[-\frac{8}{9} + \frac{1}{3}\mathsf{L}_s\right] \\ & + \left[\frac{4}{\epsilon_{\rm IR}}\mathsf{L}_{t/u} - 4\mathsf{L}_s\mathsf{L}_{t/u} - f(s,t)\right]\frac{(C_d + C_A)}{4}\Big\} \\ A_{2LL} = \frac{\alpha^2}{s}\left[\frac{4}{\epsilon_{\rm IR}}\mathsf{L}_{t/u} - 4\mathsf{L}_s\mathsf{L}_{t/u} - f(s,t)\right] & C_1 \end{aligned} \tag{A23}$$

which are the coefficients of $A_{LL}(T^a \otimes T^a)$ and $A_{LL}(\mathbf{1}\otimes\mathbf{1})$, respectively.

The counterterms of the full theory have been used to cancel to the $1/\epsilon_{\rm UV}$ terms and the remaining poles are all $1/\epsilon_{\rm IR}$ infrared divergences. These infrared divergent terms agree with the ultraviolet divergences in the effective theory. The finite parts of Eq. (A23) give the high scale matching condition at $\mu \sim Q$.

Equation (A23) gives the one-loop matching result for fermions which are distinguishable. If the fermions are identical, then there are also one-loop graphs in the crossed channel, analogous to the crossed channel tree graph Fig. 38. They are obtained by the crossing relation Eq. (A12) used earlier for the tree-level graphs.

The one-loop matching conditions for initial and final fermions of the same chirality (i.e. LL or RR) is Eq. (A23). If the fermions have opposite chirality, then one can obtain the matching coefficients using charge conjugation. The right-handed field ψ_R is replaced by the charge conjugate field ψ_L^c. This reverses the sign of the fermion arrow on the fermion line, and exchanges the box and crossed box

graphs. One can now use Eq. (A23) for the same-chirality case, and then use charge conjugation on the final amplitude to rewrite the ψ_L^c spinors in terms of the original ψ_R spinors. The result of this procedure is that the matching Eq. (A23) for opposite chirality (i.e. LL or RR) is given by Eq. (A23) with the replacement $C_1 \to -C_1$, $C_d \to -C_d$ and $t \leftrightarrow u$.

APPENDIX B: PARAMETER INTEGRALS

The parameter integrals tabulated below arise from vertex and wave function graphs where the gauge boson has mass M, the external particle has mass $m_{\rm ext}$, and the internal particle has mass m. They depend on the variables $w = m_{\rm ext}^2/M^2$ and $z = m^2/M^2$. For any function $f(w, z)$ defined below, we define the corresponding function of a single argument by $f(z) \equiv f(z, z)$. In the standard model, where the only fermion with mass comparable to the gauge boson masses is the top quark, we need the integrals $f(z, z)$, $f(z, 0)$ and $f(0, z)$, with $z = m_t^2/M_W^2, m_t^2/M_Z^2, m_t^2/M_H^2$.

For $4z \geq 1$, the $f(z, z)$ results can be analytically continued using $\sqrt{1-4z} \to i\sqrt{4z-1}$ and $\tanh^{-1}(\sqrt{1-4z}) \to i\tan^{-1}(\sqrt{4z-1})$. In each integral, the factors of i cancel, and the function remains real. The $f(w, 0)$ formulas are given by using $f(w + i0^+, 0)$ for $w \geq 1$. They have an imaginary part for large values of w.

1. Fermions

The gauge boson vertex graph leads to the integral

$$f_F(w, z) = 2\int_0^1 dx \frac{1-x}{x} \log\left(\frac{1-x+zx-wx(1-x)}{1-x}\right). \tag{B1}$$

$$\begin{aligned} f_F(z, z) = {} & 2 + \left(\frac{1}{z} - 2\right)\log(z) + \frac{1}{2}\log^2(z) \\ & + \frac{2\sqrt{1-4z}}{z}\tanh^{-1}\sqrt{1-4z} \\ & - 2(\tanh^{-1}\sqrt{1-4z})^2. \end{aligned} \tag{B2}$$

The function $f_F(z) = f_F(z, z)$ was used in CGKM2.

$$f_F(0, z) = \frac{\pi^2}{3} + \frac{2z}{1-z}\log z - 2{\rm Li}_2(1-z) \tag{B3}$$

$$f_F(w, 0) = 2 + 2\frac{1-w}{w}\log(1-w) - 2{\rm Li}_2(w) \tag{B4}$$

The inverse propagator including the gauge boson wave function graph is

$$S^{-1} = \not{p}[1 + A(p^2)] - m_{\rm ext}[1 + B(p^2)]. \tag{B5}$$

The parameter integrals required are

$$\begin{aligned} a(p^2/M^2, m^2/M^2) &= A(p^2/M^2, m^2/M^2) \\ b(p^2/M^2, m^2/M^2) &= p^2\frac{\partial B}{\partial p^2}(p^2/M^2, m^2/M^2) \\ c(p^2/M^2, m^2/M^2) &= p^2\frac{\partial A}{\partial p^2}(p^2/M^2, m^2/M^2) \end{aligned} \tag{B6}$$

where m is the mass of the internal fermion, and the integrals are evaluated on-shell, with $p^2 = m_{\rm ext}^2$, where $m_{\rm ext}$ is the mass of the external fermion.

$$\begin{aligned} a(w, z) &= -2\int_0^1 dx(1-x)\log\left(\frac{1-x+zx-wx(1-x)}{1-x}\right) \\ b(w, z) &= \int_0^1 dx \frac{4\sqrt{wz}x(1-x)}{1-x+zx-wx(1-x)} \\ c(w, z) &= \int_0^1 dx \frac{2wx(1-x)^2}{1-x+zx-wx(1-x)} \end{aligned} \tag{B7}$$

$$\begin{aligned} a(z, z) = {} & \frac{5}{2} - \frac{1}{z} - \frac{(1-2z)(1-4z)}{z^2\sqrt{1-4z}}\tanh^{-1}\sqrt{1-4z} \\ & - \frac{1-4z+2z^2}{2z^2}\log z \\ a(0, z) = {} & -\frac{z}{(1-z)} - \frac{z^2}{(1-z)^2}\log z \\ a(w, 0) = {} & \frac{3}{2} - \frac{1}{w} - \frac{(1-w)^2}{w^2}\log(1-w) \end{aligned} \tag{B8}$$

$$\begin{aligned} b(z, z) = {} & -4 + \frac{4(3z-1)}{z\sqrt{1-4z}}\tanh^{-1}\sqrt{1-4z} \\ & + 2\left(1 - \frac{1}{z}\right)\log z \\ b(0, z) = {} & 0 \\ b(w, 0) = {} & 0 \end{aligned} \tag{B9}$$

$$\begin{aligned} c(z, z) = {} & \frac{2}{z} - 3 + \frac{2(1-5z+5z^2)}{z^2\sqrt{1-4z}}\tanh^{-1}\sqrt{1-4z} \\ & + \frac{1-3z+z^2}{z^2}\log z \\ c(0, z) = {} & 0 \\ c(w, 0) = {} & \frac{2}{w} - 1 + \frac{2(1-w)}{w^2}\log(1-w) \end{aligned} \tag{B10}$$

The function

$$h_F(z) = a(z, z) - 2b(z, z) + 2c(z, z) \tag{B11}$$

was used in CGKM2 and is the wave function correction in a vectorlike theory.

The corresponding functions for radiative corrections due to a virtual scalar are

$$\tilde{a}(w,z) = \frac{1}{2}a(w,z)$$
$$\tilde{b}(w,z) = -\frac{1}{4}b(w,z) \quad \text{(B12)}$$
$$\tilde{c}(w,z) = \frac{1}{2}c(w,z)$$

and

$$\tilde{h}_F(z) = \tilde{a}(z,z) - 2\tilde{b}(z,z) + 2\tilde{c}(z,z) \quad \text{(B13)}$$

was used in CGKM2.

2. Scalars

The gauge boson vertex graph for scalar particles leads to the integral

$$f_S(w,z) = \int_0^1 \mathrm{d}x \frac{(2-x)}{x}\log\frac{1-x+zx-wx(1-x)}{1-x}. \quad \text{(B14)}$$

$$f_S(z,z) = 1 - \left(1-\frac{1}{2z}\right)\log(z) + \frac{1}{2}\log^2 z + \frac{\sqrt{1-4z}}{z}\tanh^{-1}(\sqrt{1-4z}) - 2(\tanh^{-1}\sqrt{1-4z})^2 \quad \text{(B15)}$$
$$f_S(0,z) = \frac{\pi^2}{3} + \frac{z}{1-z}\log z - 2\mathrm{Li}_2(1-z)$$
$$f_S(w,0) = 1 + \frac{1-w}{w}\log(1-w) - 2\mathrm{Li}_2(w).$$

Scalar wave function renormalization due to gauge boson exchange gives the integral

$$h_S(w,z) = \int_0^1 \mathrm{d}x\left\{(3x^2-6x+4) \times \log\left(\frac{1-x+zx-wx(1-x)}{1-x}\right) - \frac{wx(1-x)(2-x)^2}{1-x+zx-wx(1-x)}\right\} \quad \text{(B16)}$$

$$h_S(z,z) = \frac{3}{2} - \frac{1}{z} + \left[\frac{3}{2z} - \frac{1}{2z^2}\right]\log(z) - \frac{\sqrt{1-4z}(1-z)}{z^2}\tanh^{-1}(\sqrt{1-4z})$$
$$h_S(0,z) = \frac{z(1-3z)}{2(1-z)^2} - \frac{z(2z^2-2z+1)}{(1-z)^3}\log z \quad \text{(B17)}$$
$$h_S(w,0) = -\frac{1}{2} - \frac{1}{w} + \left(2 - \frac{1}{w^2}\right)\log(1-w)$$

Scalar wave function renormalization due to scalar exchange gives:

$$\tilde{h}_S(w,z) = -\int_0^1 \mathrm{d}x \frac{zx^3}{1-x+zx-wx(1-x)} \quad \text{(B18)}$$

$$\tilde{h}_S(z,z) = -\frac{1}{2} - \frac{1}{z} + \left[\frac{1}{2z} - \frac{1}{2z^2}\right]\log(z) + \frac{3z-1}{z^2\sqrt{1-4z}}\tanh^{-1}(\sqrt{1-4z})$$
$$\tilde{h}_S(0,z) = \frac{z(2z^2-7z+11)}{6(1-z)^3} + \frac{z}{(1-z)^4}\log z \quad \text{(B19)}$$
$$\tilde{h}_S(w,0) = 0.$$

APPENDIX C: ERRATUM

The low-scale matching for the t-quark in CGKM2 is incorrect. The corrected expressions are

$$[\bar{\xi}^{(Q_t)}_{n,p_2}W_n]\gamma^\mu P_L[W^\dagger_{\bar{n}}\xi^{(Q_t)}_{\bar{n},p_1}] \to a_1\bar{t}_{v_2}\gamma^\mu P_L t_{v_1} + a_2[\bar{\xi}^{(b')}_{n,p_2}W_n]\gamma^\mu P_L[W^\dagger_{\bar{n}}\xi^{(b')}_{\bar{n},p_1}],$$
$$[\bar{\xi}^{(t)}_{n,p_2}W_n]\gamma^\mu P_R[W^\dagger_{\bar{n}}\xi^{(t)}_{\bar{n},p_1}] \to a_3\bar{t}_{v_2}\gamma^\mu P_R t_{v_1}, \quad \text{(C1)}$$

where the matching coefficients a_{1-3} are given by

$$\log a_1(m_t) = \frac{\alpha_{\mathrm{em}}}{4\pi\sin^2\theta_W\cos^2\theta_W}[g^2_{Lt}F_g(Q,M_Z,m_t) + 2U_1] + \frac{\alpha_{\mathrm{em}}}{4\pi\sin^2\theta_W}\left(\frac{1}{2}\right)[F_g(Q,M_W,m_t) + 2W_1] + \left(\frac{\alpha_s}{4\pi}\frac{4}{3} + \frac{\alpha_{\mathrm{em}}}{4\pi}\frac{4}{9}\right)\left(\frac{\pi^2}{6}+4\right) + 2H(t_L),$$
$$\log a_2(m_t) = \frac{\alpha_{\mathrm{em}}}{4\pi\sin^2\theta_W\cos^2\theta_W}g^2_{Lb}F_g(Q,M_Z,m_t) + \frac{\alpha_{\mathrm{em}}}{4\pi\sin^2\theta_W}\left(\frac{1}{2}\right)[F_g(Q,M_W,m_t) + 2W_2] + 2H(b'_L),$$
$$\log a_3(m_t) = \frac{\alpha_{\mathrm{em}}}{4\pi\sin^2\theta_W\cos^2\theta_W}[g^2_{Rt}F_g(Q,M_Z,m_t) + 2U_2] + \frac{\alpha_{\mathrm{em}}}{4\pi\sin^2\theta_W}\left(\frac{1}{2}\right)[-c(w_t,0)] + \left(\frac{\alpha_s}{4\pi}\frac{4}{3} + \frac{\alpha_{\mathrm{em}}}{4\pi}\frac{4}{9}\right)\left(\frac{\pi^2}{6}+4\right) + 2H(t_R), \quad \text{(C2)}$$

and the required functions $U_{1,2}$, $X_{1,2}$, $H(t_L)$, $H(t_R)$, and $H(b'_L)$ are given in Eqs. (117), (133), and (139).

[1] J.-Y. Chiu, F. Golf, R. Kelley, and A. V. Manohar, Phys. Rev. Lett. **100**, 021802 (2008).
[2] J.-Y. Chiu, F. Golf, R. Kelley, and A. V. Manohar, Phys. Rev. D **77**, 053004 (2008).
[3] M. Ciafaloni, P. Ciafaloni, and D. Comelli, Phys. Rev. Lett. **84**, 4810 (2000).
[4] P. Ciafaloni and D. Comelli, Phys. Lett. B **446**, 278 (1999); **476**, 49 (2000).
[5] V. S. Fadin, L. N. Lipatov, A. D. Martin, and M. Melles, Phys. Rev. D **61**, 094002 (2000).
[6] J. H. Kuhn, A. A. Penin, and V. A. Smirnov, Eur. Phys. J. C **17**, 97 (2000).
[7] B. Feucht, J. H. Kuhn, A. A. Penin, and V. A. Smirnov, Phys. Rev. Lett. **93**, 101802 (2004).
[8] B. Jantzen, J. H. Kuhn, A. A. Penin, and V. A. Smirnov, Phys. Rev. D **72**, 051301 (2005); **74**, 019901(E) (2006).
[9] B. Jantzen, J. H. Kuhn, A. A. Penin, and V. A. Smirnov, Nucl. Phys. **B731**, 188 (2005); **B752**, 327(E) (2006).
[10] M. Beccaria, F. M. Renard, and C. Verzegnassi, Phys. Rev. D **63**, 053013 (2001).
[11] A. Denner and S. Pozzorini, Eur. Phys. J. C **18**, 461 (2001).
[12] A. Denner and S. Pozzorini, Eur. Phys. J. C **21**, 63 (2001).
[13] M. Hori, H. Kawamura, and J. Kodaira, Phys. Lett. B **491**, 275 (2000).
[14] W. Beenakker and A. Werthenbach, Nucl. Phys. **B630**, 3 (2002).
[15] A. Denner, M. Melles, and S. Pozzorini, Nucl. Phys. **B662**, 299 (2003).
[16] S. Pozzorini, Nucl. Phys. **B692**, 135 (2004).
[17] B. Jantzen and V. A. Smirnov, Eur. Phys. J. C **47**, 671 (2006).
[18] M. Melles, Phys. Lett. B **495**, 81 (2000); Phys. Rev. D **63**, 034003 (2001); Phys. Rep. **375**, 219 (2003).
[19] A. H. Mueller, *Perturbative Quantum Chromodynamics* (World Scientific, Singapore, 1989).
[20] C. W. Bauer, S. Fleming, and M. E. Luke, Phys. Rev. D **63**, 014006 (2000).
[21] C. W. Bauer, S. Fleming, D. Pirjol, and I. W. Stewart, Phys. Rev. D **63**, 114020 (2001).
[22] C. W. Bauer and I. W. Stewart, Phys. Lett. B **516**, 134 (2001).
[23] C. W. Bauer, D. Pirjol, and I. W. Stewart, Phys. Rev. D **65**, 054022 (2002).
[24] C. W. Bauer, S. Fleming, D. Pirjol, I. Z. Rothstein, and I. W. Stewart, Phys. Rev. D **66**, 014017 (2002).
[25] M. Beneke and T. Feldmann, Nucl. Phys. **B685**, 249 (2004).
[26] V. A. Smirnov and E. R. Rakhmetov, Theor. Math. Phys. **120**, 870 (1999); Teor. Mat. Fiz. **120**, 64 (1999).
[27] C. W. Bauer, A. V. Manohar, and M. B. Wise, Phys. Rev. Lett. **91**, 122001 (2003); C. W. Bauer, C. Lee, A. V. Manohar, and M. B. Wise, Phys. Rev. D **70**, 034014 (2004); C. W. Bauer and M. D. Schwartz, Phys. Rev. Lett. **97**, 142001 (2006); M. Trott, Phys. Rev. D **75**, 054011 (2007).
[28] M. E. Luke, A. V. Manohar, and I. Z. Rothstein, Phys. Rev. D **61**, 074025 (2000).
[29] J. C. Collins, Phys. Rev. D **22**, 1478 (1980).
[30] A. H. Mueller, Phys. Rev. D **20**, 2037 (1979).
[31] A. Sen, Phys. Rev. D **24**, 3281 (1981).
[32] A. V. Manohar, Phys. Rev. D **68**, 114019 (2003).
[33] C. W. Bauer and A. V. Manohar, Phys. Rev. D **70**, 034024 (2004).
[34] S. Mert Aybat, L. J. Dixon, and G. Sterman, Phys. Rev. D **74**, 074004 (2006); Phys. Rev. Lett. **97**, 072001 (2006).
[35] A. H. Hoang *et al.* (unpublished).
[36] A. V. Manohar and I. W. Stewart, Phys. Rev. D **76**, 074002 (2007).
[37] A. Idilbi and T. Mehen, Phys. Rev. D **75**, 114017 (2007).
[38] A. Idilbi and T. Mehen, Phys. Rev. D **76**, 094015 (2007).
[39] J. C. Collins, D. E. Soper, and G. Sterman, Adv. Ser. Dir. High Energy Phys. **5**, 1 (1988).
[40] C. Lee and G. Sterman, Phys. Rev. D **75**, 014022 (2007).
[41] A. V. Manohar, Phys. Rev. D **56**, 230 (1997).
[42] A. V. Manohar, arXiv:hep-ph/9606222.
[43] M. Bohm, H. Spiesberger, and W. Hollik, Fortschr. Phys. **34**, 687 (1986).
[44] M. Roth and A. Denner, Nucl. Phys. **B479**, 495 (1996).
[45] C. W. Bauer, M. P. Dorsten, and M. P. Salem, Phys. Rev. D **69**, 114011 (2004); A. V. Manohar, Phys. Lett. B **633**, 729 (2006).
[46] A. V. Manohar and I. W. Stewart, Phys. Rev. D **62**, 074015 (2000).
[47] I. Z. Rothstein, Phys. Rev. D **70**, 054024 (2004).
[48] A. K. Leibovich, Z. Ligeti, and M. B. Wise, Phys. Lett. B **564**, 231 (2003).
[49] A. V. Manohar and M. B. Wise, *Heavy Quark Physics* (Cambridge University Press, Cambridge, 2000).
[50] I. A. Korchemskaya and G. P. Korchemsky, Phys. Lett. B **287**, 169 (1992).
[51] D. B. Kaplan and A. Manohar, Nucl. Phys. **B310**, 527 (1988); A. V. Manohar, Phys. Lett. B **242**, 94 (1990).
[52] M. Melles, Phys. Rev. D **64**, 014011 (2001).
[53] N. Kidonakis, G. Oderda, and G. Sterman, Nucl. Phys. **B531**, 365 (1998).
[54] S. Moch, J. A. M. Vermaseren, and A. Vogt, Nucl. Phys. **B688**, 101 (2004).
[55] P. Nason, S. Dawson, and R. K. Ellis, Nucl. Phys. **B303**, 607 (1988).
[56] W. Beenakker, H. Kuijf, W. L. van Neerven, and J. Smith, Phys. Rev. D **40**, 54 (1989).
[57] P. Nason, S. Dawson, and R. K. Ellis, Nucl. Phys. **B327**, 49 (1989); **B335**, 260(E) (1990).
[58] W. Beenakker, W. L. van Neerven, R. Meng, G. A. Schuler, and J. Smith, Nucl. Phys. **B351**, 507 (1991).
[59] E. Laenen, J. Smith, and W. L. van Neerven, Nucl. Phys. **B369**, 543 (1992).
[60] N. Kidonakis and J. Smith, Phys. Rev. D **51**, 6092 (1995).
[61] E. L. Berger and H. Contopanagos, Phys. Rev. D **57**, 253 (1998).
[62] M. Cacciari, S. Frixione, M. L. Mangano, P. Nason, and G. Ridolfi, J. High Energy Phys. 04 (2004) 068.
[63] J. H. Kuhn, A. Scharf, and P. Uwer, Eur. Phys. J. C **51**, 37 (2007).